THE REPUBLIC OF TURKEY

BAHCESEHIR UNIVERSITY

COMPUTATIONAL FLUID DYNAMIC ANALYSIS OF AXIAL-FLOW LEFT-VENTRICULAR ASSIST DEVICE

Master Thesis

KORAL TOPTOP

ISTANBUL 2013

THE REPUBLIC OF TURKEY

BAHCESEHIR UNIVERSITY

THE GRADUATE SCHOOL OF NATURAL AND APPLIED SCIENCES

M.S. BIOENGINEERING

COMPUTATIONAL FLUID DYNAMIC ANALYSIS OF AXIAL-FLOW LEFT-VENTRICULAR ASSIST DEVICE

Master Thesis

KORAL TOPTOP

Supervisor: Dr. KAMURAN KADIPAŞAOĞLU

ISTANBUL 2013

THE REPUBLIC OF TURKEY

BAHCESEHIR UNIVERSITY

THE GRADUATE SCHOOL OF NATURAL AND APPLIED SCIENCES

M.S. BIOENGINEERING

Name of the thesis: **Computational Fluid Dynamic Analysis of Axial-Flow Left-Ventricular Assist Device**

Name/Last Name of the Student: **KORAL TOPTOP**
Date of the Defense of Thesis : **16.01.2013**

The thesis has been approved by the Graduate School of Natural and Applied Sciences.

Graduate School Director

I certify that this thesis meets all the requirements as a thesis for the degree of Master of Arts.

PROF. DR. EROL SEZER
Program Coordinator

This is to certify that we have read this thesis and we find it fully adequate in scope, quality and content, as a thesis for the degree of Master of Arts.

Examining Committee Members Signature

Thesis Supervisor
DR. KAMURAN KADIPAŞAOĞLU

Thesis Co-supervisor
PROF. DR. EROL SEZER

Member
PROF. DR. EMİN TACER

Member
PROF. DR. OKTAY ÖZCAN

Member
ASST. PROF. DR. M. BERKE GÜR

ABSTRACT

COMPUTATIONAL FLUID DYNAMIC ANALYSIS

OF

AXIAL-FLOW LEFT-VENTRICULAR ASSIST DEVICE

Koral Toptop

Bioengineering

Thesis Supervisor: Dr. Kamuran Kadıpaşaoğlu

January, 2013

Heart failure (HF) is the most mortal disease all over the world and last stage HF only can be recovered with heart transplantation. In case of lack of available donor, ventricular assist devices (VADs) were used to keep last stage HF patients alive, especially by supporting left ventricle. These devices aren't produced by Turkey and absence of VADs results as high economic load because of importing cost. Moreover, lack of products limits academic and clinical studies on field and restricts success in implantation and post-implantation device support. So, researcher group in Bahcesehir University started program to produce left-ventricular assist device (LVAD) and this project contains initial 3D design depending on preliminary calculations, computational fluid dynamic (CFD) analysis and optimization of geometry to reach final prototype that satisfies all design criteria.

Firstly, requirements of LVAD were determined as hemodynamic and hemocompatibility (hemolysis and coagulation) criteria. Then, initial 3D design was constructed via SolidWorks CAD software according to size restrictions for implantation i.e. anatomic constraints and tested via ANSYS Fluent commercial CFD package. Hemodynamic performance was studied by observing head pressure-flow and hydraulic efficiency characteristic and effects on hemolysis were estimated by studying shear stress, transition time, backflow and vortex zones. Then, possible coagulation was studied by observing stagnant flow regions.

Then, 3D virtual geometry was re-designed by changing pump geometric parameters by deeply considering CFD results to reduce deviation from design criteria. CFD analysis were performed on new design and this re-design and analyzing process were iteratively continued until reaching final prototype which satisfies all hemodynamic and hemocompatibility criteria. At the end of project, 2 different prototypes were developed to use them in physical tests (Mock Circuit and Particle Image Velocimetry) i.e. in-vivo and in-vitro testing as next steps of LVAD development program.

Keywords: Left Ventricular Assist Device, Computational Fluid Dynamic Analysis, Hemodynamics, Hemocompatibility, Hemolysis

ÖZET

EKSENEL-AKIŞLI SOL-VENTRİKÜL DESTEK CİHAZI
HESAPLAMALI AKIŞKANLAR DİNAMİĞİ ANALİZİ

Koral Toptop

Biyomühendislik

Tez Danışmanı: Dr. Kamuran Kadıpaşaoğlu

Ocak, 2013

Dünya çapında en ölümcül hastalıklardan biri olan kalp yetmezliğinin son aşaması ancak organ nakli ile tedavi edilebilinir. Nakil için uygun organın eksikliği gibi durumlarda, ventrikül destek cihazları hastanın yaşamsal fonksiyonlarının idamesi için kullanılır. Bu cihazlar Türkiye'de üretilmemektedir ve bu eksiklik ithalat masrafından dolayı ekonomi üstüne ağır yükler doğurmaktadır. Ayrıca cihaz eksikliğinden dolayı üniversitelerde ve kliniklerde alan üstüne çalışmalar yapılamamakta, bu yüzden de ameliyatlarda ve cihazın sonraki kullanımlarında çok başarı sağlanamamaktadır. Bu yüzden Bahçeşehir Üniversitesinden bir grup araştırmacı, yerli sol-ventrikül destek cihazı tasarımı ve üretimi için bir program başlatmıştır. Bu proje öncül hesaplamalar doğrultusunda 3B başlangıç tasarımı, tasarımın hesaplamalı akışkanlar dinamiği (HAD) yöntemi ile test edimesi ve 3B tasarımın en-iyileştirilerek bütün dizayn gerekliliklerini yerine getiren nihai prototipin elde edilmesi aşamalarını kapsamaktadır.

İlk olarak, cihaz gereksinimleri, hidrolik performans ve kan-uyumluluğu (hemoliz ve pıhtılaşma) olmak üzere belirlenmiştir. Daha sonra implantasyon için boyut kıstasları ve turbomakinalar üzerine yapılmış öncül hesapamalar göz önüne alınarak 3B başlangıç tasarımı Solidworks CAD yazılımı ile yapılmış ve ANSYS Fluent CFD yazılımı ile de hesaplamalı akışkanlar dinamiği analizi gerçekleştirilmiştir. Cihazın hidrolik performansı basma basıncı-debi ve hidrolik verim karakteristiği ile gözlemlenmiş, hemoliz etkisi ise kayma gerilimi, kan parçacığı geçiş süresi, vorteks ve geri akım bölgeleri ile tahmin edilmeye çalışılmıştır. Pıhtılaşma ise akışın durağanlaştığı bölgeler gözlemlenerek tahmin edilmeye çalışılmıştır.

Daha sonra, HAD sonuçları doğrultusunda dizayn gereksinimlerinden sapmayı azaltacak şekilde tekrarlamalı 3B tasarım pompanın geometrik parametreleri değiştirilerek yapılmış ve tekrardan HAD yöntemleri ile sınanmıştır. Bu tekrarlamalı tasarım ve HAD testleri, tüm hidrolik ve kan-uyumluluğu gerekliliklerini yerine getiren nihai prototip elde edilene kadar devam etmiştir. Proje sonunda, sol-ventrikül destek cihazı geliştirme programının sonraki aşamalarını oluşturan fiziki testlerde (Mock Circuit ve Görüntülü Parçacık Hız Analizi) kullanılmak üzere 2 farklı nihai prototip elde edilmiştir.

Anahtar Kelimeler: Sol Ventrikül Destek Cihazı, Hesaplamalı Akışkanlar Dinamiği Analizi, Hidrolik Performans, Kan-Uyumu, Hemoliz

CONTENTS

TABLES

PLOTS

FIGURES

ABBREVIATIONS

BDCM	:	Brushless Direct Current Motor
Bi-VAD	:	Both Ventricular Assist Device
BF	:	Back Flow
CAD	:	Computer Aided Design
CFD	:	Computational Fluid Dynamics
DC	:	Direct Current
EM	:	Electro Magnetic
FF	:	Forward Flow
FP	:	Final Prototype
HF	:	Heart Failure
LF	:	Leakage Flow
LV	:	Left Ventricle
LVAD	:	Left Ventricular Assist Device
MCSS	:	Mechanically Circulation Support Systems
NIH	:	Normalized Index of Hemolysis
PIV	:	Particle Image Velocimetry
pfHb	:	Plasma Free Hemoglobin
RANS	:	Reynolds Averaged Navier Stokes
RBC	:	Red Blood Cell
RV	:	Right Ventricle
RVAD	:	Right Ventricular Assist Device
R&D	:	Research & Development
TAH	:	Total Artificial Heart
UDF	:	User Defined Function

SYMBOLS

	Angles (relative to axial direction)	Units
α	Inducer trailing	Deg.
β	Flow (Relative in rotor, Absolute in Diffuser) or blade	Deg.
θ	Incidence	Deg.
δ	Deviation	Deg.
	Kinematics	
v	Absolute velocity of fluid	m/s
w	Relative velocity of fluid according to rotor	m/s
u	Blade linear velocity	m/s
ω	Blade angular velocity	Rad/s
	Geometry	
r	Radius	m
A	Area	m^2
l	Length	m
	Blade Geometric Constants	
c	Chord Length	m
s	Pitch (Space)	m
σ	Solidity ($^c/_s$)	(-)
n	Number of blades	
t	Blade thickness	
g	Gap	
C_D	Drag Coefficient	(-)
k	Sign factor depending on stages	(-)
κ	Rotor-to-diffuser drag coefficient ratios	(-)
P	1x9 constant matrix that depends on stage trailing angles	(-)
N	Trailing angle constant of P matrix ($tan(\alpha_1) + tan(\beta_{f2})$ for rotor and $tan(\beta_{f4}) - tan(\beta_{f2})$ for diffuser)	(-)
Z	Trailing angle constant of P matrix $\left(tan(\alpha_1) - tan(\beta_{f2})\right)$	(-)
	Hydrodynamic	
ρ	Density	kg/m^3
μ	Viscosity	kg/s.m
m	Mass of fluid	kg
$\dot{m}$	Mass flow rate	kg/s
Q	Volumetric Flow Rate	m^3/s
$Q(\eta_{max})$	Volumetric flow rate at peak efficiency	m^3/s
H	Total Pressure	Pa
P	Static Pressure	Pa
KE	Dynamic Pressure	Pa
h_{loss}	Pressure Losses	Pa
BF	Back flow (BF1 for rotor inlet, BF2 for rotor outlet)	
LF	Leakage flow	
R_h	Hydraulic resistance	$kg/m^4.s$
σ_{ss}	Shear stress	Pa
t_e	Transition time of fluid	ms

Force		
F	Force	N
T	Torque (also Torque Load)	N.m
X	Axial force on blade at unit depth	Pa.m
Y	Tangential force on blade at unit depth	Pa.m
D	Drag force on blade at unit depth	Pa.m
Motor		
L	Load	A.Turn
i	Armature Current	Amper (A)
N	Coil turns (all active coils)	Turn
R_e	Electrical Resistance (all active coils)	ohm
ρ	Electrical Resistivity	ohm.m
B_g	Magnetic Field Strength at gap	Tesla
K_b	Torque constant	N.m/A
General		
W	Power	$kg.m^2/s^3$
J	Moment of inertia of rotor	$Kg.m^2$
V	Volume of rotor	m^3
m	Mass of rotor	gr
η	Efficiency	(-)
Δ	Change across two point	

Subscripts

Direction		Stage	
x	Axial	r	Rotor Stage
u	Tangential	d	Diffuser Stage
y	Tangential	$total$	Sum of all stages
Type		**System**	
f	Fluid	h	Hydraulic
b	Blade	m	Mechanical
m	Magnet	e	Electrical
w	Wire	out	Output
Location		in	Input
m	At median plane	**Others**	
t	At tip plane	c	Cross Sectional
h	At hub plane	m	Mean
1	Rotor inlet	i	Ideal
2	Rotor outlet	max	Peak (Maximum)
3	Diffuser inlet	min	minimum
4	Diffuser outlet	nom	Nominal (optimum)
o	Outlet of concerned stage	r	Regurgitant
i	Inlet of concerned stage		

1. INTRODUCTION

Generally, this project is a part of developing and manufacturing Left Ventricular Assist Device (LVAD) for heart failure patients. LVAD is a turbomachine, can also be described as pump that helps function of heart's left ventricle (LV) by providing blood flow from LV to the aorta in one direction. It was invented to be used by implanting into the body as a temporary assistance during heart failure or long term assistance to regulate blood circulation by supporting the heart pumping function.

Heart failure (HF) is dysfunction of heart and it can be irregularity of beat, muscle contractility problem, inefficient blood flow, low blood pressure or inborn problems. Heart attacks are caused by blockage of coronary arteries that feed heart with oxygen rich blood. So, oxygen rich blood cannot reach heart muscles and muscle cells cannot be fed by circulatory system sufficiently. As a result, it decreases heart performance especially performance of LV that feeds circulation system by providing blood flow directly to the aorta.

Coronary heart disease cause death of more than 2 million people in European Union and 5.3 million people in Europe region each year by being most important death reason. %50 of coronary heart disease death occurs before age 75 and %15 occurs before age 65 in Europe. Moreover, 5.2 million adults within 40 to 70 years old in USA have HF. 1 million of these patients have periodic heart attack and the half dies in one year. Also, each year 550.000 new HF cases occur.

Heart attacks can cause damage on heart muscles and performance. In order to recover the decrease in heart performance, there are a few treatment methods. First method for treatment is medicine and the other is surgery; but medicine doesn't provide permanent solution for diseases. Surgery provides permanent solution but isn't appropriate for emergency situations. However, the heart in the last stage of failure reaches permanent damage on muscles and it is incurable. So heart of patients who reached last stage of HF, must be transplanted with another heart as an only solution.

So, heart transplantation are performed to patients in the last stage of HF and annually around 3500 transplantations are done worldwide with survival rates around %80, %65 and %46 respectively for 1, 5 and 10 years life period after surgery.

Plot 1.1. Survival Rates by Life Periods After Transplantation

According to statistics, in Turkey, 500.000 people have HF and %20 of them reaches last stage of HF. Moreover, 3000 of them needs immediate heart transplant each year, however only around 50 transplantations can be done due to lack of available heart. So, rest of the HF patients has to wait until available organ can be found for transplantation, however most of them dies in 2 years.

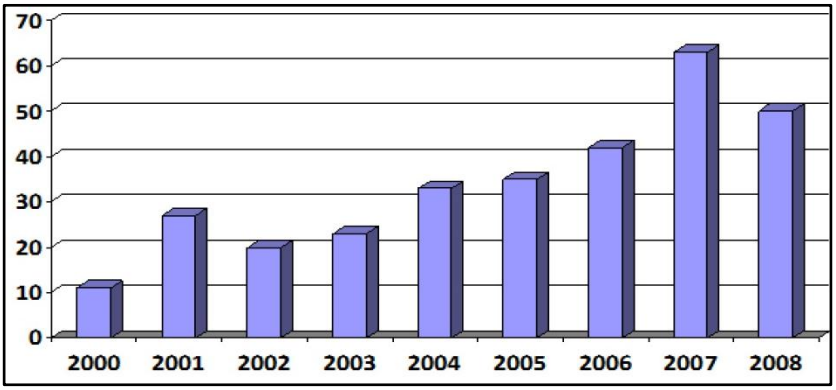

Fig 1.1: Annual Distribution of Heart Transplantations in Turkey

1.1. MECHANICAL CIRCULATORY SUPPORT SYSTEMS (MCSS)

Mechanical circulatory support systems (MCSS) were invented to keep patients alive until available organ can be found for transplantation. MCSS is pump implanted as bridge to transplant between relevant tissues to support blood circulation and generally it is used to assist to LV function. This type of MCSS called Left Ventricular Assist Device (LVAD) and it implanted between LV and aorta by connecting device inlet cannula to LV and outlet cannula to Aorta (Fig 1.2). It gives hemodynamic support to heart thanks to unloading LV by draining blood away from here and directing it to aorta. Thus, it increases survival period of patients during waiting period for transplantation by supporting heart function. Moreover, it results in increased health after transplantation thanks to feeding organs such as lungs and kidneys by providing blood circulation during its usage, although failure heart couldn't do it. Since 1963, its size was reduced from large room size to the small hand size products with increasing technology and now LVADs can be implanted to body by locating it into the body, so portability option for HF patients was provided during device usage instead of staying in hospital during long term support. Moreover, some type of LVADs can save patients from oncoming transplantation by providing them good life quality with long term survival period without any tissue damage.

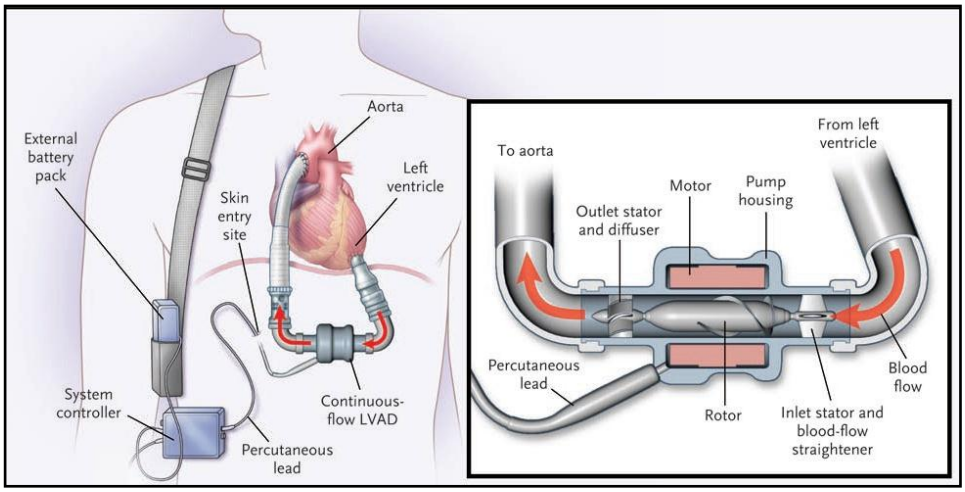

Fig 1.2: LVAD as Bridge to Transplant System in Patients Body at Left and Inner Design at Right Side

The 2010 Registry of the International Society for Heart and Lung Transplantation indicated that the percentage of adult heart transplant recipients who received an LVAD prior to transplantation, increased from 13.4 between 1992 and 2001 to 44.5 between 2002 and June 2009; while the percentage receiving IV inotrope therapy only decreased from 55.3 to 44.5 during the same respective periods.

In the US, the Interagency Registry for Mechanically Assisted Circulatory Support (INTERMACS) reported that 12-month actuarial survival increased from 50% in 314 adults receiving a LVAD in the 75 participating institutions between 23 June 2006 and 31 December 2007, to 79% in the 2506 patients on LVAD enrolled from the same beginning date to 30 September 2010 in 79 US centers. For 1936 of these 2506 patients (77%) who received an intra-corporeal continuous flow (CF) LVAD, survival at 12 and 24 months was 83% and 75%, respectively; whereas in the remaining 570 who were implanted with a pulsatile flow device, survival remained at 67% and 45%, respectively.

These data point to a steady increase in the use of mechanical circulatory assistance for the management of end-stage heart disease. The emerging trends seem to be a preference of assist devices over inotropes when stratified by era; of LVADs over RVAD, Bi-VAD or TAHs[I] by assistance modality, and of continuous flow devices over pulsatile pumps by device type. In turkey, First LVAD implantation was performed on a patient in Ankara in 2002 and device of Dr. DeBakey was used According to data from Turkish Society of Organ Transplantation, Table 1.1 below shows LVAD usage until 2010.

	Higher Education	Akdeniz University	9 Eylül University	Ege University	Gazi University	Ankara University	Yeditepe University	Total
MicroMed DeBakey	4	1	1	-	-	-	1	7
Thoratec HeartMate II	-	-	1	-	-	-	-	1
Berlin Heart INCOR	-	-	-	8	-	-	-	8
Berlin Heart EXCOR	-	2	2	28	1	-	1	34
ABIOMED 5000	-	-	-	2	1	-	-	3
Cardiowest Symbion	-	-	-	1	-	1	-	2
Total	4	3	4	39	2	1	2	55

Table 1.1: LVAD experiences in Turkey until 2010

[I] RVAD and Bi-VAD are MCSS used to support right ventricle and both ventricles respectively. TAH is total artificial heart.

1.1.1. Blood Pump Technology

Until today, many heart pumps were designed in order to reduce the HF effects on human circulation system by supporting blood flow. These heart pumps are classified in two categories depending on flow type (pulsatile and continuous flow) and in three categories (1-3 generations) depending on their bearing technologies.

Flow Type:

- Pulsatile Flow (Displacement Pumps)
- Continuous Flow (Rotary Pumps)
  - Axial Flow
  - Centrifugal (Radial)
  - Mixed Flow (Diagonal)

Generations:

- 1st generation : Displacement (Pulsatile) pumps,
- 2nd generation : Rotary pumps with mechanical bearings,
- 3rd generation : Rotary pumps with magnetic or hydrodynamic bearings

a. <u>Types:</u>

Displacement pumps (1st generation pumps) provide blood flow by taking the blood in closed volume and increasing inside pressure via mechanical system especially piston. Increased pressure causes blood flow from one valve of closed volume by forcing it to open. These types of pumps provide pulsatile blood flows. Further generations (2nd and 3rd) are rotary blood pumps that provide blood flow by transferring mechanical energy as kinetic energy to blood via propeller inside of pump and rotary pumps provide continuous flow. However, current technology allows controlling propeller speed to create pulsatile flow.

Displacement pumps can be easily broken down because of fatigue of mechanical system, so it is for shorter term use compared to rotary pumps (further generations). Moreover instant acceleration of mechanical system in displacement pumps causes demolishment of red blood cells (hemolysis). However, rotary blood pumps cause less

hemolysis than displacement blood pumps. Also, rotary pumps have less volume than displacement pumps, so implantation to body and transportability by patients is much easier than displacement pumps. Also, less blood capacity inside of pump allows to more sensitive control on volumetric flow via controlling propeller speed. These kinds of advantages of rotary blood pumps cause to prefer this type in order to support heart.

Rotary blood pumps are also divided to three categories in terms of propeller geometry; these are axial, centrifugal (radial) and mixed (diagonal) pumps. The axial flow pumps provides low pressure and high flow rate up to 20 L/min; however centrifugal pumps provides low flow rate with high pressure rise up to 500-600 mmHg and mixed flow blood pumps provides high flow rate with high pressure increase. In terms of physiological parameters of human body, the pressure difference between LV and aorta is up to 120 mmHg and blood flow rate is within 2-15 L/min. So, the heart pumps should operate within these ranges.

Commonly, centrifugal and axial flow pumps are used to support HF patients according to blood kinematic values at pump outlet and hemocompatibility. However, the smaller size and lower weight of axial flow pumps provides easier implantation to patient and less transportability limitation than centrifugal pumps. Also, smaller size allows smaller diameter and it decreases the hemolysis by reducing stress that exerted on blood particles via propeller. So, axial pumps cause less damage on red blood cells (RBCs) than centrifugal. Moreover, axial pumps generally consume less power than centrifugal pumps thanks to motor and propeller geometry; so it is available for smaller and lighter power supply package. All these advantages of axial blood pumps make it more preferred design for heart support systems.

- **Technique of Axial Flow Pumps:**

Axial flow pumps provide blood flow at direction of rotation axes and include 3 main components, one is rotary and the others are stationary. First component of turbomachine is called flow straightener, also known as inducer. It is a stationary component located at inlet of flow channel. Aim of this component is preventing pre-rotation of fluid at inlet of impeller (rotary component). When fluid enters to rotary zone, non-smooth fluid and rotary blade action may cause flow to turn in backward

direction with high tangential velocity. Then, this backflow may cause prerotation of fluid at front of inlet of rotary component. So, inducer blades reduce prerotation by parallelizing blood flow to its blades and generally inducer blades are designed as parallel to the flow channel (0^0 with rotation axes).

Then, fluid enters to second component of device, named as rotor (impeller or rotary component) and designed to gain hydraulic energy to fluid by converting mechanical energy. Blades are rotated by mechanical energy that produced via electromechanical motor mechanism. Then, torque and rotational velocity are converted to flow and pressure rise via impeller. So, rotor is the most important component in device because it had to be accelerated via electromagnetic mechanism to impart energy to fluid. That means permanent magnets of brushless DC motor are located at rotor component. So, turbomachinery calculations are not enough to design rotor blades. It also requires making calculations with electromagnetic formulas to design this component. Moreover, because of high rotational velocity of these blades, most of the hemolysis occurs at this section. So, these design requirements bring many concepts to rotor design.

When fluid exits from rotor, it has high tangential velocity or kinetic energy. Third component of axial flow pump called diffuser that is stationary component of device, and is designed to decelerate flow in tangential direction to lead it parallel to rotation axis and prevent circulative flow motion at pump exit. This function results as conversion of tangential velocity into static pressure rise. Shortly, diffuser converts kinetic energy of fluid to potential energy. Furthermore, inducer and diffuser components include bearings for mechanical support of rotary component.

b. <u>Bearing:</u>

In addition to selecting the pump type, bearing selection is also one of the most important criteria that define hemocompatibility, because most of the hemolysis occurs around bearing region of pump. So, pump generations were divided according to bearing mechanism due to importance on hemocompatibility and support period.

In the 1st generation pumps, bearings were isolated from the blood via plastic cover, that method was commonly used in displacement pumps. However, plastic cover demolishes with the time because of material fatigue, bearing oil disperses into the blood flow and limits usage period of displacement pumps. Then, rotary pumps were used in further generations to support heart functions. Mechanical bearings were used to support impeller in 2nd generation rotary blood pumps and lubrication of bearing was provided with blood. However, high friction at this section caused high hemolysis at bearings.
Then, hydro-dynamic levitation was used in some 3rd generation pumps to support impeller rotation by just allowing blood plasma to washing bearings thanks to forming bearing gaps smaller than red blood cells.

Finally, magnetic levitation of impeller was performed in other 3rd generation rotary pumps by locating same polarity magnet one at inner surface of stator (pump housing) and one at rotor. Magnetic field interaction of these magnets holds impeller up without any contact with pump housing. Contact-free manner of magnetic levitation reduces frictional losses and hemolysis. Furthermore, coagulation is also reduced by removing mechanical bearings which causes stagnant flow. However, extra magnets are increasing mass of device and all technological ads have extra costs.

c. Permanent Magnets:

Furthermore, although some rotary blood pumps were designed as same type, they have different configurations on brushless EM DC motor design. These configurations depend on permanent magnet installations. Permanent magnets located at rotary component of devices, are used to create magnetic field, which interacts with another magnetic field created by copper coils located at stator section of DC motor. Both field interactions create rotational movement of impeller. In initial rotary pumps, these permanent magnets were located at hub of impeller, this configuration has large gap between magnets and stator coils and results as high magnetic flux losses. Magnetic flux losses can be recovered by increasing magnet volume and it results in increased device mass. So, some technological developers moved permanent magnets inside of impeller blades and made them closer to the stator coils. However, in this configuration, blades limits magnet volume for installation. Smaller magnet volume also reduces magnetic field strength created by permanent magnets which can be recovered by

increasing coil turn numbers or armature current. However, this enhancement causes high electrical loses at stator coils and results in motor overheating.

So, in this project permanent magnets were designed as cylinder and flow channel was opened interior of this magnetic cylinder. Then, blood acceleration and pressure head was provided by locating blade inside of this channel. Hereby, large magnetic distance problem as in first configuration and small magnet size problem as in second configuration was eliminated with new configuration that was developed during this project. Also, there are some heart pump developer groups that work on same configuration too such as Baykut Doğan from Coras Medical (AG, Switzerland) and his colleagues from Helmholtz Inst. (Institute of Applied Medical Engineering, Aachen Germany).

1.1.2. Current Products

There are many companies that work on their own MCSS. Most of them work in collaboration with universities. Because when company designs device, they need feedbacks from doctors by depending on clinical trials on patients. Furthermore, educated technician for the field is required to help doctors for device implantation during surgery and correct usage of device to increase life quality of patients after surgery. Proportion at the collaboration depends on their choices; but commonly companies do the production of prototypes and final product when universities do experiments on animals and humans to provide feedback to companies. Moreover product design, its computer based simulations and laboratory based physical tests can be done by companies or universities too by depending on their agreements. Also, medical technicians are educated during this clinical testing process in universities to use company products more efficiently in hospitals. According to pump generations, some LVAD and their producers are:

- **1st Generation Pumps:**

— HeartMate I XVE/IP (Thoratec Corporation -Pleasanton CA, USA):

The HeartMate I is implantable pneumatic left-ventricular assist system. Pump operation relies on actuation of pusher plate (plastic diaphragm) to produce pulsatile blood flow to ascending aorta. Device designed with 110 mm width, 40 mm height and 1190 gr weight and achieves support up to 10 L/min at 120 Beat/min. Blood contact surface was covered by sintered titanium to prevent coagulation.

— ExCor (Berlin Hertz Centrum):

The Berlin Heart Excor is pneumatically actuated VAD (capable of left, right or biventricular support). Different models of device are available up to 80ml depending on body surface area. Largest device delivers maximum 10 L/min flow at maximum beat rate, 150 Beat/min.

— Novacor (World Heart Corporation, Novacor Corp, Oakland, CA-USA):

Novacor LVAS was manufactured by World Heart Corporation (WHC) and Stanford University researches helped WHC by providing feedback from clinical trials. Novacor LVAS was designed as totally implantable pulsatile blood pump to provide therapy for end-stage heart failure. Pusher plate is used to pump blood and it is driven by magnetic field created by coils and permanent magnets located in pusher plate.

- **2nd Generation Pumps:**

— Hemopump (Medtronic Incorporation - Minneapolis, USA):

As a result of the investigation and research by Dr. Rich Wampler, Hemopump was produced and developed with co-operation between Medtronic Company and Utah Artificial Heart. Hemopump can provide 3.5 to 4.5 L/min blood flow to aorta with 17000-26000 rpm. This device has 8.1 mm diameter, 16 mm length, 6 gr weight and 5 cc volume. Moreover, the test on the humans showed that Hemopump had mean 50 hour continuous support period without causing any negative effect on blood as hemolysis, infection or vessel damage. However, this device isn't currently used.

— Jarvik 2000 (Jarvik Heart Incorporation – New York, USA):

Jarvik 2000 axial flow pump was developed by Dr. Robert Jarvik with co-operation between Oxford Heart Center, Texas Heart Institute and Jarvik Heart Corporation. This heart pump has 25 mm diameter, 55 mm length, 85 gr weight and 25 cc volume. Moreover, it can produce up to 7 L/min blood flow with 100 mmHg pressure difference between LV and aorta at 8000-12000 rpm. As a result of the experiments on calves made by Texas Heart Institute, normalized index of hemoglobin (NIH) was observed 0.00082 ± 0.00054 mg/dl after 70 days support period. Animal trials of Jarvik 2000 had been started in 2001. According to results in end of 2002, this device provides %56 survival rate after one year transplantation period. It has a power supply that produces 10 Watt, 8-10 hour duration. Brushless EM DC motor is used in Jarvik 2000 to turn propellers for providing blood flow. Also, rotor includes permanent magnets assembled in the center of rotor (hub) with diameter of 5 mm and length of 20 mm. Rotation was

supported with two ceramic bearings and their durability is 10 year. All surfaces of device that contact blood were covered by titanium to prevent reaction with blood.

— IVAP (Sun Medical Corporation -Nagano, JAPAN):

IVAP was developed by Sun Medical Corporation and Waseda University and has 170 gr weight, 8 mm hub and 13.5 mm housing diameter with 0.1 mm blade tip gap. It produces 8 L/min blood flow under 100 mmHg pressure difference at 13000 rpm. It works with 8 W power requirement. In IVAP device, the blood contact surface of rotor was reduced more than the other LVAD, so it causes less hemolysis effect.

— DeBakey VAD (MicroMED Technology Corporation):

MicroMED Co. produced DeBakey VAD by working with NASA Johnson Space Center and Baylor College of Medicine. This device has 25 mm diameter, 75 mm length, 95 gr weight and 15 cc volume. Furthermore, it can work with less than 10 W power and produce 5-6 L/min blood flow under 100 mmHg pressure difference at 10000 rpm. Blood flow up to 10 L/min can be achievable with maximum motor velocity. The blood contact surface of device was covered with titanium material. Also, mechanical bearings (covered by ceramic) were used to support rotor, so flow straightener and diffuser contains ceramic bearings. The specialty of DeBakey VAD is, the permanent magnets of rotor were installed into rotor blades. Producers reduced magnetic gap between permanent magnets and stator coils with this configuration. According to the experiments on calves, after 90 days from implantation normalized index of hemolysis (NIH) was remained below 0.0002 mg/dl which is within acceptable range. As reported in 2000, in terms of the in-vivo tests on 37 adult patients, %81 survival rate after 30 days from implantation and mean 47 day continuous support period were observed.

— HeartMate II (Thoratec Corporation -Pleasanton CA, USA):

Thoratec Co. produced and developed HeartMateII LVAS by co-operating with Texas Heart Institute. HeartMateII is an axial flow heart pump that has 40 mm diameter, 60 mm length, 375 gr weight and 62 cc volume. This device can produce 3-4 L/min blood flow with 80-100 mmHg pressure rise at 8000-9000 rpm. Power supply of device

provides 10 W power up to 4 hours duration. Permanent magnets of rotor were installed into rotor center (hub) to rotate propellers. HeartMateII also has ceramic bearings like DeBakey VAD. According to generated reports, levels of pfHb varies from 3 to 4 gr per day. Tests on animals were begun in 1997 and the first human implantation was performed in Israel in July 2000. According to experiments in calves, the NIH was observed within acceptable range for human physiology.

— Impella (Abiomed - Aachen, GERMANY):

Impella AD was developed as a result of the Abiomed's research and experiments. Impella AD has 6.4 mm diameter, 60 mm length, 5 gr weight and 2 cc volume. This device produces 7 L/min blood flow and 100 mmHg pressure rise at 30,000 rpm with hydraulic efficiency approximately %30. The reason for producing same blood flow at high rpm operation is lower volume of Impella. Impella has 12 W power supply in order to provide blood flow. Also, Impella has 2 blades on rotor with 0.3 mm thickness, moreover the gap between blades and housing (shroud, stator wall) is 0.1 mm. According to experiments on animals, no effective hemolysis level was observed.

— Valvo Pump (Keio University & Hokkaido University -Tokyo, JAPAN):

Valvo Pump has 138 gr weight, 40 mm length, 38 mm outer diameter and 40 cc volume. Rotor cylinder has 4 blades that have 22 and 13 mm outer and hub diameter with 0.5 gap clearance. Permanent magnets of brushless EM DC motor were installed into the hub. Valvo Pump can produce 5 L/min under 100 mmHg pressure difference at 7000 rpm. This device needs more than 20 W to produce 5 L/min blood flow. Also, device contains ball bearings to support rotor shaft. Pump operation at optimum operation point (5L/min & 100 mmHg) during 200 min, caused 50 mg/dl plasma free Hb and normalized index of hemoglobin (NIH) was calculated as 0.030 ± 0.003 mg/dl.

— NIVADIII (Shangai-China):

NIVADIII was started to be developed by Zhong and his colleagues in Tongjoi University in 2001. Device was designed as axial flow heart pump and its permanent magnets formed as ring which locates at blade tip and blood flow was provided inside of this ring formation. In 2010, NIVADIII was tested on animals and survival period

more than 93 hours couldn't be obtained because of high hemolysis; hereby device isn't in commercial use yet.

— Heart Turcica (Koc & Yeditepe University, Istanbul-Turkey):

In Turkey, Prof. Dr. Ismail Lazoglu from Koc University and Prof. Dr. Suha Kucukaku from Yeditepe University started a program for developing Heart Turcica I as centrifugal LVAD and aimed to manufacture it in 2009. Although, they visually designed 3D pump geometry and tested via computer based simulations, there is no literature about laboratory dependent experiments until 2011.

- **3rd Generation Pumps:**

— Streamliner (McGowan Center & Pittsburg University):

Streamliner was developed by the McGowan Center for Artificial Organ Development that is a subdivision of Department of Surgery at the Pittsburgh University. James Antaki was the team leader and director for artificial heart research of the McGowan Center. Streamliner has 19 mm blade diameter and can produce 6 L/min blood flow under 100 mmHg pressure difference at 7000 rpm with %28 hydraulic efficiency. Also, it has 5 blades on rotor and 6 blades on diffuser. Rotor is levitated by magnets instead of mechanic bearings. Also, permanent magnets act as radial support for rotor. Magnetic levitation causes less friction than mechanic shaft design, hereby it prevents heating due to friction. According to in-vivo experiments conducted on 87 kg calf during 34 days with average 5.9 L/min flow support and 96 mmHg mean arterial pressure, streamline caused average 7.3 ± 3.9 mg/dl pfHb (NIH = 0.0015 ± 0.0010 mg/dl).

— HeartMate III (Thoratec Corporation -Pleasanton CA, USA):

Thoratec Co. and collaborated universities designed HeartmateIII as a centrifugal pump with magnetically levitated rotor for long-term use. Mass of device is 475 g and pump has been optimized by in vitro testing to achieve design point of 7 L/min blood flow against 135 mmHg at 4500-500 rpm and hydraulic efficiency was observed as 30%.

Furthermore in-vivo tests on calves during 30 to 60 days period, resulted average 4-10 mg/dl pfHb level.

— INCOR (Berlin Heart Group):

Berlin heart group developed INCOR I axial flow pump that has 30 mm diameter, 120 mm length and 200 gr weight. INCOR I can provide 5 L/min blood flow to aorta from LV with 100 mmHg head pressure at 8000 rpm. This device needs 2-4 W power and it also has magnetic bearings for rotor levitation. According to the experiment results of INCOR I, normalized index of hemolysis (NIH) was calculated as 0.006 mg/dl. After acceptable trials, the first clinical implementation was made to two patients that have coronary heart diseases in Berlin Heart Institute in June 2002.

— Terumo DuraHeart (Japonya):

The DuraHeart is an implantable 3rd generation (magnetically levitated) centrifugal heart pump. The device has 72 mm diameter, 45 mm height and 540 gr weight. Magnetic levitation allows impeller to be suspended within fluid volume with contact-free manner. NdFeB type permanent magnets were integrated into rotor component to design brushless Dc motor. The output power of motor is 4.5 W when it rotates around 2000 rpm and exerts 0.0215 N.m torque. Also pump is capable to operate within range 1200-2600 rpm and provide 2-10 L/min blood flow. Titanium material is used to prevent thrombosis formation in pump. Clinical implantations of DuraHeart were started in January 2004, however it only implanted to around 118 patients due to size limitations and some cannula placement difficulties according to data in 2011.

— Levitronix CentriMag (Pharos Corporation, Boston MA):

The Levitronix CentriMag is a continuous-flow, centrifugal-type rotary blood pump that is placed outside the body (extra-corporeally) and aimed to support patient during 2 weeks or longer (short-term use) by being single-use device. The rotating component of device (rotor) was magnetically levitated and it results as lower hemolysis than other pumps. The centrifugal pump design permits rotation of the impeller at speeds of 2500

to 3300 rpm to provide 4 to 6 L/min blood flow. Moreover, it can produce 9.9 L/min blood flow when operating around 5000 rpm.

― HeartWare (HeartWare Corp- Miami, Florida, USA):

The HeartWare HVAD model is a magnetically levitated centrifugal heart pump. Smallest and lightest version of device has 50 mm diameter and 145 gr weight. Device operates within 1800-4000 rpm range and produces up to 10 L/min flow. A ceramic-titanium blood contacting surface is used to reduce thrombosis formation. Clinical trials were started in 2008 and device implanted to more than 700 patients worldwide according to data at 2011.

― DexAide RVD, CorAide LVD-4000 (Cleveland Clinic-Cleveland, OH):

DexAide and CorAide designed by Cleveland Clinic respectively as an implantable centrifugal pump for right and left ventricular support. DexAide RVAD produces 4 L/min flow and 20 mmHg pressure rise at 2000 rpm with 1.9 W power consumption. In vivo studies showed acceptable hemodynamic characteristic.

There are many other attempts to design and produce LVAD or other heart support systems. However, most of them cannot obtain success in the long-terms use because of their hemocompatibility results. Mostly, US of American, German and Japan products are commercially used in hospitals. Rest of the attempts still continues to enhance device to achieve compatibility for human physiology.

1.1.3. Cost

As explained above, most of the commercially used LVAD are manufactured by USA, Japan or Germany. Turkey isn't the only country that hasn't enough research, development and production on LVAD; almost all countries suffer from lack of works on this subject and they have to import these MCSS from developed countries.

Resource Category	Average Cost	% of Total Cost
LVAD	$67,085	48%
Professional paymt	$23,935 ± 10,897	17%
Length of stay		
Special care days	$14,765 ± 10,874	10%
Regular floor	$7,071 ± 7,376	5%
Operating room	$10,818 ± 1,725	8%
Diagnostics	$3,900 ± 3,574	3%
Laboratory	$3,407 ± 1,767	2%
Blood products	$2,873 ± 2,562	2%
Drugs	$3,257 ± 3,229	2%
Miscellaneous	$3,235 ± 1,695	2%
Rehabilitation	$670 ± 423	0%

Table 1.2: Hospitalization Cost of LVAD for Patients

Table 1.2 shows the cost of LVAD including hospitalization, importation and maintenance. Because of technologic level in LVADs, generally one surgery to implant LVAD is around 130.000 USD and this cost increases with special surgery methods or observation period after surgery. Also, un-known stay period in hospital increases cost of treatment. As shown in Table 1.2, the most expensive factor is importation cost of LVAD. So, development on LVAD technologies is most necessary option for offering cheaper and better solutions for patients. When it was considered that around 3000 patients need these devices annually just in Turkey, the high load of importation cost on economies can be better appreciated.

1.1.4. Process to Develop LVAD

LVAD is a turbomachine that creates head pressure and flow by using electrical energy. Brushless electromagnetic DC motor is used to convert electrical energy to mechanical energy as torque and angular velocity to rotate impeller. Rotary component (impeller) in device converts mechanical energy to hydraulic energy as head pressure and flow. So, design process of LVAD basically consists of two main steps: electro-magnetic motor design to produce mechanical energy (required torque and angular velocity) and pump design to satisfy hemodynamic performance and hemocompatibility by using mechanical energy. Actually, computational performance testing of pump geometry will determine required performance of electro-magnetic motor. In addition, bearing for mechanic components, controller unit for consistency with physiology, portable battery unit and cannula to connect device to LV and aorta, should be designed for implantable device.

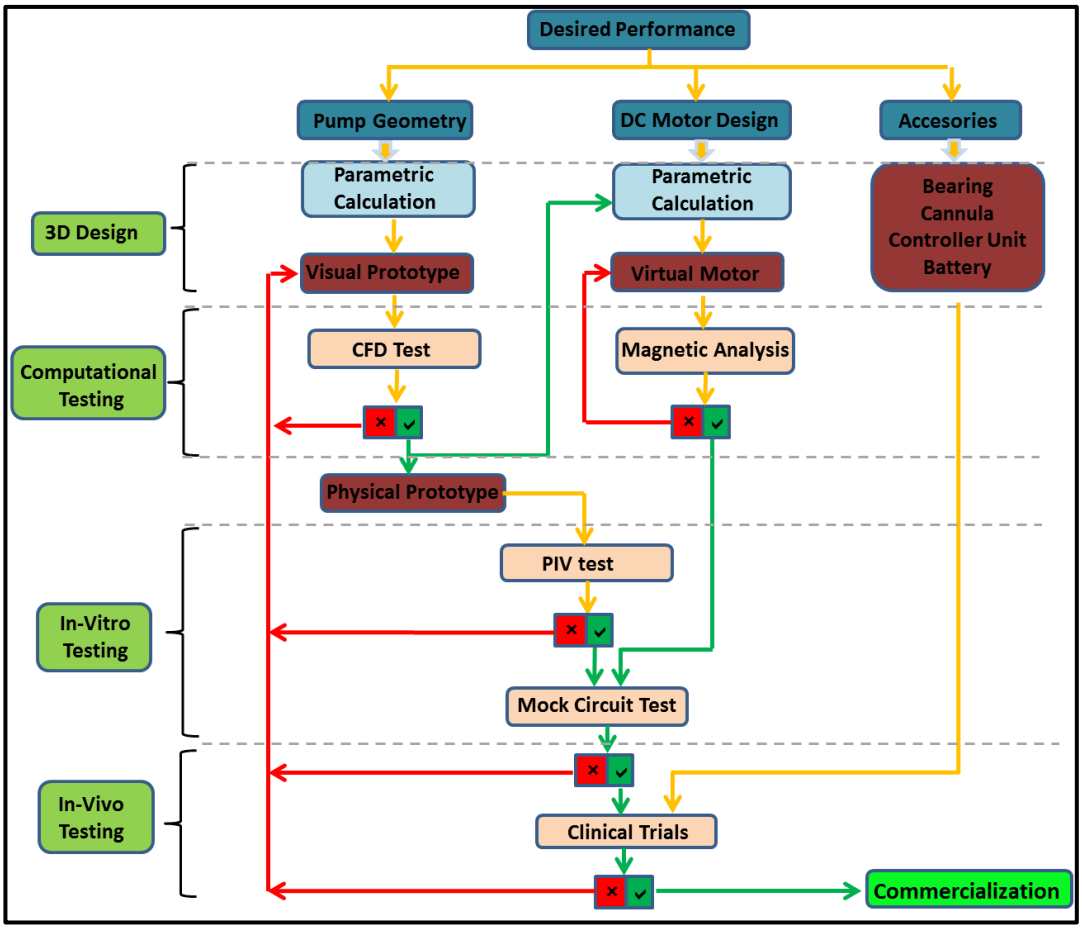

Fig 1.3: R&D Steps of LVAD

Pump geometric design is the first step of LVAD development process from point zero until reaching commercial usage. In first, geometric parameters (blade tip, cross sectional area and blade angles etc.) are calculated by applying turbomachinery principles to satisfy human physiological needs within anatomic constraints. Then, 3D initial pump model is created via computer aided design (CAD) tools depending on parametric analysis and performance of 3D visual model is simulated via computational fluid dynamic (CFD) solvers. According to computational results, deviation from the design criteria is determined and initial 3D visual design is modified to converge simulation results to desired results. This CFD analysis and iterative modification process continues until achieving all hemodynamic and hemocompatibility criteria within anatomic constraints. Then, physical prototype (plastic) can be produced to simulate its performance under real physical conditions.

First, particle image velocimetry (PIV) method is applied to physical prototype to validate CFD results. If there are large differences between computational and physical test results and deviation from the design criteria, 3D visual prototype is modified according to achieve design criteria in real environment. Then, optimization on pump geometry continues until CFD and PIV tests results converge to acceptable results when compared to design criteria.

After completing PIV tests, mock circuit [I] (hydrodynamic simulation mechanism of circulation system) test can be done to see possible physiological effects of device by using metal wear physical prototype (including motor). Moreover, mock circuit test is used to develop controller algorithm for device to provide consistency with pump operation and physiology. However, motor design should be completed before starting mock circuit testing. According to pump hydraulic characteristic determined by CFD and PIV performance tests, required rotational velocity and torque are known and motor parameters such as coil turns and magnet volume are initially calculated. However,

[I] Mock circuit is a hydraulic model of human cardiovascular system. It is used to simulate blood circulation in body by modelling circulation system as reservoirs. For examle, left and right ventricle, pulmonary arteries, aorta artery are some reservoirs and they connected to each other via plastic tubes serving as arteries and veins.

motor design should be computationally tested by using finite element method (FEM) to optimize motor variables.[I] After optimization depending on computational results, motor of device can be tested in mock circuit physical testing.

After all acceptable results of physical testing, laboratory experimentation can be started with animal tests. After observing acceptable hemocompatibility on animal physiology, the LVAD can be tried on human subjects in clinical trials as last step for design.

Some of these steps are performed by companies and some of them are performed by universities and clinics. When universities do the laboratory based research & development steps such as mock circuit and PIV tests, clinics do the biological tests on animals and patients. The company takes the responsibility on most expensive side of the process and does the manufacturing of prototypes and final product. Moreover, educating medical technicians during laboratory based experiments are necessary for clinics and hospitals for the effective implantation and full-capacity usage of devices.

[I] Magnetic field analysis can be performed by some finite element method softwares such as ANSOFT® Maxwell or ANSYS® Magnetostatic.

1.1.5. Gap

As explained above, annually more than 3000 patients just in Turkey are in the waiting list for available donor; however heart transplantation can be done for only 50-60 of them. Rest of the patients have to be supported by mechanically circulation support systems especially LVADs to stay alive. Since most commercially used LVADs are manufactured by corporations from US, Germany or Japan; under-developed countries have to import from these countries to recover patient needs. However importation and maintenance cost for hospitals and hospitalization cost for patient brings high loads on economy. Moreover, countries that don't have research on concerned field, cannot efficiently use LVAD on patients, as these devices should be used by personal that have enough experience with it. So, educating technicians especially by having them to join physical testing and clinical testing process, will help doctors to use device to keep patients alive. Because, joining development process of device and its physical testing will help to know the possible technical problems that can be observed during implantation and immediate intervention to fix them. Moreover, joining clinical experiences will help the personal to know possible physiologic effects of devices during its usage.

So, under-developed countries also have to develop LVADs to remove economic loads and recover patients' needs by providing device and technical personal sophisticated on concerned field. However, these medical devices should be developed according to international medical standards for commercial use. Fig 1.3 explains the way to develop LVAD from point zero to commercial use. These researches and development steps require high investment and only can be recovered by high collaboration that includes universities, clinics and companies. So, if this collaboration can be provided by under-developed countries, they have a chance to develop their own LVADs for commercial use. In Turkey, until 2010 academic group from Koc and Yeditepe University has completed a centrifugal pump development process steps that include computer based fluid dynamic simulations (CFD step). However they couldn't start physical testing on real prototype. So, In Turkey there are attempts to developing LVAD, however there are still missing steps to complete device design such as physical testing (PIV and mock circuit tests) and clinical testing (animal and human tests).

1.1.6. Project Field

A research group from Bahcesehir University started a program to develop axial flow LVAD to fill these missing steps in Turkey and reach commercially used product. This program includes all steps in Fig 1.3, until now small projects such as develop mock circuit for physical tests and attempts to provide hardware for PIV tests and research lab for animal tests as beginning of R&D program for device. The present Master Thesis is a sub-project of axial flow LVAD development program and starts from point zero.

This project includes;

- Literature search on devices,
- Parametric calculation for initial LVAD design
- Initial 3D design via SolidWorks (CAD tool),[I]
- Computational fluid dynamic analysis on 3D visual prototype via ANSYS Fluent[II]
- Optimization on visual prototype to achieve all design criteria (hemodynamic and hemocompatibility within anatomic constraints) by iteratively repeating 3D visual design and CFD testing,
- Virtual motor design and performance analysis via FEM based electro-magnetic solvers [III]
- Optimization on motor design to achieve required mechanical performance in terms of device hemodynamics

This project aims to develop LVAD prototype that achieves all hemodynamic and hemocompatibility criteria within anatomic constraints on computer based performance results (CFD analysis). After completion of this project, physical prototype will be produced without active motor part and will be prepared for PIV physical testing. So, as shown in Fig 1.4, this project only covers R&D process of LVAD from beginning to PIV performance testing that is first physical testing of device to validate computer based performance results.

[I] Dassault Systèmes SolidWorks Corp.®: Waltham, Massachusetts, USA
[II] ANSYS Inc.- ANSYS® Fluent- Canonsburg,Pennsylvania,USA
[III] ANSYS Inc. - ANSOFT® Maxwell - Canonsburg,Pennsylvania,USA

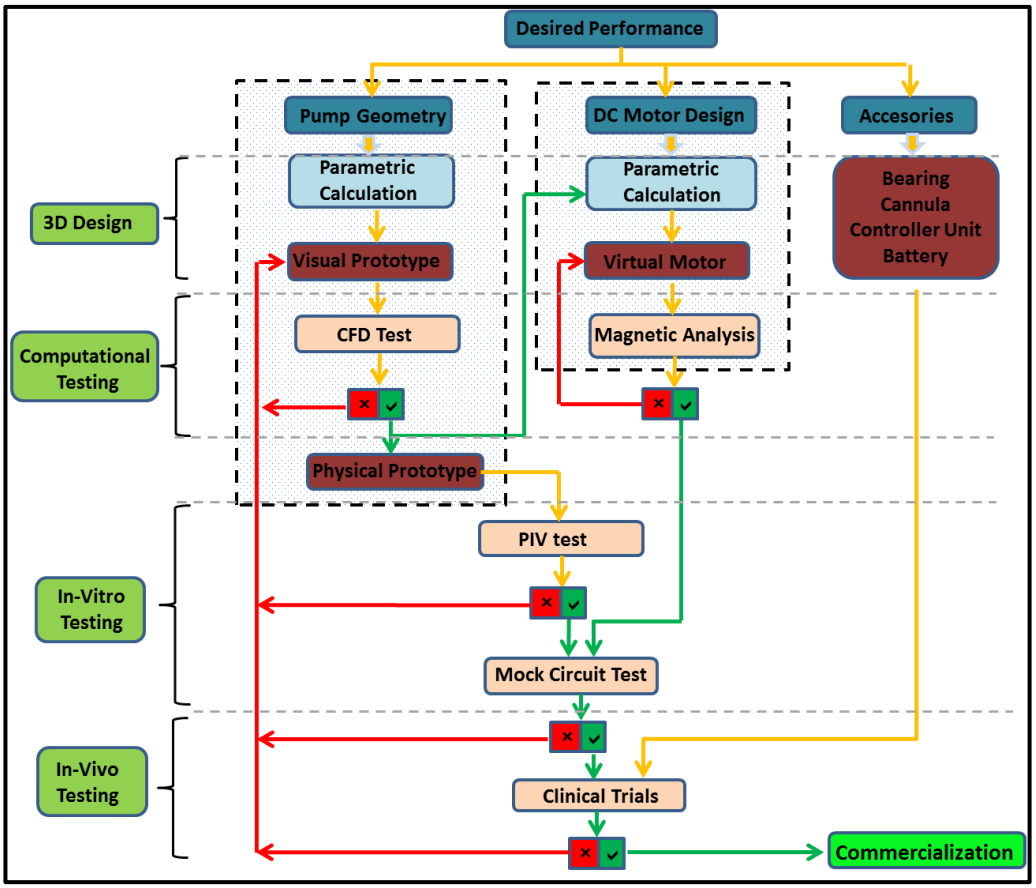

Fig 1.4: R&D Steps of LVAD. Dashed Boxes Indicate the Subject-Matter of the Present Thesis.

Furthermore, after successful results of this project, there are many important steps to manufacture LVAD for commercial use and also there are attempts to go further. These attempts will be explained in discussion and future works section.

1.1.7. Design Criteria

Device	Weight (gr)	Volume (cc)	Diameter (mm)	Length (mm)	Power (Watt)	Flow (L/min)	Rpm*10^3	Magnet Location	NIH (mg/dl)*10^{-3}
Hemopump	6	5	8,1	16	-	4,5	17-26	-	NH
Jarvik2000	85	25	25,0	55	10	2,0-7,0	8-12	Hub	0,82 ± 0,54
IVAP	170	-	13,5	-	8	8,0	13	-	NH
DeBakey	95	15	25,0	75	10	5,0-6,0	10	Blade	< 0,20 ± 0,00
HeartMateII	375	62	40,0	60	10	3,0-4,0	8-9	Hub	NH
Impella	5	2	6,4	60	12	7,0	30	-	NH
Valvo	138	40	38,0	40	> 20	5,0	7	Hub	30,00 ± 3,00
Streamliner	-	-	>19,0	-	-	6,0	7	-	1,50 ± 1,00
INCOR I	200	-	30,0	120	3	5,0	8	-	6,00 ± 0,00

Table 1.3: Axial-Flow Pumps and Specifications (at 100 mmHg pressure rise). NH = Not Harmful pfHb Level.

As summarized in Table 1.3, although each device has its own technical specifications (dimensions, weight, volume) and operation characteristic, all were developed to achieve the same purpose, which is supporting human circulation system by pumping blood from LV to aorta in terms of physiological needs. Moreover, achieving this aim isn't enough to use these devices in human body, also it should be compatible with physiology, i.e. means it shouldn't have negative effects on body. In short, LVAD should be designed to achieve hemodynamic performance to support patient by satisfying hemocompatibility (no negative effects on physiology).

As seen from Table 1.3, heart pumps were commonly designed to provide blood flow up to 10 L/min for adults under 80-120 mmHg pressure difference between LV and aorta. This hemodynamic performance can be achieved with high rotational velocities (around 7000-13000 rpm) because of small device sizes. This high rotation of impeller increases shear stress exerts on red blood cells (RBCs) and it results as demolishment of RBCs, named hemolysis.[I] Mostly RBCs are demolished in pump at inlet and outlet

[I] RBCs are generally 6-8 μm in diameter and have 2.2 μm thickness. Their average volume and surface area are 92 μm^3 and 140 μm^2 respectively.

section where fluid accelerates or decelerates instantly. When RBCs membrane tears, hemoglobin is released into the blood plasma (plasma free hemoglobin, pfHb).

Hemoglobin content of the blood is 150 g/L for a healthy person. It is reported that renal threshold in man for hemoglobin is above 150 mg% and if it exceeds, kidney excretes Hb into the urine. Normal renal function allows purify blood from doses up to 14 g of plasma free Hb in 24 hour. So, increase rate of pfHb level should be less than 583 mg/hour for kidney function capacity. In short, acceptable hemolysis for device hemocompatibility can be defined to not causing accumulation of pfHb in blood and it can be observed by evaluating concentration and increment rate of pfHb. However, pfHb accumulation in blood depends on supporting period, volumetric flow rate and head pressure. Hereby, American Society for Testing and Materials (ASTM) standardized hemolysis effect of different heart pumps into normalized index of hemoglobin (NIH) that is calculated under same operating conditions (5 L/min flow under 100 mmHg pressure rise during 6 hour). So, NIH value of device should be less than threshold defined by ASTM to satisfy international standards.

Evaluating parameters of both increment level of pfHb and NIH, can be evaluated only by taking samples from real blood and isn't calculable with mathematical methods. However, this project only covers computationally performance testing of LVAD and most of the works are conducted in computers. So, some predictions on pfHb should be done to define hemocompatibility of device during virtual design and testing process instead of actually evaluating them with in-vivo or in-vitro tests.[I] There is no accurate mathematical model of RBC damage occurred in heart pump, however it empirically determined that magnitude and duration of stress exerted on cells determine RBC damage. Shear stress and exposure time are two parameters used to empirically determine pfHb. According to studies, RBCs start to explode under shear stress larger than 100 pa without depending on time. Furthermore shear stress up to 500 pa is acceptable on RBCs, if exposure time isn't longer than 100 ms. Although two

[I] Computational estimations only acceptable for comparision between prototypes and optimization process in virtual domain. After starting physical tests, actual values should be evaluated from samples of real blood and then optimization should be re-performed according to real results to achieve hemocompatibility.

parameters can be used in some predictions on hemolysis, it doesn't gives exact damage factor on RBCs. Empirical formula that was used by Behbahani et al, gives numerical estimation of pump damage by calculating pfHb from stress tensor and exposure time. This model still doesn't provide accurate results on hemolysis, however it is the best in computational evaluations with current technology.

Previous pump design experience indicates that excessive hemolysis happens where backflow occurs. The reason of backflow is non-smooth contact of fluid and impeller and it creates vortex region in flow field. These vortex regions increase residence time of RBCs in pump and longer duration causes more pfHb. So eliminating vortex by minimizing backflow is also one of the design requirements to enhance hemocompatibility of pump. Backflow in flow field cannot be totally eliminated, but there were some attempts to minimize it. Anderson et al. reduced total percentage backflow to % 16 by changing blade clearance of CFVAD3 prototype (Centrifugal Pump). Then, Chua et al. calculated percentage leakage flow as %16 at blade tip clearance in axial flow pump prototype made by Nanyang Technological University. It is known that both devices aren't in commercial use, so at least it is concluded that acceptable backflow shouldn't be greater than %16 for commercial product that satisfies medical standards. Actually, backflow should be reduced as much as possible for enhancing flow lines; however indirect relationship with hemolysis limits optimization of device according to backflow with computational methods. So, threshold value for acceptable percentage backflow was reduced to %10 as a challenge in this project in order to pass in-vitro tests to evaluate hemolysis.

A second negative effect of pump on blood is coagulation. It is known that, coagulation occurs where blood flow gets stagnant. According to accumulated design experiences, most coagulation occurs at bearing section of pump where velocity gets lower. So bearing selection is the most important factor to eliminate coagulation, but also coagulation can be observed in pump where blade geometry causes low velocity field.

Furthermore, LVADs are implanted into the body, so device should be designed according to anatomic constraints to be suitable for in body use. As seen from the Table 1.3, these devices commonly have up to 30 mm in diameter and 100 mm in length.

Moreover, when we consider that patient carries these devices into their bodies during long-term support, device should be lighter. So, device weight shouldn't exceed 300 gr for portability. Also, other factor that effects portability, is size of device battery. Batteries locate at outside of body and provide power to run device via cable that gets into the body through the skin. Size of battery directly depends on power need and it is mainly determined by hydraulic efficiency of pump. So, maximizing pump efficiency (hydraulic, magnetic, mechanical and electrical) is also better option to provide lighter battery i.e. portability. Shortly, LVAD should achieve:

Hemodynamic Performance

- *Head pressure (ΔP) :* $80 < \Delta P < 120$ *mmHg*
- *Blood Flow (Q) :* $1 < Q < 10$ *L/min*

Hemocompatibility Criteria

- *Rate of Plasma Free Hemoglobin ($\Delta pfHb$)* $\Delta pfHb < 583$ *mg/h*
  - Exposure time (t_s) t_s < 100 ms
  - Shear Stress (σ) σ_{ss} < 500 Pa
  - Backflow (BF) BF < %10

- *Coagulation* *Not Tolerated*
  - Stagnation Not Tolerated

Anatomic Constraints

- *Portability* *Required*
  - Length (l) l < 100 mm
  - Width (w) w < 30 mm
  - Weight (h) h < 300 gr

2. METHODS

As known from the literature search, all of the heart pumps (LVAD, RVAD, BiVAD or TAH) are designed to provide blood flow against the pressure difference between the corresponding tissues. On the other hand, they pump blood from heart (LV or RV) to aorta or pulmonary artery. Rotary heart pumps of both centrifugal and axial flow type, achieve this performance by accelerating blood by converting mechanical energy (speed and torque) to hydraulic energy (flow and pressure rise). In short, rotary heart pumps are small turbomachines that support dysfunctional heart by pumping blood. So, firstly turbomachine principles should be studied to understand physics of pumping blood via rotational machines.

2.1. INITIAL DESIGN:

2.1.1. Pump Design (Axial-Flow Pump)

In this project, axial flow heart pump was aimed to develop to pump blood from LV to aorta. Although both rotational pumps have same principles, they include different components that effect hydrodynamic performance and require different design procedure.

Axial-flow blood pumps consist of 3 main components that direct blood flow, one is rotary and the others are stationary blades. Three blade sets should be designed according to their performance requirements. These blade sets (inducer, rotor and diffuser) can be considered as two dimensional cascades to analyze hydraulic performance in theory. Cascade performance analysis starts with velocity triangle that formulates flow direction and magnitude (velocity vectors) in terms of blade parameters such as inlet and outlet vane (attack and trailing) angles and dimensions. Then, velocity vectors can be used to calculate kinetic energy and potential energy rise of fluid. On the other hand, it gives hydraulic performance of turbomachine. Then, resultant hydraulic performance gives individual and overall efficiency of stages (each cascade or each blade sets).

2.1.1.1) Velocity Triangles

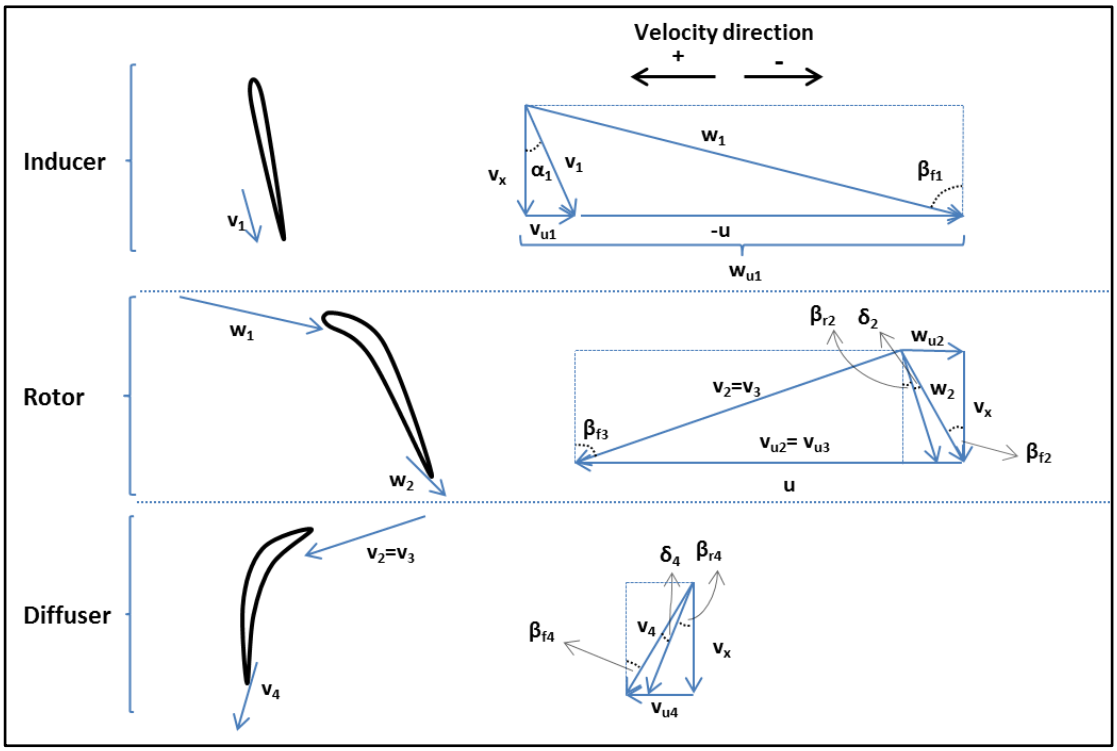

Fig 2.1: Velocity Vector Diagrams of Blade Stages

Inducer blades lead blood flow parallel to its blades, so inducer trailing angle (α_1)[I] creates tangential component of absolute velocity at rotor inlet(v_{u1}).

$$v_{u1} = -v_x tan(\alpha_1) \qquad \textbf{Eq 2.1}$$

Where the minus sign accounts for the direction of velocity with respect to the tangential velocity (u) of rotor blade at the medial plane [II], such that

$$u = \omega\, r_m \qquad \textbf{Eq 2.2}$$

Where ω is rotor angular velocity in radian per second (rps) and r_m is the rotor radius at the median plane in meter. Also in Eq 2.1, axial velocity of fluid (v_x) can be formulated as

[I] α_1 is positive if inducer blade is twisted at –u direction (opposite to rotation direction).
[II] Some turbomachinery books formulate tangential velocity (u) at tip plane or they are using another approach to determine radial distance for calculations.

$$v_x = \frac{Q}{A_c} \qquad \textbf{Eq 2.3}$$

Where Q is volumetric flow rate in m^3 per second and A_c is cross sectional flow area of pump in m^2. Tangential component of the fluid velocity at rotor inlet relative to rotor blades (w_{u1}) is given by:

$$w_{u1} = v_{u1} - u \qquad \textbf{Eq 2.4}$$

Fluid enters to rotor blades with attack angle β_{f1} (angle between velocity vector of w_{u1} and rotation axis) relative to the rotary blades,

$$\beta_{f1} = tan^{-1}\left(-\frac{w_{u1}}{v_x}\right)$$
$$\beta_{f1} = tan^{-1}\left(\frac{u}{v_x} + tan(\alpha_1)\right) \qquad \textbf{Eq 2.5}$$

Fluid exits from the rotary frame parallel to its blades in theory, however experiments shows that fluid differs from this action. Deviation between actual flow and blade metal angle at rotor outlet is described with deviation angle(δ_2) that is generally estimated from empirical models. Relative fluid angle at rotor outlet (β_{f2}, angle between w_{u2} and rotation axis) is a function of blade metal angle (β_{b2}) and deviation angle(δ_2).[I]

$$\beta_{f2} = \beta_{b2} + \delta_2 \qquad \textbf{Eq 2.6}$$

Tangential component of fluid at rotor outlet relative to rotor blade (w_{u2}) is calculated from:

$$w_{u2} = -v_x\, tan(\beta_{f2}) \qquad \textbf{Eq 2.7}$$

Absolute fluid velocity at rotor exit (v_{u2}) is,

$$v_{u2} = u + w_{u2} \qquad \textbf{Eq 2.8}$$

[I] β_{b2} and δ_2 are positive if blade twisted in $-u$ direction

$$v_{u2} = u - v_x \tan(\beta_{f2})$$

Applying the same procedure to the stationary diffuser section, and assuming no loss in tangential component of the fluid velocity between the rotor and diffuser ($v_{u3} = v_{u2}$), fluid attack angle to diffuser (β_{f3}, angle between v_{u3} and rotation axis) can be evaluated from [I],

$$\beta_{f3} = \tan^{-1}\left(\frac{v_{u3}}{v_x}\right)$$

$$\beta_{f3} = \tan^{-1}\left(\frac{u}{v_x} - \tan(\beta_{f2})\right) \quad \textbf{Eq 2.9}$$

Fluid exit from the diffuser according to outlet angle of diffuser (trailing, β_{b4}), however it doesn't exit totally parallel to the blade because of deviation. Deviation at diffuser outlet was defined as δ_4.[II] So, fluid exits from diffuser with angle, β_{f4} (angle between v_{u4} and rotation axis).

$$\beta_{f4} = \beta_{b4} + \delta_4 \quad \textbf{Eq 2.10}$$

The tangential component of absolute fluid velocity (v_{u4}) at diffuser exit is

$$v_{u4} = v_x \tan(\beta_{f4}) \quad \textbf{Eq 2.11}$$

As seen from Eq 2.8 and Eq 2.11, absolute velocity of fluid increases at rotor outlet (v_{u2}) and decreases at diffuser outlet (v_{u4}). That means fluid accelerates through rotor and decelerates through diffuser. On the other hand, blood gains kinetic energy through rotor and loses kinetic energy through diffuser. Decrement on kinetic energy generates potential energy rise as increment on static pressure. Angular momentum change i.e. absolute velocity change between two points, can be used to calculate exerted force at this stage. Velocity change through inlet and outlet is equal to change in tangential fluid

[I] Fluid attack angles are calculated from relative velocity. However relative to blade equals to absolute velocity in stationary frames. So, absolute velocity is used if blades are stationary.
[II] β_{b4} and δ_4 angles are positive if blade twisted in + u direction.

velocity across this stage(Δv_u) if cross sectional flow area is uniform (axial velocity of flow doesn't changes).

$$\Delta v_u = v_{uo} - v_{ui} \qquad \textbf{Eq 2.12}$$

where the subscripts "o" and "i" define the outlet and inlet point of a frame, respectively. If absolute tangential velocities at inlet and outlet of both stages are substituted in Eq 2.12, change in velocity across concerned stage becomes,

$$\begin{aligned} \Delta v_{ur} &= u + v_x \left(tan(\alpha_1) - tan(\beta_{f2})\right) \\ \Delta v_{ud} &= v_x \left(tan(\beta_{f4}) + tan(\beta_{f2})\right) - u \end{aligned} \qquad \textbf{Eq 2.13}$$

where the subscripts "r" and "d" define the rotor and diffuser blade stage, respectively.

As seen from velocity triangle formulas, velocity change across blade stage is a function of axial velocity of fluid (v_x), linear velocity of rotary blade (u) and trailing angle of all blades ($\alpha_1, \beta_{b2}, \beta_{b4}$). Trailing edge design of blade can be done by calculating effects on kinetic energy rise through blade stage via these formulas. However, blades attack edges (β_{b1}, β_{b3}) effects cannot be observed via formulas above. These angles should be designed directly according to attack angles of fluid (β_{f1}, β_{f3}). Eq 2.5 and Eq 2.9, specify attack angle of fluid at rotor and diffuser inlet respectively. Moreover its known that difference (incidence) between fluid $(\beta_{f1})$and blade attack angle (β_{b1}) exists to provide smoother contact between flow and blade attack edge. Greater or less incidence can reduce quality of flow field and may cause backflow. So, incidence angle is an optimum angle value for blade attack edge design to provide less backflow and better hemodynamic performance.

$$\begin{aligned} \beta_{b1} &= \beta_{f1} - \theta_r \\ \beta_{b3} &= \beta_{f3} - \theta_d \end{aligned} \qquad \textbf{Eq 2.14}$$

$\theta_r$and θ_d are incidence angles for rotor and diffuser inlet edge and can be specified after computational or experimental tests, because there is no physical formula to define it.

Mean fluid angle, β_m, across any stage is defined by depending on relative flow angle at inlet (β_{fi}) and outlet (β_{fo}) of that stage.

$$\beta_m = tan^{-1}\left(\frac{tan(\beta_{fi}) + tan(\beta_{fo})}{2}\right) \quad \textbf{Eq 2.15}$$

When, fluid angles according to selected stage, are substituted formula above; mean fluid angle for rotor (β_{mr}) and diffuser (β_{md}) become,

$$tan\,(\beta_{mr}) = \frac{1}{2}\left(\frac{u}{v_x} + tan(\alpha_1) + tan(\beta_{f2})\right)$$
$$tan\,(\beta_{md}) = \frac{1}{2}\left(\frac{u}{v_x} + tan(\beta_{f4}) - tan(\beta_{f2})\right) \quad \textbf{Eq 2.16}$$

Mean velocity of fluid (v_m) at any stage is defined as

$$v_m = \frac{v_x}{cos(\beta_m)} \quad \textbf{Eq 2.17}$$

After trigonometric substitutions, v_m becomes,

$$v_m = v_x\sqrt{(tan\,(\beta_m))^2 + 1} \quad \textbf{Eq 2.18}$$

2.1.1.2) Momentum Equation

According to most fundamental principles in mechanics (Newton's second law of motion), sum of the external forces acting on fluid by rotary blades accelerates fluid at rate of change in fluid momentum in force direction.

$$\sum F = \frac{d}{dt}(m\, v) \qquad \textbf{Eq 2.19}$$

If rotary machine cross sectional flow area is uniform through stage and fluid is incompressible, there is no chance at axial velocity of fluid at inlet and outlet of a stage. So, only tangential component of external force[I] (described as Y directional force) effects angular momentum change of fluid. So, equation above gives steady flow momentum equation (acceleration term, $\dot{v}$ neglected) such that

$$F_y = \dot{m}\, \Delta v_u \qquad \textbf{Eq 2.20}$$

Where $\dot{m}$ is mass flow rate in kg/s and can be specified in terms of volumetric flow rate ($Q, m^3/s$) and fluid density ($\rho, kg/m^3$) [II] as $\dot{m} = \rho\, Q$. External energy transfer only occurs at rotational frame and tangential force exerted by rotational stage is referred to applied torque. So, Eq 2.20 becomes

$$T = \rho\, Q\, r_m\, \Delta v_{ur} \qquad \textbf{Eq 2.21}$$

Where T is torque in *N.m* and $r_m$is radius of blades at medial plane in *m*. If Δv_{ur} is substituted into the torque equation, required torque for desired hemodynamic performance can be formulated in terms of flow rate and blade linear velocity (u):

$$T = Q^2\, \frac{\rho\, r_m}{A_c} \left(tan(\alpha_1) - tan\left(\beta_{f2}\right)\right) + Q(\rho u\, r_m) \qquad \textbf{Eq 2.22}$$

[I] Force is exerted by blade to fluid in rotary stage or reacted by fluid to blade in stationary stage. Just sign of force changes depending on stage.
[II] Density of blood is 1050 kg/m^3 at 37 C^0.

Required torque formulated above is the input of hydraulic system, also output torque of mechanical system i.e. torque load (T_l). Moreover, motor and electronic circuit designer should consider that, system should work against mechanical losses such as inertial and frictional losses in order to produce this torque. So, torque generated by motor isn't equal to T_l, which is input of hydraulic system.

2.1.1.3) The Euler Work Equation

According to energy conservation, input energy is transferred to hydraulic system at rate of hydraulic efficiency. Hydraulic system output is defined as

$$W_{out} = \eta_h W_{in} \quad \textbf{Eq 2.23}$$

$$\Delta H\, Q = \eta_h T\, \omega \quad \textbf{Eq 2.24}$$

Where ΔH is total pressure rise in Pascal and ω is angular velocity in radian per second. If we assume no hydraulic loss through blade ($\eta_h = 1$), output becomes ideal total pressure rise(ΔH_i). Eq 2.21 was substituted instead of torque in Eq 2.24. So, Euler work equation was formed to formulate ideal total pressure rise of system.

$$\Delta H_i = \rho\, u\, \Delta v_{ur} \quad \textbf{Eq 2.25}$$

Note that, u (blade linear velocity) equals to zero for stationary blade; so it proves that no external energy transfer occurs across stationary blades.[I] Furthermore, It is important that ΔH (total pressure rise) includes both energy increase such that kinetic and potential i.e. dynamic and static pressure respectively. In order to separate energy levels, Bernoulli and kinetic energy equations should be derived for both stages individually.[II] If we substitute Δv_{ur} into the Euler work equation (Eq 2.25), external energy transfer across rotor blade can be derived by depending on flow rate and blade linear velocity:

$$\Delta H_i = u^2\rho + u\left(\frac{\rho\, Q}{A_c}\left(tan(\alpha_1) - tan\left(\beta_{f2}\right)\right)\right) \quad \textbf{Eq 2.26}$$

[I] There is no external energy transfer across diffuser blades. $\left(\Delta H_{diffuser} = 0\right)$
[II] For details look "APPENDIX A - APPLYING BERNOULLI EQUATION TO BOTH STAGE- P:133"

2.1.1.4) Rotational Speed

LVADs operate to achieve exact hemodynamic performance as physiologic need explained in "*1.1.7.Design Criteria-P:24*". So, Torque (T) and angular velocity$(\omega)$of pump should be formulated as a function of hydraulic outputs (ΔH and Q) for blade and motor design to obtain the desired hemodynamic performance. Eq 2.22 already formulated torque depending on hydraulic outputs. Eq 2.26 was modified as 2nd order polynomial of blade linear velocity, u.[I]

$$u^2 + u\left(\frac{Q}{A_c}\left(tan(\alpha_1) - tan(\beta_{f2})\right)\right) - \frac{\Delta H}{\eta_h\,\rho} = 0 \qquad \textbf{Eq 2.27}$$

where η_h is the overall pump efficiency. Roots of the above polynomial are evaluated to calculate blade linear velocity for the desired hemodynamic performance $(\Delta H\ \&\ Q)$. Then by selecting pump size (r_m), angular velocity of impeller (ω) can be calculated to select motor parameters. It should be noted that the calculation process is iterative since η_h is initially unknown and should be obtained from the CFD results.

2.1.1.5) Force on Blades

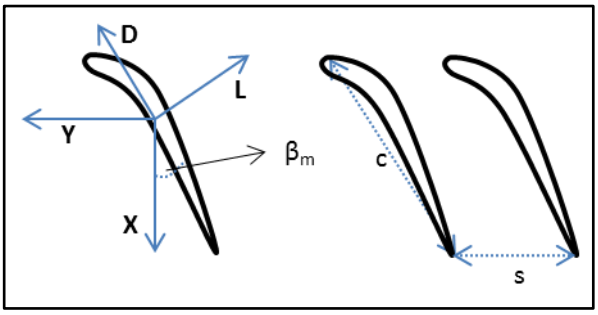

Fig 2.2: Force Diagrams on Blade at Left and Blade Geometric Parameters at Right

In Fig 2.2, X and Y represents axial and tangential force exerted on fluid at unit depth of blade. Axial force exerted on the fluid causes an increase in the static pressures (ΔP) of both the stationary and rotary frames, because there is no kinetic energy transfer at axial direction due to uniform axial velocity profile.

[I] However, it is better to use linear velocity (u) instead of angular velocity(ω) for geometric design; because u removes geometric parameters from Euler work equation (Eq 2.26) by recalling $u = \omega\, r_m$.

$$X = s\,\Delta P \qquad \textbf{Eq 2.28}$$

where, ΔP is static pressure rise (Pascal) across inlet and outlet of blade and s is the space between adjacent blades in the axial direction (meter).

By contrast, in the tangential direction, the dynamic pressure of the fluid is increased in the rotary frame only, where tangential forces (Y_r) exerted on the fluid can increase the tangential fluid velocity. Whereas in the stationary diffuser blades, where such kinetic energy transfer cannot occur (as formulated above, Δv_{ud} has negative value, so kinetic energy decreases), tangential forces (Y_d) become reactive due to the interaction between the moving flow and the stationary blade. Specifically, Y_r is in the same direction as Δv_{ur}, whereas Y_d is in the direction opposite to Δv_{ud}. Letting k represents the direction of tangential force (Y) according to which frame is selected and k=+1 and -1 respectively for rotor and diffuser stage calculations to define magnitude of force.

$$Y = s\,k\,\rho\,v_x\,\Delta v_u \qquad \textbf{Eq 2.29}$$

In Fig 2.2, D and L are the reaction forces exerted by fluid to blade respectively parallel and perpendicular to the mean velocity vector. These forces exert to blade with angle of β_m to rotation axes. From trigonometric relations, drag force exerted (D) by fluid can be derived as a function of tangential (Y) and axial force (X) by blade for any frame.

$$D = Y\sin(\beta_m) - X\cos(\beta_m) \qquad \textbf{Eq 2.30}$$

This formula can be modified to find axial force (X) exerted on fluid to formulate static pressure rise (ΔP) across blade stage.

$$X = Y\tan(\beta_m) - \frac{D}{\cos(\beta_m)} \qquad \textbf{Eq 2.31}$$

Drag force exerted by fluid (D)cannot be evaluated in theory, so there are empirical formulas were derived after physical tests, to model drag force characteristic of cascades. After many studies, drag force exerted on cascade was empirically formulated by depending on drag coefficient (C_D) of used cascade.

$$D = C_D \frac{\rho\, c}{2} \frac{{v_x}^2}{\cos(\beta_m)^2} \qquad \textbf{Eq 2.32}$$

where c is the chord length of blade in meter. Generally drag coefficients are predetermined constants with experiments on specially designed cascades. However, there is no specified drag constant for helical blades used in axial flow heart pumps. So, C_D brings unknown to evaluate static pressure rise through system. C_D can be numerically determined by CFD analysis or physical testing to add it to literature.

2.1.1.6) Pressure Rise (Static and Dynamic)

By substituting Eq 2.28, Eq 2.29 and Eq 2.32 into Eq 2.31, static pressure rise across any blade (ΔP) set can be formulated as

$$\Delta P = k\, \rho\, v_x\, \Delta v_u \tan(\beta_m) - \frac{\rho\, C_D\, \sigma\, {v_x}^2}{2\cos(\beta_m)^3} \qquad \textbf{Eq 2.33}$$

Where σ is solidity of a blade, space-chord ratio ($\sigma = {}^{c}/_{s}$), or the rate of total area of pressure surface in any blade stage and flow cross sectional area.

The dynamic pressure rise (kinetic energy, ΔKE) across the blade set is equal to the difference between the squares of absolute velocities at inlet and outlet of the respective blade stage. However, it is assumed that cross sectional flow area is uniform through all stages and fluid is incompressible, so axial velocity of fluid is assumed as uniform through all pump ($v_{xo} = v_{xi}$). Kinetic energy chance of fluid for any stage can be expressed as below,

$$\Delta KE = \rho\, \frac{({v_{uo}}^2 - {v_{ui}}^2)}{2} \qquad \textbf{Eq 2.34}$$

Bernoulli equation defines external energy transfer through any stage as

$$\Delta H_i = \Delta P + \Delta KE + h_{loss} \quad \textbf{Eq 2.35}$$

Where sum of static and dynamic pressure rise is the transferred energy to fluid $(\Delta P + \Delta KE)$ or the output energy and h_{loss} represents pressure losses through the blade. Ideal total pressure rise through rotary blade is known from Eq 2.25 and it is known that there is no external energy transfer through diffuser blades $(\Delta H_d = 0)$. By substituting static pressure rise and kinetic energy with formulas from velocity triangle, h_{loss} for any blade set can be expressed as below, [I]

$$h_{loss} = \frac{\rho\, C_D\, \sigma\, {v_x}^2}{2\cos(\beta_m)^3} \quad \textbf{Eq 2.36}$$

So, it's clear that pressure loss through any blade set is a function of drag coefficient (C_D) and solidity(σ) constants of blade. So, blade selection is important to increase hydraulic efficiency of pump. As said before, there is no numerical result in the literature about C_D of helical or screw type blades that are generally used in axial flow heart pumps.

2.1.1.7) Efficiency and Optimal Flow Rate

Efficiency of pump directly related to the pressure losses through pump stages. Overall pump pressure losses can be formulated by considering all stages together, so pressure loss for all stages should be calculated individually and sum of them gives total pressure losses through pump.[II]

$$h_{loss-total} = \frac{\rho\, C_{Dr}\, \sigma_r\, {v_x}^2}{2\cos(\beta_{mr})^3} + \frac{\rho\, C_{Dd}\, \sigma_d\, {v_x}^2}{2\cos(\beta_{md})^3} \quad \textbf{Eq 2.37}$$

Overall efficiency of pump can be expressed from rate of pressure losses and ideal total pressure rise (output/input).

[I] For proof, look "APPENDIX A- A.1 APPLYING BERNOULLI EQUATION TO BOTH STAGE- P:133"
[II] Pressure losses through inducer blades were neglected.

$$\eta_h = 1 - \frac{h_{loss}}{\Delta H_i} \qquad \textbf{Eq 2.38}$$

Also overall pump ideal pressure rise is equal to rotor stage because there is no external energy transfer through diffuser section. So, by substituting Eq 2.26 and Eq 2.37 into Eq 2.38, overall hydraulic efficiency becomes,[I]

$$\eta_h = 1 - \frac{\left(\frac{{v_x}^2}{2}\right)\left(\frac{C_{Dr}\,\sigma_r}{\cos(\beta_{mr})^3} + \frac{C_{Dd}\,\sigma_d}{\cos(\beta_{md})^3}\right)}{u^2 + u\,v_x\left(tan(\alpha_1) - tan\left(\beta_{f2}\right)\right)} \qquad \textbf{Eq 2.39}$$

Another important design consideration, stemming from the need for lighter and smaller batteries, is the maximization of power efficiency. This condition is satisfied by,

- increasing the absolute value of overall pump efficiency,
- shifting peak of efficiency curve (η_{max}) to desired operational flow rate determined in terms of human physiology,
- having as flat efficiency curve as possible to providing wide range of pump flow spectrum that yields efficiency close to maximum.

These methods mostly reduce overall power consumption of pump and results as possibility to use smaller batteries. As obviously seen from Eq 2.39, peak of hydraulic efficiency is directly affected by drag coefficient (C_D) and blade solidity (σ). Although solidity already formulated and evaluated from 3D CAD softwares, there is no empirical formula for helical or screw type blades commonly used in axial flow heart pumps. So, this option only can be achieved by using computational simulation methods.

Second option to increase overall pump efficiency can be achieved by some modifications on pump. In order to find flow rate that gives maximum efficiency $(Q@\eta_{max})$ point on operation curve of pump, firstly derivative of efficiency formula according to flow rate $\left(\frac{d\eta_h}{dQ}\right)$ should be formulated. The flow rate (Q) that makes

[I] For proof, look APPENDIX A- A.2 HYDRAULIC EFFICIENCY- P:136

derivative of efficiency zero, can be evaluated by finding roots of $\frac{d\eta_h}{dQ}$. This flow rate is optimal flow rate of current design, $Q(\eta_{max})$ (flow rate at peak of efficiency curve (η_{max})). Then, derived formula can be used to see pump parameters that effect pump optimal flow rate ($Q(\eta_{max})$ or roots of $\frac{d\eta_h}{dQ}$). These parameters can be modified to matching optimal operation flow rate of the pump to desired flow rate to reduce power consumption.

So, after taking derivative of η_h and reformulating with a condition of $\frac{d\eta_h}{dQ} = 0$, following equivalence was observed,[I]

$$0 = \sum_{k=0}^{8} \left(Q^{(8-k)} (u\, A_c)^k \left(P_{d\,(9-k)} - P_{r\,(9-k)} \left(\frac{C_{Dr}\, \sigma_r}{C_{Dd}\, \sigma_d} \right)^2 \right) \right) \qquad \textbf{Eq 2.40}$$

Where P_r & P_d is a 1x9 matrix and conditional function of another matrix P that defined as:

$$P \xrightarrow{N=tan(\alpha_1)+tan(\beta_{f2})} P_r$$

$$P \xrightarrow{N=tan(\beta_{f4})-tan(\beta_{f2})} P_d$$

Where

$$P = \begin{bmatrix} 1 \\ 4Z \\ (4Z^2 - 6N^2 + 6NZ - 12) \\ (-4N^3 - 12N^2Z + 12NZ^2 - 24N - 24Z) \\ (9N^4 - 28N^3Z + 9N^2Z^2 - 96NZ + 36N^2) \\ (12N^5 - 12N^4Z - 4N^3Z^2 - 72N^2Z - 24NZ^2 + 96N^3 + 192N - 96Z) \\ (4N^6 + 6N^5Z - 6N^4Z^2 + 48N^4 + 48N^3Z - 36N^2Z^2 + 96NZ + 192N^2 - 48Z^2 + 256) \\ (4N^6Z + 48N^4Z + 192N^2Z + 256Z) \\ (N^6Z^2 + 12N^4Z^2 + 48N^2Z^2 + 64Z^2) \end{bmatrix}$$

and constant Z is a function of trailing angles of inducer and rotor blades such that,

$$Z = \left(tan(\alpha_1) - tan(\beta_{f2}) \right)$$

[I] For Proof look, APPENDIX A- A.3 DERIVATIVE OF EFFICIENCY- P:137

So, P_r & P_d are design constants determined by geometric parameters of pump such as trailing angles of inducer(α_1) and rotor (β_{f2}) blades. In addition, P_d is also effected by trailing angle of diffuser blades (β_{f4}) too. Roots of this polynomial which lay in a range 3 to 10 L/min, identifies pump optimum flow rate (flow rate that satisfies maximum efficiency, $Q(\eta_{max})$).

2.1.1.8) Drag Coefficients

As seen in Eq 2.40, blade linear velocity (u) and other pump geometric parameters such as cross sectional flow area (A_c), trailing angles (α_1 , β_{f2} & β_{f4}), drag coefficients (C_D) and solidity of blades (σ) effect optimum flow rate of pump, $Q(\eta_{max})$. Effect of these parameters should be studied firstly to shift peak of efficiency curve (moving (η_{max})) to desired flow rate point. All geometric parameters such as flow area (A_c), trailing angles (α_1 , β_{f2} & β_{f4}) and solidities (σ) can easily be determined by using CAD design softwares. However, drag coefficient of blades are known for common blade designs from literature by being experimentally pre-determined and it is unknown for helical or screw type blades. This unknown $C_D$parameter restricts numerically calculating $\eta_{max}$and $Q(\eta_{max})$. So, Eq 2.40 can be used to numerically calculate $C_D$of helical blade by using it with backward engineering methods.

— CFD analysis allows evaluating hydraulic efficiency and pressure rise of pump. So, optimum flow rate $(Q(\eta_{max}))$of pump can be determined by plotting efficiency vs. flow rate curve via CFD analysis.

— Then by using $Q(\eta_{max})$ and design constants such as trailing angles and solidity of blade stages in Eq 2.40, drag ratio of rotor and diffuser stage $\left(\kappa = \frac{C_{Dr}}{C_{Dd}}\right)$ can be calculated.

— Drag coefficient of any stage can be defined by depending on the other stage coefficient via drag ratio($C_{Dr} = \kappa\, C_{Dd}$).

— Eq 2.39 can be modified to formulate remaining C_D as showed in Eq 2.41.

– As final, remaining drag coefficient can be calculated by inserting hydraulic efficiency and ideal total pressure rise values that are numerically evaluated via CFD analysis.[I]

$$C_{Dd} = \frac{2\,(1-\eta_h)\,\Delta H_i}{\rho\, {v_x}^2 \left(\frac{\kappa\,\sigma_r}{\cos(\beta_{mr})^3} + \frac{\sigma_d}{\cos(\beta_{md})^3}\right)} \qquad \textbf{Eq 2.41}$$

Where,

$$\kappa = \frac{C_{Dr}}{C_{Dd}}$$

[I] Look APPENDIX A- A.4 DRAG COEFFICIENTS- P:144, for derivation of drag coefficient formulas

2.1.2. Motor Design

According to aimed hemodynamic performance $(\Delta H\,, Q)$ to support failed heart sufficiently, required mechanical performance $(T_l\,, \omega)$, were formulated by individually defining torque load and rotational velocity in Eq 2.22 and Eq 2.27. Now, electromagnetic brushless DC motor (BDCM) parameters should be formulated to optimize them by depending on mechanical performance requirements.[I] Relation between torque load transferred to hydraulic system and mechanical torque generated by BDCM can be defined as,

$$T = \eta_m T_m \qquad \textbf{Eq 2.42}$$

Where $\eta_m$is mechanical efficiency of pump mechanism, however it is unknown for presently, because there is no study on bearing design or frictional losses by viscous effects of blood. So, this parameter will be defined arbitrarily initially until bearing selections, inertial and frictional losses calculations are done.

2.1.2.1) Magnetic Field

Dc motor produces mechanical motion via interaction between two magnetic fields created separately by rotor and stator. In order to use this technique into the LVAD, rotor compartment of device shouldn't include contact with wire due to rotation in blood volume. To provide electrically contactless rotation, rotor part creates permanent magnetic field and stator part creates varying magnetic field created by switched electrical current flow in coils. So, power generated by brushless DC motor directly depends on these two magnetic fields strength known respectively as electrical loading (L_e) and magnetic loading (L_m). Strength of magnetic field created by stator coils (Electrical load) depends on coil turns(N) and armature current feed (i) and magnetic field created by permanent magnets (Magnetic load) is function of magnetic field intensity $\left(B_g\right)$ and magnet surface area $(A_m = 2\,\pi\, r l_m)$.

[I] Note that calculated torque in Eq 2.22, is a load torque that should be transferred to fluid. In addition, BDCM has to produce torque against mechanical losses i.e. inertial effects and frictions. So,mechanical torque must be greater than load torque.

$$L_m = 2\,\pi\, r l_m B_g \quad \textbf{Eq 2.43}$$

$$L_e = N\, i \quad \textbf{Eq 2.44}$$

Where r is outer radius of permanent magnets installed in magnetic cylinder block in meter, l_m is magnet length in meter, B_g is magnetic field intensity at fluid gap in Tesla, N is the number of coil turns (all active phases together) and i is the armature current of motor drained by power source in Amper.[I] So; mechanical power (W_{mech},Watt) produced by BDCM, is formulated as

$$W_{mech} = L_m L_e\, \omega$$
$$W_{mech} = 2\,\pi\, r l_m B_g N\, i\, \omega \quad \textbf{Eq 2.45}$$

Form the literature, it is known that mechanical power generated by DC motor is also a function of rotational velocity, current feed and motor torque constant (K_b),

$$W_{mech} = i\, K_b\, \omega \quad \textbf{Eq 2.46}$$

By using both W_{mech}equations (Eq 2.45 and Eq 2.46), motor torque constant was formulated as,

$$K_b = 2\,\pi\, r l_m B_g\, N \quad \textbf{Eq 2.47}$$

Also it should be noted that magnetic field intensity at fluid gap (B_g) is a function of magnet material and magnetic efficiency affected by magnetic reluctances of materials used in pump design (impeller material, stator and rotor core material or cover materials etc.) and flow passage gap. Moreover, it's known that $T_m = K_b\, i$, so we can write load torque as $T_l = \eta_m K_b\, i$. By substituting it into Eq 2.22, K_b was formulated as;

$$K_b = \frac{Q^2\ \frac{\rho\ r_m}{A_c}\left(tan(\alpha_1) - tan(\beta_{f2})\right) + \ Q(\rho u\, r_m)}{\eta_m\, i} \quad \textbf{Eq 2.48}$$

[I] If motor coils were connected with Y-type connection.

By using Eq 2.47 K_b formula as a function of motor design parameters, into the Eq 2.48 K_b formula as a function of flow rate and blade linear velocity; motor parameters such as magnet length(l_m) and coil turn (N) product, can be formulated as a direct function of Q and ω.[I]

$$l_m\, N = \frac{Q^2\ \frac{\rho\ r_m}{A_c}\left[\ tan(\alpha_1) - tan\left(\beta_{f2}\right)\right] +\ \ Q(\rho\omega {r_m}^2)}{2\ \pi\ r\ i\ B_g\ \eta_m} \qquad \textbf{Eq 2.49}$$

As said earlier magnetic field intensity at gap (B_g) is a function of magnet material and device material, however it is also a function of some geometric parameters of pump such as magnetic gap between magnet and stator (hub-to-shroud distance if permanent magnets located inside of rotor hub or blade tip clearance if magnets located into rotor blades). Extending flow gap between rotor and stator may cause increase on pump flow capacity by increasing optimal flow rate, however it reduces magnetic field intensity by increasing magnetic gap between rotor magnets and stator coils in configurations which include magnets in rotor hub. So, possible decrease on B_g requires increase on product of magnet length and coil turn ($l_m * N$) to provide same torque and rotational velocity characteristic. However, increase on both parameters have disadvantage on device. Increase on magnet length results as heavier device and limitation of portability and increase on coil turn number results in more electrical loss and overheat on motor.

So, decrease on B_g because of flow passage modifications aimed to be eliminated by creating permanent magnets as cylindrical formation that contains hole at interior by being a flow channel (internal, central or alternative flow channel) to alternatively canalize flow through inside of rotor. So it eliminated the necessity for exterior gap to adjust pump flow capacity thanks to extra flow passage. So, the channel thickness (magnetic gap) located at exterior of magnet was reduced to improve magnetic efficiency. As a result, this formation provides advantage to use smaller magnet size or fewer coil turns by decreasing magnetic flux losses at magnetic gap.

[I] N is the total coil turn number of all active phases ($N = N_a + N_b$).For example, if two phase is active, one coil has N/2 turn.

2.1.2.2) Electrical Circuit

Electrical resistance of wire (all active phases together) is defined as;

$$R_e = \rho_w \frac{l_w}{A_w} \quad \textbf{Eq 2.50}$$

Where, ρ_w defines electrical resistivity of wire in ohm.m [I], A_w is cross sectional area of wire in m^2 and l_w is total length of wire (all active phases together) in m. l_w can be defined as a function of motor active length and total coil turns.

$$l_w = 2\ k\ l_m\ N \quad \textbf{Eq 2.51}$$

Where k is electrical resistance estimation error factor due to non-accurate coil length calculation from product of $l_m * N$, and it's greater than 1. Then by substituting Eq 2.51 into Eq 2.50, electrical resistance becomes as a direct function of l_m and N.[II]

$$R_e = 2\ k\ \rho_w \frac{l_m\ N}{A_w} \quad \textbf{Eq 2.52}$$

In this project, 3 phase coils with Y type connection is used for driver design of BDCM; so 2 of them are always active and serial connected as shown in Fig 2.3.

[I] Electrical resistivity is $1.68*10^{-8}$ ohm.m at 20 C° for copper wire.
[II] R_e is the total electrical resistance of all active phases if they connected serial (Y type connection). $R_e = R_a + R_b$.

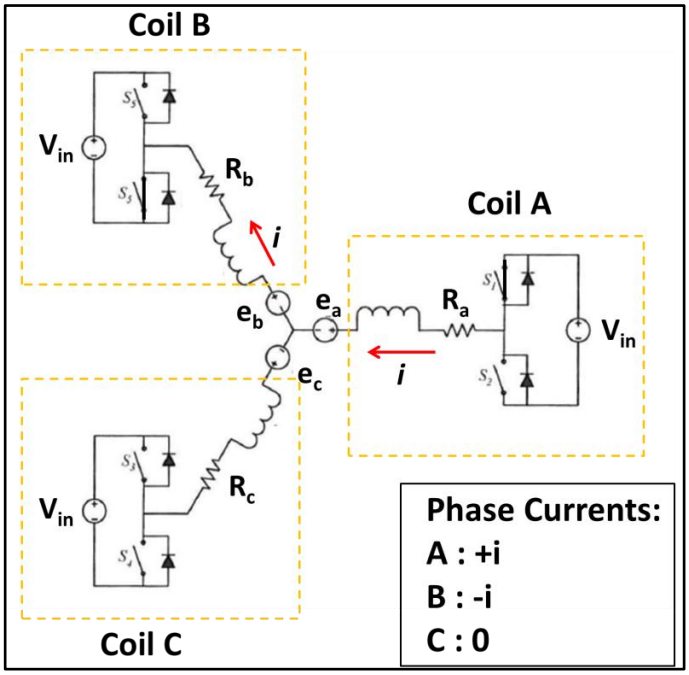

Fig 2.3: Y connected Coils and Electrical Circuit (Phase A, B and C are respectively +, - and 0)

So, electrical model of system can be written as below.

$$V_{in} = i\,R_e + K_b\omega \qquad \textbf{Eq 2.53}$$

Where $K_b\omega$ is voltage across motor ($K_b\omega = e_a + e_b$). Then, Eq 2.49 was inserted in Eq 2.52 and it was used in Eq 2.53 to define voltage drained by motor ($K_b\omega$) as a function of hydraulic torque (torque load in Eq 2.22) and magnet specifications.

$$K_b\omega = V_{in} - \frac{k\,\rho_w}{\eta_m \pi\, B_g r\, A_w}\,T \qquad \textbf{Eq 2.54}$$

Then, product of magnet length and coil turn number (all active phases) can be formulated as independent from armature current by substituting Eq 2.47 in Eq 2.54.

$$l_m N = \frac{1}{2\,\pi\, r\, B_g\, \omega}\left(V_{in} - \frac{k\,\rho_w}{\eta_m \pi\, B_g r\, A_w}\,T\right) \qquad \textbf{Eq 2.55}$$

2.1.3. Design Procedure (for Parametric Calculation)

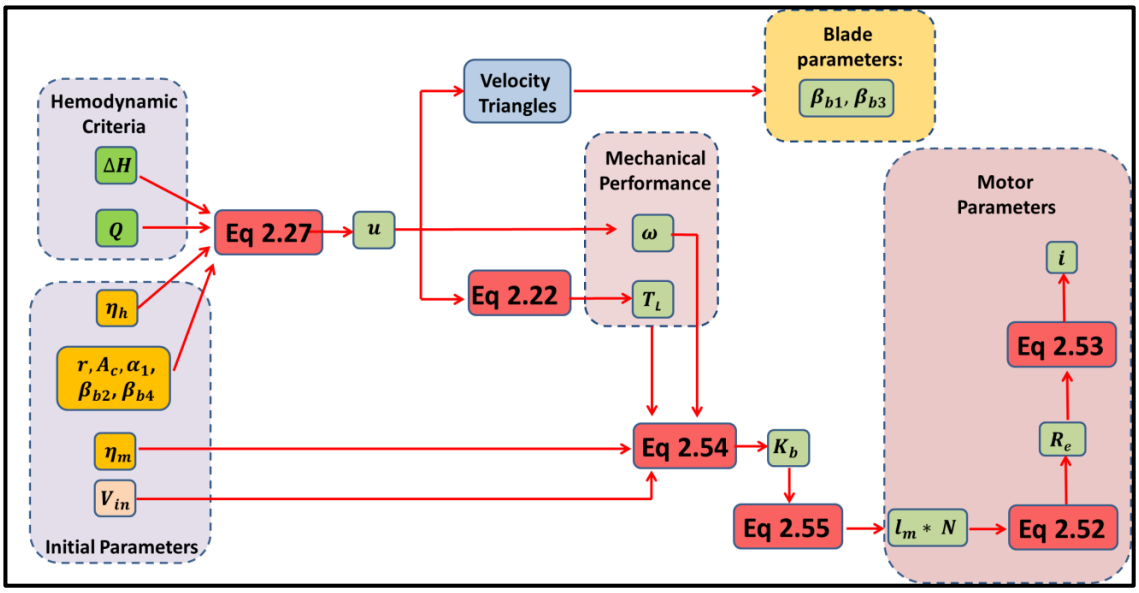

Fig 2.4: Design Process for Parametric Calculation (In Theory)

LVADs are designed to achieve hemodynamic performance $(\Delta H, Q)$ specified according to human physiology. So, these parameters are normally output of design in real operation; however they can be used as input for backward engineering method to make parametric calculations as an initial design step.

First, Eq 2.27 was used to numerically determine required linear velocity (u) of blades that satisfies hemodynamic performance $(\Delta H, Q)$. For this calculation, η_h should be initially specified according to conventional designs because there is no helical blade drag coefficient (C_d) in literature to empirically calculate it. Then linear velocity of blade was converted to angular velocity (ω) with initial blade dimension(r) selections. Next, load torque that is input of hydraulic system was calculated by using Eq 2.22. These two calculated parameters $(T \; and \; \omega)$ was required mechanic output of motor. Then, motor torque constant (K_b) was determined from Eq 2.54 which performs required mechanical performance with initially specified mechanical efficiency [I] and input voltage which is also selected from conventional battery types of LVADs. Then,

[I] Initial mechanical efficiency for these calculations should be determined from conventional designs; because without any bearing selection and shaft design, friction losses can't be known. Also inertial and extra frictional losses due to blood viscous effects should be studied to evaluate actual mechanical efficiency.

Eq 2.55 was used to make selection for magnet length (l_m) and coil turns(N) as being independent from armature current. Total electrical resistance of all active phases (R_e) was calculated by using $l_m * N$ in Eq 2.52 and voltage across motor $(K_b * \omega)$ was subtracted from input voltage (Eq 2.53) to calculate voltage across active coils, armature current (i) and electrical loss through resistance.

Also, blade attack angles was determined to provide smooth contact between fluid and blade by using velocity triangle formulas. However, unknown incidence angle (θ) restricted exact calculation for blade attack edge. Furthermore, initial hydraulic efficiency was only useful for having some idea about rotational velocity and load torque. Also, effects of initial geometric parameters such as tip and hub radius of blade, attack and trailing angles and blade clearances on pump hemocompatibility couldn't be known via these formulas. So, these parameters should be specified and tested by using experimental or computational simulation methods to optimize them. By using calculated mechanical performance especially ω as a boundary condition in finite element based computational fluid dynamics program, initial geometry should be computationally simulated to evaluate hydraulic efficiency and blade attack edge effects on flow field. These computational analyses are requirement of R&D process of LVAD because design criteria (Hemodynamic, hemocompatibility) cannot be achieved by only formulas above.

In addition to parametric analysis in theory, optimum flow rate $\left(Q(\eta_{max})\right)$ and hydraulic efficiency (η_h) was numerically evaluated after CFD analysis on design. Then, drag coefficient (C_d) of helical type blades were calculated by using this optimum flow rate with some other additional geometric parameters such as solidity in Eq 2.40.

2.2. 3D VIRTUAL DESIGN (SOLIDWORKS®)

This step of R&D process of LVAD, consists of 3-D virtual design of pump geometry to enable CFD analysis, as CFD programs require solution domain in CAD (Computer Aided Design) format to compute. By depending on CFD solver selection, geometry of device should be specified. For example, some CFD solvers require only impeller geometry (Solid volume), however others such as ANSYS Fluent® [I] need fluid volume (inverse of impeller geometry) to compute. These solution domains should be designed as 3D by CAD tools. There are many softwares as CAD tool; furthermore CFD packages also include CAD tool. However in this project, SolidWorks® [II] software was used as CAD tool to design pump in terms of parameters that was specified according to equations above.

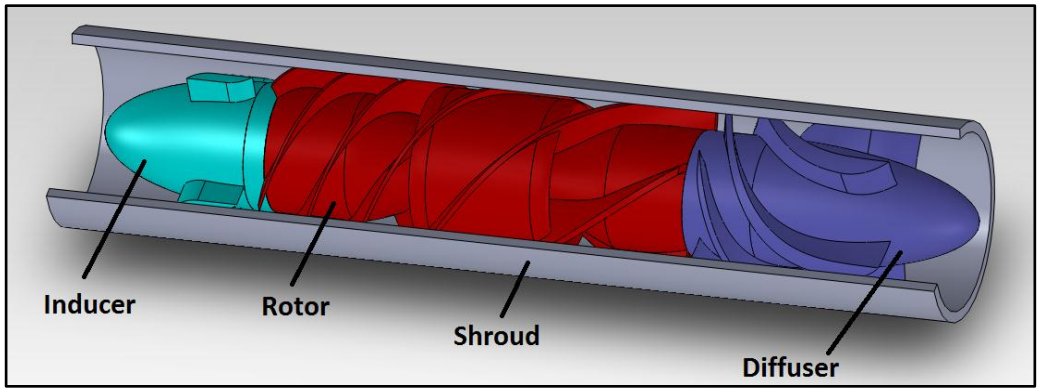

Fig 2.5: 3D Virtual Design of Axial Flow Heart Pump (3D Design Only Includes Concerned Geometries for CFD)

Axial flow heart pumps include three blade stages called inducer, rotor and diffuser. Each stage has its own performance requirements. When inducer regulates flow field to prevent prerotation of fluid at rotor inlet, rotor imparts kinetic energy to fluid and diffuser converts this kinetic energy to potential energy. So, all stages have their own design considerations depending on their functions.

[I] ANSYS Inc.®: Canonsburg,Pennsylvania,USA
[II] Dassault Systèmes SolidWorks Corp.®: Waltham, Massachusetts, USA

2.2.1. Inducer

As seen from Fig 2.5, inducer is the first component of device which contacts blood. It is a stationary component combined with shroud (stator or pump housing). The function of inducer is preventing prerotation of fluid by adjusting flow lines at axis direction. When blood comes back from rotary component (backflow), it has higher tangential velocity and it causes radial circulation of blood at pre-stage (prerotation at interface between inducer and rotor). So, inducer blades should block tangential displacement of blood flow and lead it to forward direction. If it can't direct it forwardly, duration of flow gets longer in inducer stage.

Inducer blades are conventionally designed parallel to the flow axis (leading angle of inducer equals to zero, $\alpha_1 = 0$) , to adjust flow lines parallel to axes. However, axial length of interface between inducer and rotor blades (gap, g_1) is more important to block radial circulation of backflow and reduce its duration. Furthermore, number of inducer blades (n_i) is also important factor to enhance flow field in this section.

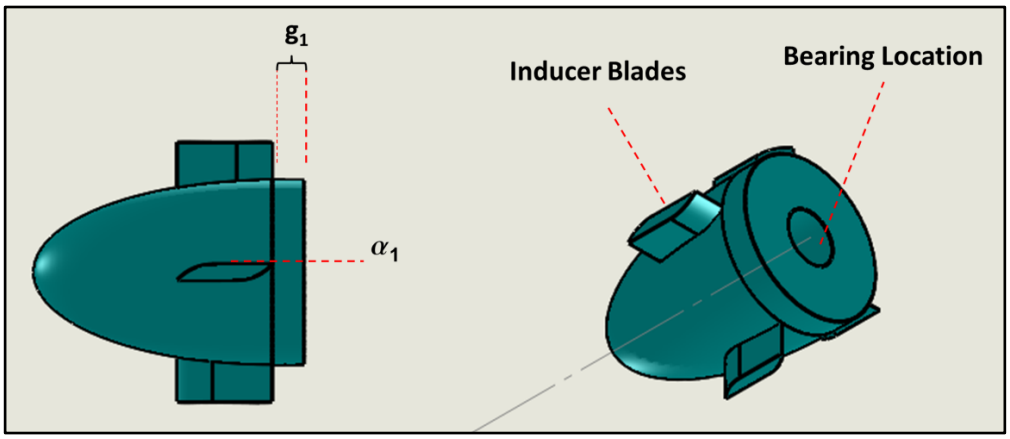

Fig 2.6: Inducer Component Side View and Isometric View at Left and Right Respectively

Moreover, inducer is used as radial support for rotary motion by containing mechanical bearings installed in hole at interior of inducer to locate rotor shaft onto them.

2.2.2. Rotor

Rotor is the component that imparts kinetic energy to fluid by increasing its velocity in tangential direction (u) by applying force at same direction (Torque) and potential energy as static pressure rise by exerting axial force to fluid. As understood from equations above, this component has to move rotationally to increase total energy on fluid. This motion is provided by interactions of two magnetic fields, one is caused by coils in stator and the other is caused by permanent magnets of Brushless DC motor into this component. Conventionally, there are two methods to install permanent magnets.

First method is locating permanent magnets into hub (rotor center), which provides unrestricted volume for locating magnets. It is known that effect of permanent magnet on rotor performance can be evaluated from magnetic flux that reaches stator (Magnetic load). Large gap between magnet and stator increases magnetic resistance and reduces magnitude of flux that reaches stator. However, shortening this gap causes smaller blade height and it negatively effects transferred energy on fluid and cross sectional flow area that represents flow capacity of pump. So, in this configuration, negative effects (high magnetic losses) can be recovered by increasing permanent magnet volume which results in increase on device mass or electrical loading, e.g. by increasing armature current or coil turns (Eq 2.55) which result in higher electrical losses in motor and overheating. Moreover, increase on power requirement causes need for heavier battery and may lead to restricting patient portability.

In second method, permanent magnets are located in rotor blades to improve magnetic efficiency by reducing distance between magnets and stator coils. However, in this configuration, rotor blades have restricted available volume for installing permanent magnets and it showed in Eq 2.55, magnetic load is proportional to magnet length [I]. In this configuration, possible disadvantages (less magnetic load or flux) can be recovered only by increasing electrical loading, which results in electrical losses and overheating as explained above.

[I] Magnetic loading also described as magnetic flux. It is known that magnetic flux equals the product of magnet surface area and magnetic field intensity of magnetic material. So magnetic flux becomes magnetic loading in Eq 2.43.

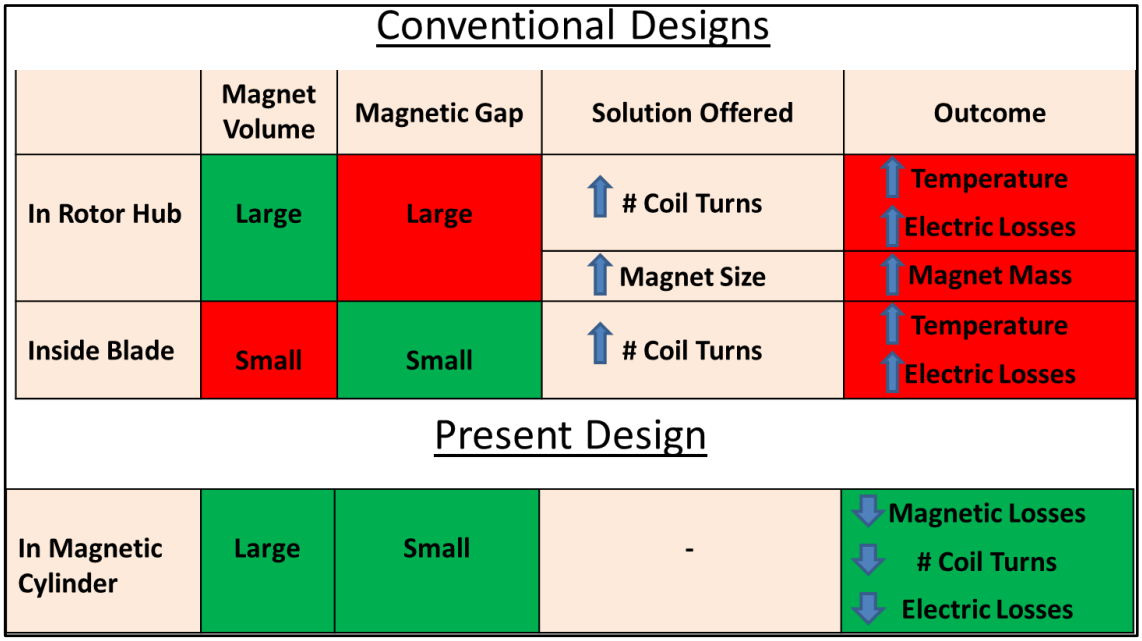

Fig 2.7: Advantages and Disadvantages of Conventional and Present Designs

In this project, a radically new configuration was developed. As shown in Fig 2.8, permanent magnet was designed as cylinder and flow channel was opened at interior of this magnetic cylinder. Then by locating blade inside of this channel blood acceleration and pressure rise were provided mostly through interior channel. Magnetic cylinder was located closer to shroud by reducing necessity for exterior (Peripheral) channel thanks to transporting flow through central flow channel. Moreover, blood flow through peripheral channel is accelerated by smaller height blades located at exterior of magnetic cylinder to prevent possible stagnation. Hereby, large magnetic distance problem as in first configuration and small magnet size problem as in second configuration were removed. So, this configuration provides possibility to reduce electrical losses by reducing necessity for higher current and coil turns by increasing magnetic load thanks to less flux losses and larger volume (Fig 2.7).

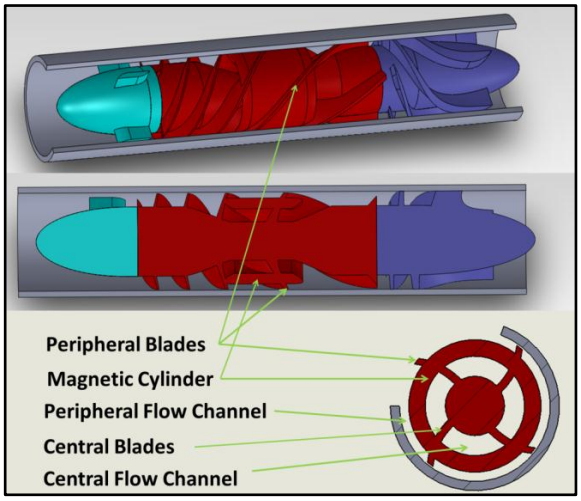

Fig 2.8: Details of New LVAD Configuration (Isometric view on top, horizontal cross sectional view in the middle and vertical cross sectional view below)

As explained and formulated above, blade attack (β_{b1}) and leading (β_{b2}) angle design can be preliminary done according to parametric analysis in 2D (Fig 2.1), however their effects on hemodynamic performance and flow field cannot be known without CFD tests in 3D flow domain. Blade attack edge should be designed to provide smooth contact with incoming flow and trailing design should be done to lead blood flow to diffuser and adjust kinetic energy rise (Eq 2.13). Other geometric parameters such as tip and hub radius of rotor blade $(r_t \; and \; r_h)$ and cross sectional flow area (A_c) should be designed according to adjust pump operation point (Maximum efficiency versus flow rate) and hydraulic efficiency. There are extra parameters such as rotor blade length (l_r) and number(n_r) that effect energy transfer to fluid by changing flow passage length and width i.e. blade geometric constants such as chord length, space and solidity. Blood flow reaches its maximum velocity across rotor component. So, high shear stress and hereby hemolysis mostly occurs in rotor stage, especially around blade tip and shroud where radial forces are maximum. Also blade tip-shroud gap (g_t) is an important parameter for leakage flow through there and shear stress at shroud.

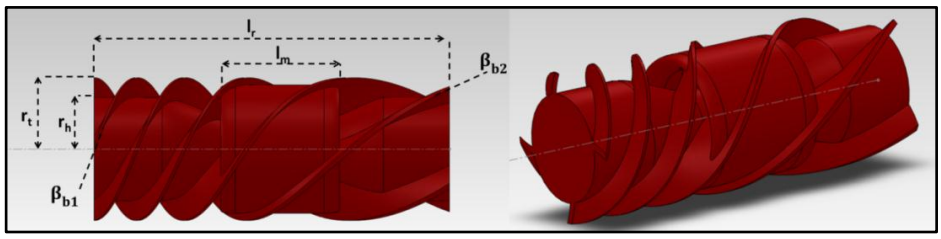

Fig 2.9: Rotor Component Side and Isometric View at Left and Right Respectively

2.2.3. Diffuser

Diffuser is a stationary component of LVAD, which increases static pressure of blood by reducing tangential velocity imparted by rotor. In other words, diffuser converts kinetic energy (dynamic pressure) of flow into the potential energy (static pressure). Diffuser attack edge (β_{b3}) should be designed in order to provide smooth contact at diffuser inlet to not cause backflow. Also, diffuser leads blood flow into axial direction by reducing tangential velocity. Hereby, leading edge (β_{b4}) should be designed in order not to cause radial flow at exit cannula. Moreover, gap between diffuser blades and rotor blades (g_2) has effect on backflow at diffuser inlet. In addition to these parameters, other parameters such as blade length, number, thickness and twisting shape possibly influence flow field through diffuser e.g. boundary flow separations and vortex in this stage by effecting flow passage length and width.

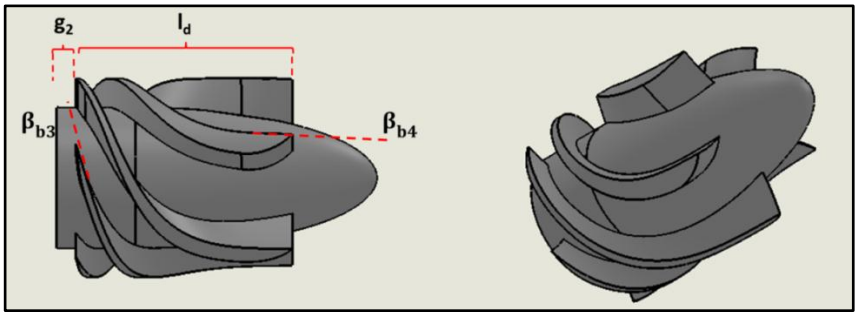

Fig 2.10: Diffuser Component Side and Isometric View at Left and Right Respectively

Diffuser component are used to radially support the rotary component by installing mechanical bearings into the central hole of diffuser as in inducer. However, this bearing configuration isn't required in designs that use magnetic levitation or hemodynamic bearing mechanism.

Parameters listed below will be main consideration point of 3D virtual design and optimization process:

- Tip and hub radius of rotor blade ($r_t and\ r_h$),
- Hub- tip radius ratio as dimensionless pump size parameter ($^{r_h}/_{r_t}$),
- Cross-sectional flow area (A_c),
- Rotor and diffuser stage length ($l_r\ and\ l_d$),

- Magnetic cylinder length and thickness ($l_m \; and \; t_m$),
- Chord length and space of rotor and diffuser blade (c_r, c_d, s_r, s_d),
- Chord-space ratio (Solidity) of rotor and diffuser blade as dimensionless blade parameter ($\sigma_r \; and \; \sigma_d$),
- Attack and trailing angles of rotor blade ($\beta_{b1} \; and \; \beta_{b2}$),
- Attack and trailing angles of diffuser blade ($\beta_{b3} \; and \; \beta_{b4}$),
- Trailing angle of inducer (α_1)
- Number of rotor, diffuser and inducer blades ($n_r, n_d and \; n_i$),
- Rotor blade tip to shroud gap (g_t),
- Inducer to rotor blade gap (g_1),
- Rotor to diffuser blade gap (g_2),

As listed, effects of some of them can be predicted from parametric analysis in 2D but the effect of others cannot. Even though formulas above give an idea about the effects of this second group of parameters on hemodynamic performance and flow field, it doesn't provide exact solution for acceptable design without doing experiments in 3D flow domain. Computational fluid dynamics methods are acceptable numerical analysis tool that give effects of these parameters on performance as close as to experiments in real conditions. After 3D virtual design (CAD data) process according to specified parameters at above, it will be imported to CFD program to analyze these parameters computationally.

2.3. COMPUTATIONAL FLUID DYNAMIC ANALYSIS (CFD)

As explained, listed turbomachine formulas are not enough to define pump characteristic, because they were derived by simplifying flow domain into 2D. All dynamics of fluid are basically defined by Continuity, Momentum (Reynolds Averaged Navier Stokes-RANS) and energy equations. Generally, CFD is numerical analysis method that uses these equation groups to simulate dynamics of fluid as close to real conditions as possible. Also, it is capable to simulate under different boundary conditions such as moving surfaces or heat transfer. This step of R&D process of LVAD consists of computational performance testing of 3D virtual geometry and ANSYS Fluent® software was used to solve the governing equations.

As a result of fluid dynamic analysis, boundary flow separation, eddy currents and turbulence characteristic of flow, dynamic and static pressure level in any location, exerted shear forces on fluid, exposure time of fluid particles, viscous effects on blades can be numerically and visually observed.

In order to provide simulation results as close to reality as possible;

- Flow model should be determined by selecting extra equations additional to governing equations (Continuity and Momentum). These extra flow modeling equations enable to define dynamics of fluid under special conditions such as turbulence, energy transfer, multiphase fluid, melting, species, acoustic or etc.

- CFD softwares firstly divide flow volume into smaller cells and solve governing and other additional model equations for each cell one by one. Division to small cells called as meshing or solution domain discretization. If extra model equations require special cell sizes for accuracy in solution, discretization should be performed according to size requirements e.g. turbulence models require to locate nodes in specific layers.

- Then, boundary conditions are determined to specify physical operation conditions in virtual environment such as moving wall, heat flow, pressure or mass flow.

- After solving equations for each cell, CFD solver takes these results as initial condition for next turn and it applies same equations to each cell again. This solving and taking it as initial for next solving process called iteratively solving, and it continues until deviation between results of two iterations become acceptable (convergence).

After solutions converged, flow dynamics results of pump can be used to compare them with design criteria to enhance effects by optimizing geometric parameters.

2.3.1. Flow Modeling

2.3.1.1) Turbulence:

Blood flow in pump has high velocity level due to rotational motion. So increasing velocity level of fluid causes increase on Reynolds Number (Re) and it is known that laminar or turbulent flow characteristic is directly defined by Re level of fluid. Where Re>2500, flow turns from laminar to turbulent characteristic and Re>10000, flow shows fully turbulent characteristic. High velocity regions in pump especially where fluid instantly accelerates and decelerates such as inlet of rotor and diffuser, fluid shows fully turbulent characteristic. So, turbulence model should be selected in addition to governing equations to model fluid flow accurately.

- **Turbulence Model:**

Generally turbulence models are determined according to application and turbomachines that have rotating walls and high Re number, are simulated commonly by Standard k-ε or SST k-ω turbulence models; where k, ε and ω designate turbulence kinetic energy, dissipation rate and frequency respectively. Both models have their own advantages and limitations on accuracy of flow dynamics results. Standard k-ε turbulence model has limitation to accurately capture fluid characteristic at flow separation along boundary at weak turbulence flow or low Re number (Re<10000). Despite this limitation, Standard k-ε turbulence model are widely used to model flow turbulence in such devices. k and ε parameters can be modified by user in ANSYS Fluent, however default values are acceptable for these applications.

- **Near Wall Treatment:**

Flow turbulence action differs at core and near wall region of flow domain. So, selecting correct turbulence model is only enough to simulate flow dynamics in general flow domain and it doesn't represent real action of fluid near wall region. Fluid turbulence characteristic near wall region (boundary) depending on distance to boundary and experts on the field grouped different turbulence actions of fluid into three layers from boundary as shown in Fig 2.11. First layer from the boundary called the "viscous sublayer"; the flow is almost laminar and the molecular viscosity plays a dominant role in momentum and heat or mass transfer. In the outer layer, called the "fully-turbulent layer", turbulence plays a major role. Finally, there is region between the "viscous sublayer" and the "fully turbulent layer" where flow turns to turbulence from laminar and it called "buffer zone". These layers were separated from each other in terms of dimensionless distance factor y^+ as shown in Fig 2.11. Dimensionless distance factor y^+ depends on actual distance of first node (corners of cell) to boundary (y) , blood viscosity (μ , $Pa.s$), blood density (ρ) and wall-shear stress (σ_{ss}, Pa).

$$\frac{y}{y^+} = \frac{\mu}{\sqrt{\sigma_{ss}\rho}} \qquad \textbf{Eq 2.56}$$

As seen in Fig 2.11, where $y^+ < 5$, first node locates within "viscous sublayer" and $y^+ > 60$, it locates within "fully turbulent region". If $y^+$is within 5 and 60, first node stands in "buffer zone" where flow turns to turbulence from laminar characteristic.

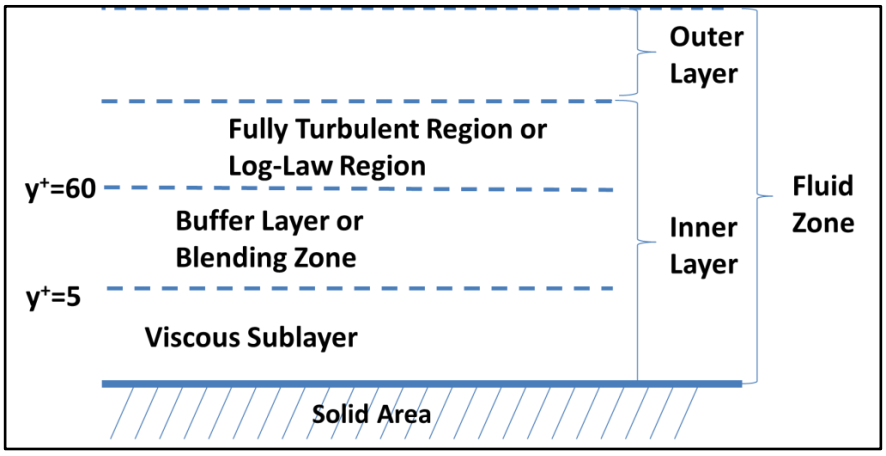

Fig 2.11: Subdivision of Near Wall Region (Boundary)

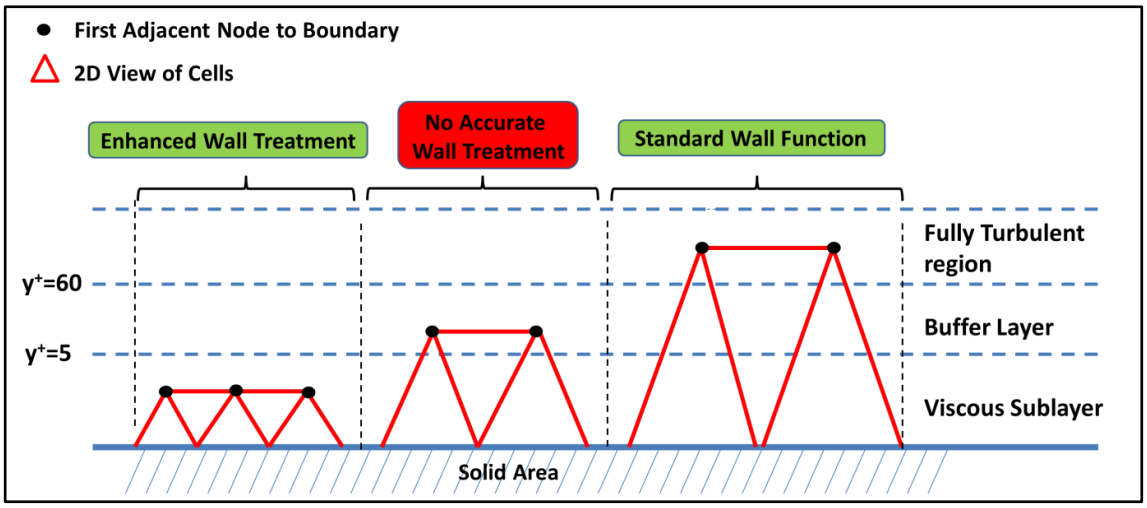

Fig 2.12: Wall Treatment Models According to First Node Location (Red Triangles Designates Meshes at Near Wall)

Flow characteristic can be modeled for "viscous sublayer" and "fully turbulent layer" with "Enhanced Wall Treatment" and "Standard Wall Function" respectively, as shown in Fig 2.12. However there is no accurate model to define flow characteristic at "Buffer Zone". Hereby, CFD solver shouldn't compute turbulence and wall treatment formulas for nodes that locates in buffer zone. Also, first nodes closest to boundary should be located within "viscous sublayer" or "fully turbulent region".

By using Eq 2.56, first cell size (y) was determined to locate first node to any of both available layer and wall treatment method was selected according to layer. Also, size should be selected to avoid locating first node in "buffer zone". However, axial flow heart pump designed in this project has small clearances between blade tip and shroud ($0.2>g_t>0.1$ mm), and it restricted to make $y^+> 60$ for first node at boundary. So, in this project "Enhanced wall function" was used as wall treatment method by locating first nodes in "viscous sublayer" ($y^+<5$) because of geometric restrictions.

Furthermore layer where first node locates depends on shear stress and it is unknown without CFD analysis. So, first nodal actual distance was determined according to preliminary estimations on shear stress. After CFD solution, it can be validated that first nodes have $y^+ < 5$ and wall treatment accurately works.

2.3.1.2) Heat Transfer Model:

Generally heat transfer model isn't used in blood pumps CFD analysis, because it doesn't simulate effect of pump geometry on fluid dynamics. So, this model isn't required for optimization of pump geometry. However, heat transfer model can be inserted to CFD solver in order to study effect of overheating through coils, on blood. This is not the topic of the present study and will constitute the next step of program.

2.3.1.3) Blood Damage Modeling (Hemolysis):

As explained in "1.1.7-Design Criteria, P:24" section, there are high shear stress zones in pump due to high rotational velocities. Red blood cells (RBCs) blow up under high forces and hemoglobin in cells releases into the blood plasma. Plasma free hemoglobin (pfHb) level is evaluated by taking samples from blood after in-vitro or in-vivo tests (physical tests of pump with blood) to specify pump hemocompatibility. However, it's not possible to take samples during computational testing process, so mathematical model is required to estimate hemocompatibility of pump in virtual domain. Experts on the field found that RBC demolishment depends on shear stress and exertion time of stress (exposure time). However, if shear stress is non-uniform such in LVADs, total damage on one RBC during passing through pump is assumed to be accumulated linearly within very short time steps. Empirical hemolysis formula as,

$$\%Hb = \sum_{inlet}^{outlet} 3.62 * 10^{-7}\ \tau^{2.416}\, \Delta t^{0.785} \qquad \textbf{Eq 2.57}$$

Where $\%Hb$ is the ratio of pfHb to the total hemoglobin, τ is the scalar shear stress acting on RBC in Pa and Δt is duration of stress in seconds. In 3D domain, scalar shear stress are formulated as a combination of 6 stress tensor:

$$\tau = \sqrt{\frac{1}{6}\ \sum \left(\tau_{ii} - \tau_{jj}\right)^2 + \sum {\tau_{ij}}^2} \qquad \textbf{Eq 2.58}$$

Respectively xy, xz and yz were substituted instead of ij in Eq 2.58 and scalar shear stress (τ) became,

$$\tau = \sqrt{\left(\frac{{\tau_{xx}}^2 - 2\tau_{xx}\tau_{yy} + {\tau_{yy}}^2}{6} + {\tau_{xy}}^2\right)\ldots+\left(\frac{{\tau_{zz}}^2 - 2\tau_{zz}\tau_{yy} + {\tau_{yy}}^2}{6} + {\tau_{zy}}^2\right)} \quad \textbf{Eq 2.58}$$

$$\sqrt{\frac{\left({\tau_{xx}}^2 + {\tau_{yy}}^2 + {\tau_{zz}}^2\right) - \left(\tau_{xx}\tau_{yy} + \tau_{xx}\tau_{zz} + \tau_{zz}\tau_{yy}\right)}{3} + \left({\tau_{xy}}^2 + {\tau_{xz}}^2 + {\tau_{zy}}^2\right)}$$

Shear stress vectors are expressed as;

$$\begin{aligned}
\tau_{xx} &= 2\,\mu_t\,\frac{\partial u}{\partial x} + \lambda\left(\frac{\partial u}{\partial x} + \frac{\partial v}{\partial y} + \frac{\partial w}{\partial z}\right)\\
\tau_{yy} &= 2\,\mu_t\,\frac{\partial v}{\partial y} + \lambda\left(\frac{\partial u}{\partial x} + \frac{\partial v}{\partial y} + \frac{\partial w}{\partial z}\right)\\
\tau_{zz} &= 2\,\mu_t\,\frac{\partial w}{\partial z} + \lambda\left(\frac{\partial u}{\partial x} + \frac{\partial v}{\partial y} + \frac{\partial w}{\partial z}\right)\\
\tau_{xy} &= \tau_{yx} = \mu_t\left(\frac{\partial v}{\partial x} + \frac{\partial u}{\partial y}\right)\\
\tau_{xz} &= \tau_{zx} = \mu_t\left(\frac{\partial w}{\partial x} + \frac{\partial u}{\partial z}\right)\\
\tau_{zy} &= \tau_{yz} = \mu_t\left(\frac{\partial v}{\partial z} + \frac{\partial w}{\partial y}\right)
\end{aligned} \quad \textbf{Eq 2.59}$$

Where u, v, w is the velocity of fluid respectively at x, y and z direction. μ_t is dynamic viscosity (0.0035 Pa.s for blood) and λ is secondary viscocity that is written as a function of dynamic viscosity.

$$\lambda = -\frac{2}{3}\mu_t \quad \textbf{Eq 2.60}$$

Combination of equations above can be used to estimate averaged ratio of pfHb to total hemoglobin level, $\%Hb$. Its known that hemoglobin content in RBCs, κ is 15000 mg/dl

for healthy person. Amount of pfHb (ΔHb in mg/dl) and rate of pfHb ($\frac{d(\Delta Hb)}{dt}$ in mg/hour) becomes;

$$\Delta Hb = \%Hb\ \kappa \quad \textbf{Eq 2.61}$$

$$\frac{d(\Delta Hb)}{dt} = 600\ \Delta Hb\ Q \quad \textbf{Eq 2.62}$$

Where Q is volumetric flow rate of pump in L/min. Then hemocompatibility of pump can be estimated by comparing $\left(\frac{d(\Delta Hb)}{dt}\right)$ with renal activities capacity to purify blood and it is reported that normal functions of kidneys can purify 583 mg/h Hb.

Although Eq 2.61 and Eq 2.62 give pfHb accumulation and increase rate in blood, these parameters cannot be used to compare different pump types due to difference on operation conditions such as volumetric flow rate, head pressure and supporting period. Hereby, American Society for Testing and Materials standardized continuous flow blood pumps effects on hemolysis by defining normalized index of hemoglobin (NIH) parameter. According to their procedure, operation of blood pump should be adjusted to 5 ± 0.25 L/min flow at 100 mmHg head pressure at 37 ± 1 C° circulating blood temperature. Then, plasma free hemoglobin, ΔHb should be evaluated from blood samples after 6 hour pump operation in closed test loop (in-vitro study) and it should be approved with 5 trials. Normalized index of hemolysis (NIH, g/100l or mg/dl) reduces ΔHb into the standardized parameter to classify blood pump hemocompatibility.

$$NIH.\ g/100l = \Delta Hb * V * \frac{(100 - Hct)}{100} * \frac{1}{Q * T} \quad \textbf{Eq 2.63}$$

Where ΔHb is plasma free hemoglobin concentration in mg/dl, V is test circuit volume in L, Q is flow rate in L/min, Hct is hematocrit that is the proportion of blood volume occupied by RBCs (%45 for healthy person) and T is sampling time interval in min. According to standards NIH should be calculated from Eq 2.63 with real blood samples, however it is only applicable if hemolysis test are performed with real blood (in-vitro or in-vivo study).

So, in such projects which contain computational methods instead of physical tests with real blood, mathematical models that applicable for computational simulations should be used such as Eq 2.57. Empirical %Hb formula was applied to more than one RBC (n, cell number) and averaged with total cell number to estimate blood damage accurately.

CFD solvers doesn't include embedded model for these formulas, extra macros (user defined functions, UDF) should be written and imported to ANSYS Fluent library to compute Eq 2.57 on streamlines [I] in static or released particles [II] (RBCs) in transient analysis. Then, averaged %Hb level can be used to evaluate $\frac{d(\Delta Hb)}{dt}$ with Eq 2.62.

[I] Streamlines are pathways that conducted from flow vectors and holds flow dynamic history as stress, time and etc in static analysis.

[II] As being advantage to use CFD tool, Lagrangian CFD method gives possibility to track fluid particles which carry fluid history depending on its flow time. Particle tracking with Lagrangian easily enables to make individual numerical calculations for each particle. Flow domain is defined as fluid-solid particle mixture and particles should be defined as size of RBC. Then, CFD solver releases particles from pump inlet and computes UDF for these particles. This method gives more accurate result than computing on streamlines.

2.3.2. Finite Element Methods (Mesh)

In finite element methods, flow volume is discretized to smaller volumes, and then CFD solver computes continuity, RANS and turbulence equations for each cell. This process is called meshing operation. Meshes can be triangular or rectangular in 2D and pyramid, tetrahedral or hexagonal elements in 3D.

Meshing operation should be performed according to provide consistency between simulation and real results. The second important objective of meshing is not causing longer computation times. Discretizing flow domain with excessive number of cells causes longer duration for computation time, however otherwise dividing to fewer cells results as deviation from reality. So, balance between both should be achieved to sufficiently use time for accuracy in simulation. Selecting smaller cells into critic flow regions instead of all flow volume, provides accuracy on simulation results in important flow zones, prevents excessive usage of time and results in faster computation.

Critical regions where flow has high velocity, shear stress, acceleration and deceleration, mostly occur at rotor and diffuser blades attack edges. Moreover, some flow volume where high turbulence and vortex possibly occur, such as boundary flow separation points on diffuser blades and prerotation in inducer zone, are also important flow areas. Non-smooth contact with incoming flow and blade attack edge causes backflow, so most of the backflow occurs between blade stages. Hereby, rotor-inducer and rotor-diffuser clearances are also important flow regions that effect biocompatibility of device.

As explained above, meshing sizes at boundary layer should be determined in terms of near wall treatment functions. In this project , “enhanced wall function” was used to simulate flow dynamics at boundary layer and it requires $y^+ < 5$ for first node to locate them in “viscous sublayer”. According to formula in Eq 2.56, it is seen that flow region where high shear stress is expected, should have smaller cell sizes than other regions to sufficiently solve turbulence equations around these areas.

2.3.3. Setting Physical Conditions

- **Material Selection:**

LVAD pumps blood from LV to aorta. So material that is used in CFD analysis should be blood. Blood is non-Newtonian [I] fluid and its density and viscosity are 1050 kg/m^3 and 0.0035 Pa.s respectively.

Moreover, surfaces of blood pump that contact with blood are covered with material that doesn't react with blood such as Titanium. So, friction coefficient of Titanium can be used for advanced CFD model of boundary effects. This is not the topic of the present study and will constitute the next step of program.

- **Zone and Boundary Conditions:**

This step includes setting physical conditions for simulation model. These conditions can be movement of any wall, heat transfer from wall, special friction effects on wall or etc. Before setting conditions, firstly surfaces and volumes of flow domain should be grouped. LVAD was designed from 3 components inducer, rotor and diffuser. So, there are 3 separate cell groups. Inducer and diffuser are the stationary components of device and there is no need to specify physical conditions to them. However rotor component was defined as "Rotating Frame" and rotational velocity was specified. Then all surfaces of rotor component were defined as "rotationally moving wall" with "zero velocity relative to adjacent cell zone". This definition, enables rotation of boundaries with adjacent cell groups at same velocity (rotor boundaries are adjacent to rotor cell zone). Then all other surfaces of pump such as shroud, diffuser blades and inducer blades were determined as non-slip stationary wall. Furthermore, intersecting surfaces of 3 components were defined as "interface".

After determining all cell and boundary types, pump operation condition should be determined for simulation. There are two methods to simulate performance of pump. In

[I] Non-Newtonian fluid represents incompressiblity of fluid. So, its density doesn't change under exerted pressure.

first method, outlet and inlet boundary should be defined as "Pressure outlet" and "Pressure inlet" respectively, then numerically static pressure value can be specified for both boundaries.[I] After simulation, flow rate at any of these boundaries can be observed to numerically evaluate pump hemodynamic performance. For second method, inlet and outlet of pump can be defined as "mass flow inlet" and "pressure outlet". After determining mass flow rate and outlet pressure, simulation can be performed and pump hemodynamic performance can be numerically evaluated by observing static pressure at pump inlet.[II] Both method gives same hemodynamic performance and flow dynamics with good qualified mesh and converged solution.

However, it is known that backflow between stages mostly occurs due to incidence angle $(\theta_r \& \theta_d)$ between attacking flow $(\beta_{f1} \& \beta_{f3})$ and blade attack angle $(\beta_{b1} \& \beta_{b3})$ as formulated in Eq 2.14 and it is a function of volumetric flow rate(Q) instead of pressure rise(ΔP). So, making simulations by specifying volumetric flow rate is easier observation method for backflow to compare different virtual designs for optimizing its geometric parameters. So, second method for operation conditions definition was used in this project.

[I] For example -13332 Pa static pressure can be set for "pressure inlet" and gauge pressure (0 Pa) can be set for "pressure outlet". It represents 13332 Pa (100 mmHg) head pressure.
[II] For example 0.0875 kg/s mass flow rate and gauge pressure is defined for "mass flow inlet" and "pressure outlet" respectively. Static pressure value at "mass flow inlet" boundary gives pressure rise.

2.3.4. Analyzing Process

CFD solvers compute continuity, RANS, turbulence and additional model formulas to each cell of flow domain one by one. After completing calculations for each cell, results of previous calculation are used as initial condition for next calculation turn and same equations are solved again for each cell. After every step of this iterative process difference between results of two successive iterations (residuals) gets closer to zero. When results between two iteration are the same or very slightly different from each other ($\Delta<10^{-4}$), solution converges.

It is important to know that converged solution only depends on difference between two iteration results and it doesn't represent accuracy on flow dynamics. Accuracy on flow results can be achieved only by correct mesh sizes and modeling method (Turbulence model and boundary conditions settings). Moreover, increasing orders of Momentum and turbulence equations to 2^{nd} order gives more accuracy on converged results, however it results increase on computation time of simulation.

At the beginning of simulation, setting initial conditions for velocity values as close to simulation results as possible, provides quicker convergence of simulation. As against, setting initial conditions as far as from simulation results cause large errors on converged solution and it doesn't simulates reality. So, in this project initial conditions were set as zero to avoid possible non correct simulation results.

During project, flow domain was divided into 5-8.000.000 mesh and computed in workstation which has 24 GB RAM and 12 processors with 2.66 GHz. Solution was converged within 1.500-2.000 iteration and it took 7-10 computation hours.

2.4. OPTIMIZATION

It is known that heart pumps should achieve exact performance depending on physiological needs and they were listed as design criteria. These criteria were divided in three main groups: hemocompatibility, hemodynamics and anatomic constraints. Pump performance should be simulated via computational methods and deviation from design criteria should be evaluated via observing dynamics of fluid e.g. backflow, leakage flow, eddy current, vortex zone, shear stress, transition time, static and dynamic pressure rise mapping studies or etc. Then optimization on geometry should be done to enhance flow field and dynamics in pump to achieve hemodynamic performance within hemocompatibility and anatomic constraints.

2.4.1. Optimization Objectives:

Implantable LVADs are for in-body use, so it should be designed according to anatomic constraints. Human anatomy brings geometric restrictions on design to fit it into body and device geometric optimization should be done within these constraints. According to conventional designs, geometric restrictions were defined as maximum 100 mm at length, 30 mm at diameter and 300 gr on weight. Furthermore, reducing dimensions and weight as much as possible improves portability and provides easier implantation.

Hemocompatibility of pump is defined as not causing excessive and unacceptable hemolysis level and coagulation in order to not negatively affect physiology. Hemolysis occurs as a result of RBCs demolishment under high forces and hemoglobin (Hb) contents in RBCs release into the blood plasma after cell demolishment. Device effects on blood damage can be evaluated by observing plasma-free hemoglobin level (pfHb), however it is only possible for in-vitro or in-vivo tests (testing with real blood). Experts on the field found that pfHb is a function of shear stress (σ_{ss}) exerted on RBCs and its duration (exposure time,t_e) and then, empirical model was derived to estimate percentage damage factor as ratio of pfHb to the total hemoglobin (Eq 2.57). Although, it doesn't provide accurate level of pfHb, it shows that less stress and shorter duration reduce pfHb level. According to studies on this subject, shear stress within range 400 to 500 Pa with 100ms exposure time is threshold for RBCs collapse. Shear stress should be

reduced as much as possible for more hemocompatible product, however is not possible to classify hemocompatibility of device without blood sampling during in-vitro and in-vivo tests. So, this range for shear stress was aimed to achieve to complete optimization process via computational methods and to pass physical testing.

Depending on computational studies in such devices, backflow and vortex as a result of backflow increase residence time of blood cells in pump and causes pfHb accumulation in blood. Less hemolysis as an objective of optimization, can be achieved by reducing shear stress and exposure time via minimizing backflow between stages. As known from accumulated experiences, %16 total backflow didn't satisfy requirements of commercial products. Actually, backflow should be reduced as much as possible for enhancing flow lines; however indirect relationship with hemolysis limits optimization of device according to backflow with computational methods. In order to minimize need for modification that is possible to arise in future physical testing process (in-vitro and in-vivo tests), threshold value for percentage backflow was determined as %10 as being achievable realistic condition for pump design.

Furthermore, coagulation cannot be modeled in CFD solver, however it's known that it occurs because of low velocity fields. So, eliminating stagnant flow is another objective of optimization.

Hemodynamic performance of pump is determined from physiological need of body as producing volumetric flow rate (Q) against head pressure (ΔP). Hemodynamic performance of pump meets this requirement by providing adequate rotational velocity $(\omega)$and torque (T). Relationship between these parameters was numerically determined via CFD analysis and then hydraulic efficiency $(\eta_h)$was calculated from this relationship.

As being objective of optimization, increasing hemodynamic performance can be achieved by increasing output power $(Q * \Delta P)$ when input power $(\omega * T)$ doesn't change i.e. increased hydraulic efficiency. Improved hydraulic performance gives chance to reduce rotational velocity and hereby shear stress that directly causes RBCs demolishment. In short, improved hemodynamic performance gives possibility to

reduce hemolysis via requiring less blade linear velocity(u). Moreover, increase on hydraulic efficiency reduces power consumption and it gives possibility to use smaller and lighter battery. As a result of efficiency maximization, more portability for patients can be provided.

So, advantages explained above shows importance of hydraulic efficiency improvement. Pump will work as fluctuating to be in synchrony with heart cycles, so it won't have any static value for hydraulic efficiency. Overall efficiency (integral according to time) can be achieved by increasing peak of efficiency (η_{max}), moving peak of efficiency as close as to desired operation point and making efficiency curve as flat as to minimize difference between efficiencies at different flow rates. Averaged area under the efficiency curve (η_{mean}) can be used as comparison parameter between two designs in terms of curve flatness and mean efficiency was formulated as below within a range 4 and 8 L/min ($Q_{\max \& \min} = 8 \ \& \ 4\ L/min$). (Fig 2.13)

$$\eta_{h_{mean}} = \frac{\int_{Q_{min}}^{Q_{max}} \eta_h \, dQ}{Q_{max} - Q_{min}} \qquad \textbf{Eq 2.64}$$

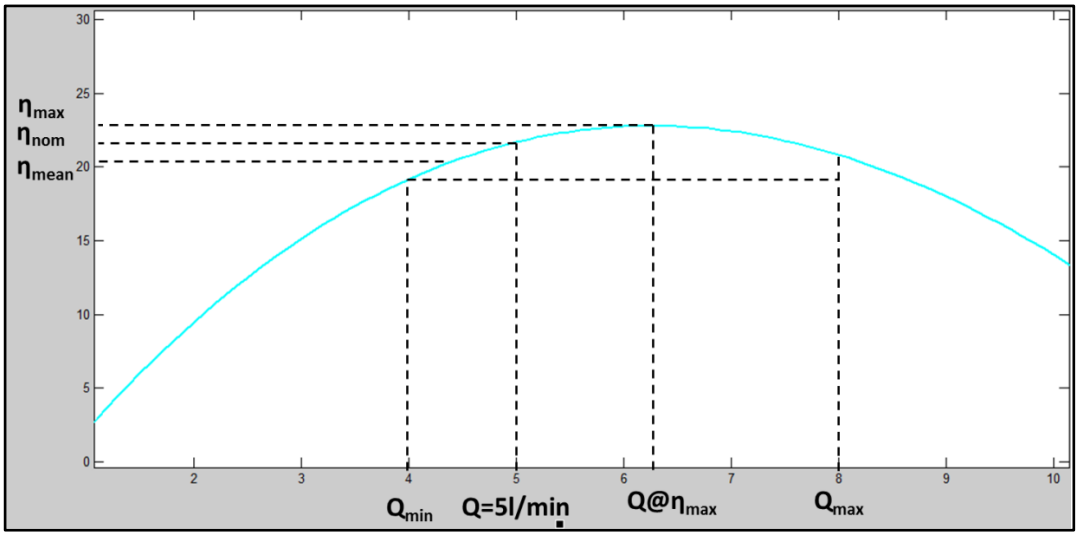

Fig 2.13: Efficiency Maximization Optimization Objectives Showed on Efficiency vs. Flow Rate Plot

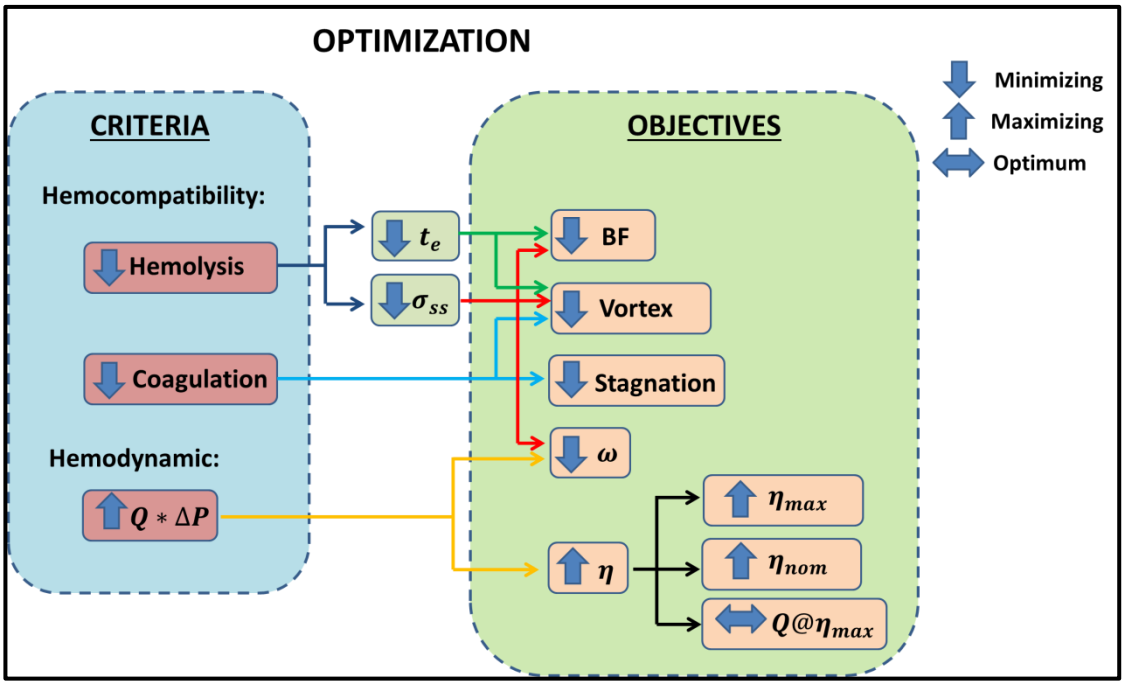

Fig 2.14: Optimization Objectives Required by Design Criteria (Optimization should be performed within anatomic constraints)

Some optimization objectives have priority over the others e.g. backflow has dominant role than rotational velocity on hemolysis. In short, optimization methods can be listed as below in terms of their importance:

1) **Minimizing backflow** between blade stages to reduce residence time of RBCs in pump
2) **Minimizing vortex zones** to reduce residence time
3) **Preventing Stagnation** to not cause coagulation
4) **Minimizing required rotational velocity** by producing same hemodynamic output ($Q * \Delta P$), to reduce shear stress (σ_{ss})
5) **Maximizing overall hydraulic efficiency** to minimize power consumption and require fewer blade linear velocity
    - Increasing peak of efficiency, η_{max}
    - Shifting peak of efficiency to desired operation point, $Q@\eta_{max}$
    - Increasing area under the efficiency curve, η_{mean}

As explained in *"1.1.7-Design Criteria, P:24"*, LVADs support heart function and it should provide sufficient blood blow against pressure difference between LV and aorta. For this project, hemodynamic output which is 5 L/min blood flow against 100 mmHg, was adjusted as desired optimum operation point of pump. So, optimization objectives were evaluated via CFD analyzing and compared between different geometries at this operation point.

Providing best for these optimization objectives is always better for LVAD designs, however it's also important that time is effective factor for development process. So, optimization process will be continued to observe objectives in acceptable range.

2.4.2. Optimization Parameters and Conventional Methods:

Pump geometric parameters were modified to achieve optimization objectives into their ranges explained above. These parameters were listed in *"2.2-3D VIRTUAL DESIGN (SOLIDWORKS®), P:51"* section.

3D visual geometry was computationally simulated by changing all geometric parameters one-by-one by keeping rest as constant to observe individual effects on flow dynamics and optimization objectives (ceteris paribus). Because when more than one geometric parameter is modified at same time, it's hard to observe weight of parameter effects on objectives (optimization variables) because of non-linearity.

Effects of some parameter modifications on flow dynamics were already studied by other researchers on field and it can be found in literature. For example, reducing cross sectional flow area (A_c) reduced flow capacity of pump and shifted optimum flow rate $(Q@\eta_{max})$ to the lower flow rates. Furthermore, tip or hub radius can be modified to reduce A_c and modification resulted as smaller blade height i.e. larger hub-tip ratio $\left({}^{r_h}/_{r_t}\right)$. Hereby, difference between pressure gradients at tip and hub plane got smaller and reduced backflow by enhancing flow field (flow pathlines). Furthermore, leakage flow occurs due to pressure difference between pressure and suction surface at blade tip region. So this leakage flow was minimized by reducing tip-shroud gap (g_t), however it caused increment on shear stress at blade tip and shroud. Also, backflow was reduced by increasing blade metal angle, however it caused drop on pressure rise. Such examples can show a way for parametric optimization.

3. RESULTS

3.1. OPTIMIZATION

3.1.1. Step-by-Step Parametric Optimization Process:

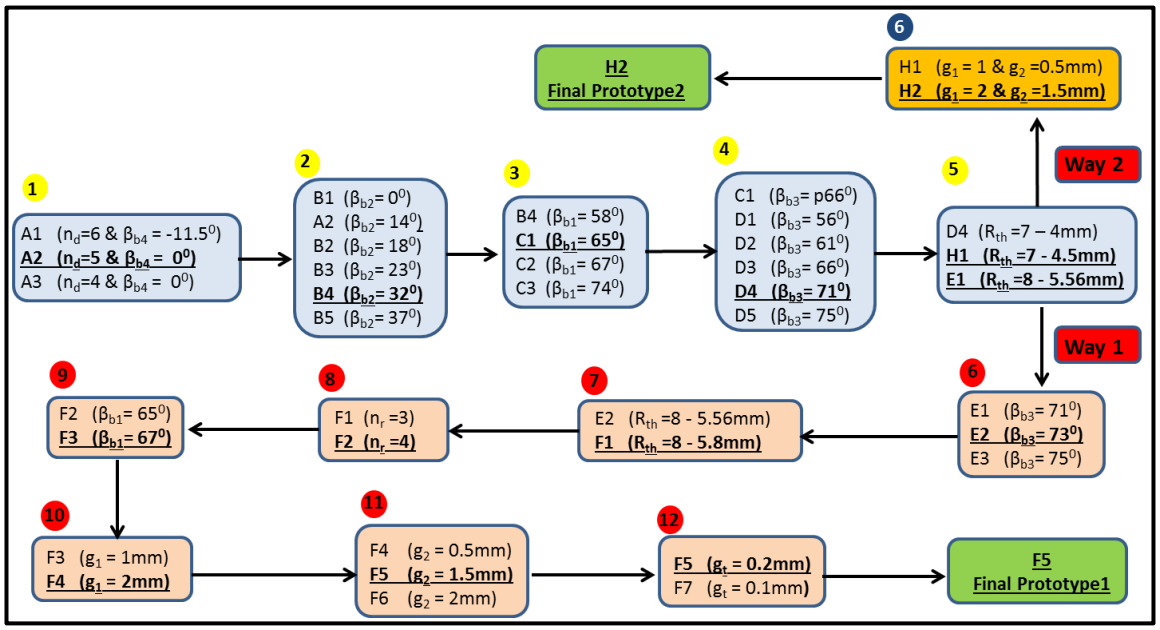

Fig 3.1: Step by Step Optimization Process Chart: Bold and underlined prototype code shows the best option among other prototypes in each step. Geometric parameter desired to be optimized, is shown on the right side of prototype codes.

Optimization of parameters was performed one-by-one for each parameter. First prototype was developed according to preliminary calculations or conventional selections on parameters. Then, only one selected parameter aimed to be optimized in any step, was modified by holding constant all other parameters and different prototypes were formed. CFD analysis was computed on different prototypes created by depending on only selected parameter. Effect of this parameter on optimization objectives (Fig 2.14) was numerically characterized by using CFD data and fitting them to plot. Then according to the comparison between different prototypes, best option of this design parameter was selected (bold and underlined prototype in Fig 3.1) and same process was repeated for other parameters in further steps. This step-by-step modification process is shown in Fig 3.1 until reaching final prototype which gives acceptable results on each optimization objectives.

Initially prototype A1 was designed with 7 and 4 mm radius at rotor blade tip and hub. Tip to shroud clearance (g_t) was selected as 0.2 mm in order not to make gap too small to cause excessive cell number for meshing operation and long computation time. So, cross sectional flow area of design A1 becomes 33π. Rotor was designed as 3 continuous helical blades and 3 smaller height blades at exterior surface of magnetic cylinder with inlet (attack, β_{b1}) and outlet (trailing, β_{b2}) vane angle respectively 58^0 and 14^0. Component length and continuous helical blade thickness were selected as 40 mm and 0.7 mm respectively. Furthermore, inducer was designed with 5 blades that have 12 mm length and 0^0 trailing angle at outlet edge (α_1). Also, Diffuser was designed with 6 blades with 18 mm length, 1 mm thickness, 66^0 and -11^0 attack (β_{b3}) and trailing (β_{b4}) angles respectively.[I] Furthermore, pressure surfaces of diffuser blades attack edges were shaped as circular instead of sharp edge, so β_{b3} doesn't match with its numeric value in 3D design. This type of attack edge designs were marked with "p" before numerical value. Moreover, gap between inducer-rotor blades (g_1) and diffuser-rotor blades (g_2) were specified as 1 mm.

		Attack Angle	Trailing Angle	Length	Blade Numbers	Blade Thickness	Gap
Prototype A1	**Rotor**	$\boldsymbol{\beta_{b1}}$ 58^0	$\boldsymbol{\beta_{b2}}$ 14^0	$\boldsymbol{l_r}$ 40 mm	$\boldsymbol{n_r}$ 3	$\boldsymbol{t_r}$ 0.7 mm	$\boldsymbol{g_t}$ 0.2 mm
	Inducer	- -	$\boldsymbol{\alpha_1}$ 0^0	$\boldsymbol{l_i}$ 12 mm	$\boldsymbol{n_i}$ 5	- -	$\boldsymbol{g_1}$ 1 mm
	Diffuser	$\boldsymbol{\beta_{b3}}$ p66^0	$\boldsymbol{\beta_{b4}}$ -11^0	$\boldsymbol{l_d}$ 18 mm	$\boldsymbol{n_d}$ 6	$\boldsymbol{t_d}$ 1 mm	$\boldsymbol{g_2}$ 1 mm

Table 3.1: Geometric Specifications of Initial Prototype (A1), $r_{t\text{-}h}$ = 7-4 mm

Then optimization process was started by using this initial geometry with one-by-one parametric approach.

Step 1: (Diffuser Blade Numbers, Trailing Angles and Thickness)

In first step of optimization process, enhancement on flow field that is affected by diffuser trailing angle and blade number, was done.

[I] Flow exits from rotor at same direction with u, so attack edge of diffuser was twisted at opposite direction of u (also opposite to rotor attack edge twisting direction) to welcome incoming flow (β_{f3}). However trailing edge of diffuser was twisted at same direction with u (opposite to β_{b3}), so β_{b4} was defined with minus sign to specify difference between diffuser edge twisting directions.

CFD analysis on prototype A1 showed that there was flow separation at 5^{th} mm from attack edge (inlet) of diffuser blades. This flow separation may occur due to space between blades or twisting shape of blade. Moreover, there was circulative flow at exit of diffuser due to camber at trailing edge.

So, prototype A2 was designed by reducing number of blades to 5 to extend space between blades. However, possible excessive increase in space between blades may cause flow separation too. So, thickness of blades was increased to 2 mm to reduce the space between blades. Moreover, trailing angle was reduced to 0^0 to minimize circulation at outlet, because reduced trailing angle minimizes tangential velocity of fluid as seen from Eq 2.11. According to CFD results, design A2 eliminated circulation at outlet and increased hydraulic efficiency. Although reduction of flow separation, it didn't eliminate all. So, prototype A3 was designed by reducing blade numbers to 4 and keeping trailing angle same with A2. However, excessive increase on space between blades resulted in worsening flow field across diffuser blades. Moreover, hydraulic efficiency decreased and backflow at inlet increased at nominal operation point (5 L/min and 100mmHg).

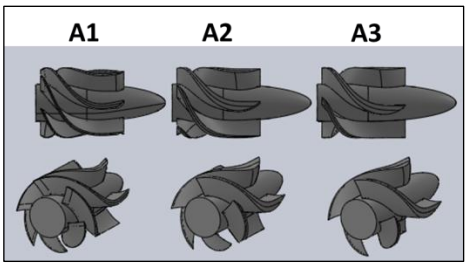

Fig 3.2: 3D View of A1-3 (All non-listed parameters are same with A1)

Prototype Codes	$\boldsymbol{\beta_{b4}}$	$\boldsymbol{n_d}$	$\boldsymbol{t_d}$
A1	-11^0	6	1 mm
A2	$\mathbf{0^0}$	**5**	**2 mm**
A3	0^0	4	2 mm

Table 3.2: Technical Specifications of A1-3 (All non-listed parameters are same with A1)

So, A2 gave best performance between all prototypes (A1, A2 and A3). According to prototype A2, blade numbers and trailing angles of diffuser was fixed as 5 and 0^0.

Step 2: (Rotor Trailing Angle, β_{b2})

As seen from Eq 2.8, rotor trailing angle (β_{b2}) is a geometric parameter that affects fluid tangential velocity at rotor outlet (v_{u2}) and hereby kinetic energy rise across rotor. Moreover, it affects incidence angle (θ_d) and backflow at diffuser inlet by effecting flow vector at this section. Furthermore, rotor trailing angle is a factor to shift optimum flow rate of pump as seen from Eq 2.40. Some of these effects of β_{b2} are more dominant than others but nothing can be decided exactly without CFD. So only by changing β_{b2} of prototype A2, 5 more designs (B1 to B5) were formed to see rotor trailing angle effects on flow field and hemodynamic performance.

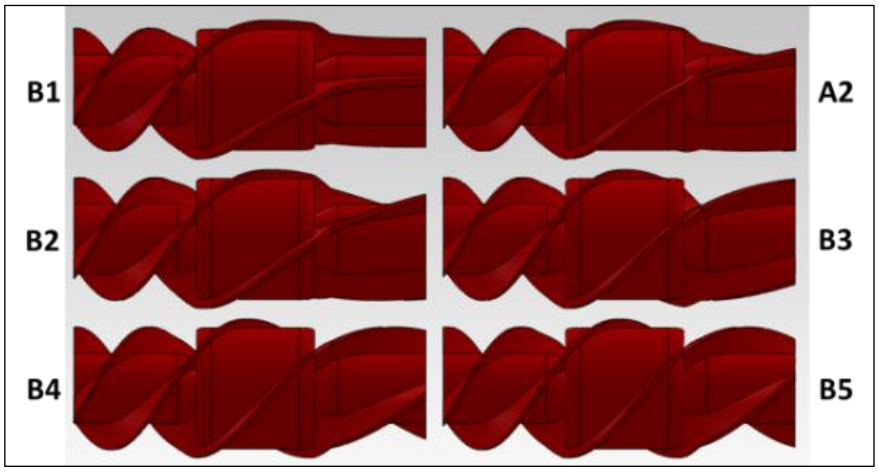

Fig 3.3: 3D View of Prototypes B1-5 and A2

Prototype Codes	β_{b2}
B1	0^0
A2	14^0
B2	18^0
B3	23^0
B4	32^0
B5	37^0

Table 3.3: Technical Specifications of Prototypes B1-5 and A2 (All non-specified Parameter are same with A2)

From Table 3.1, it is known that initially trailing angle for A2 was selected as 14^0. Other geometries B1-5 were respectively designed with 0^0, 18^0, 23^0, 32^0 and 37^0 trailing angles.

prototype code	%BF1 @ 5L	%BF2 @ 5L	η @ 5L	ΔP @ 5L (mmHg)	η max	η mean	Q@ ηmax (L/min)
B1	17,40%	35,23%	14,93%	96,8	19,50%	16,50%	9,35
A2	17,40%	36,91%	16,85%	107,2	21,31%	18,16%	9,20
B2	17,40%	35,04%	17,00%	107,0	21,95%	18,71%	9,00
B3	17,40%	34,44%	17,47%	106,4	22,38%	19,30%	8,60
B4	17,42%	32,92%	18,38%	102,4	22,81%	20,05%	8,20
B5	17,40%	32,69%	19,00%	101,8	22,62%	20,47%	7,60

Table 3.4: CFD Results of Prototype B1-5 and A2 (ω = 1060 rad/sec)

As seen from Table 3.4, there is no difference on backflow at rotor inlet because all designs have same rotor attack angle, 58^0. However, increasing trailing angle (β_{b2}) reduced incidence angle (θ_d) by reducing tangential velocity at rotor outlet(v_{u2}). As a result, backflow at diffuser inlet was decreased. However, attack angle of diffuser (β_{b3}) is more effective parameter than rotor railing angle on specifying incidence angle and therefore backflow at this location. So, backflow at diffuser inlet was mostly enhanced by modifying diffuser attack edge in further steps.

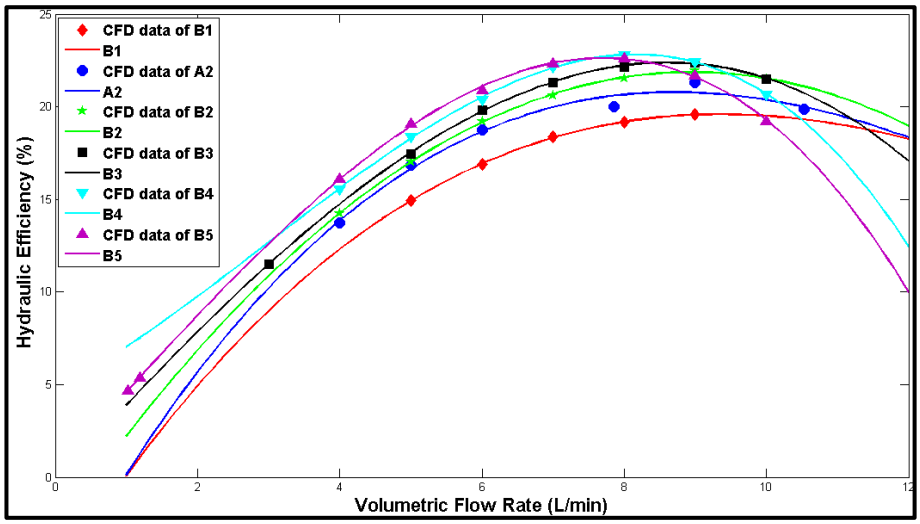

Plot 3.1: Efficiency Curve of Prototype A2 and B1-5

Increasing β_{b2} from 0^0 to 37^0 shifted peak of efficiency curve (pump nominal operation point, Q @ η_{max}) to lower flow rates from 9.35 to 7.6 L/min. Moreover, efficiency at desired operation point (η @ 5L) and average efficiency (η mean) were increased from

%14.93 to %19 and %16.5 to %20.47 by increasing β_{b2} to 37^0. Furthermore, it increased maximum efficiency of pump from %19.5 to % 22.81 until reaching 32^0, β_{b2} and then increasing β_{b2} caused drop on efficiency. Furthermore, efficiency at higher flow rates significantly dropped with increment on blade trailing angle and it can cause limitation on flow rate range for device usage.

Against these beneficial effects, increasing $\beta_{b2}$from 0^0 to 14^0 firstly increased head pressure at same rotational velocity but then increasing from 14^0 to 37^0 reduced it from 107.2 to 101.8 mmHg. It should be remembered that decrease on head pressure at desired flow rate can be recovered by increasing rotational velocity, hereby shear stress at tip and shroud will increase too.

In summary, the effects of β_{b2} on optimization criteria aren't linear. When it increases hydraulic efficiency, it causes drop on head pressure. So optimum β_{b2} exists in tried angles. However, determining this optimum value depends on optimization objectives and weights of their effects on device performance. So, optimization formula is required to exactly detect it. However, hemocompatibility especially due to backflow and shear stress, is most important criteria to achieve. So, reducing backflow and not causing drop on head pressure are effective performance comparison tools to select the best. From results in Table 3.4, increasing β_{b2} gave good result to reduce backflow but it also dropped head pressure, however 32^0 for rotor trailing angle was selected as the best trade-off between for both options, also it provided maximum of efficiency peaks. Therefore, design B4 was selected at this step.

Step 3: (Rotor Attack Angle, β_{b1})

Rotor attack angle is the most effective parameter on incidence at rotor inlet (θ_r), therefore most effective one on backflow at this location. So, 3 different designs addition to B4 were designed by changing rotor attack angle (β_{b1}) to characterize effects of incidence at rotor inlet. Flow angle at 5 L/min was calculated as 84^0 by using

Eq 2.5 and incidence angle (difference between flow and blade angle) at rotor inlet was calculated for 4 prototypes by using Eq 2.14 and listed in Table 3.5.[I]

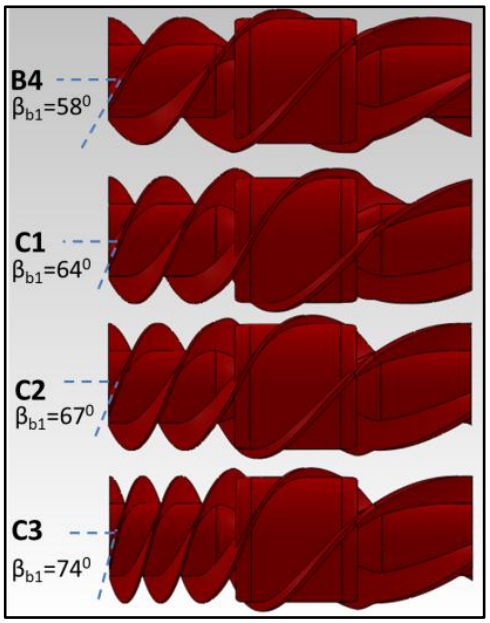

Fig 3.4: 3D View of Prototypes B4 and C1-3 (All non-specified parameters are same with B4)

Prototype Code	β_{b1}	θ_r	σ_r
B4	58^0	26^0	5,78
C1	64^0	20^0	6,31
C2	67^0	17^0	6,49
C3	74^0	10^0	7,49

Table 3.5: Technical Specifications of Prototypes B4 and C1-3 (All non-specified parameters are same with B4)

As seen from Table 3.5, increasing rotor attack angle (β_{b1}) up to flow angle, decreased difference between flow and blade metal angle (θ_r, incidence). Visualization of fluid streamlines and vectors by CFD at the inducer-rotor interface for each prototype (B4 and C1-3), illustrated the relationship between incidence and backflow. In Fig 3.5, velocity vectors (arrows) show forward (right) moving fluid around the inducer (horizontal on the left-hand side of each frame) towards the rotor blade attack edge.

[I] Incidence angle was calculated from 2D cascade analysis and it doens't give actual value in 3D flow domain.

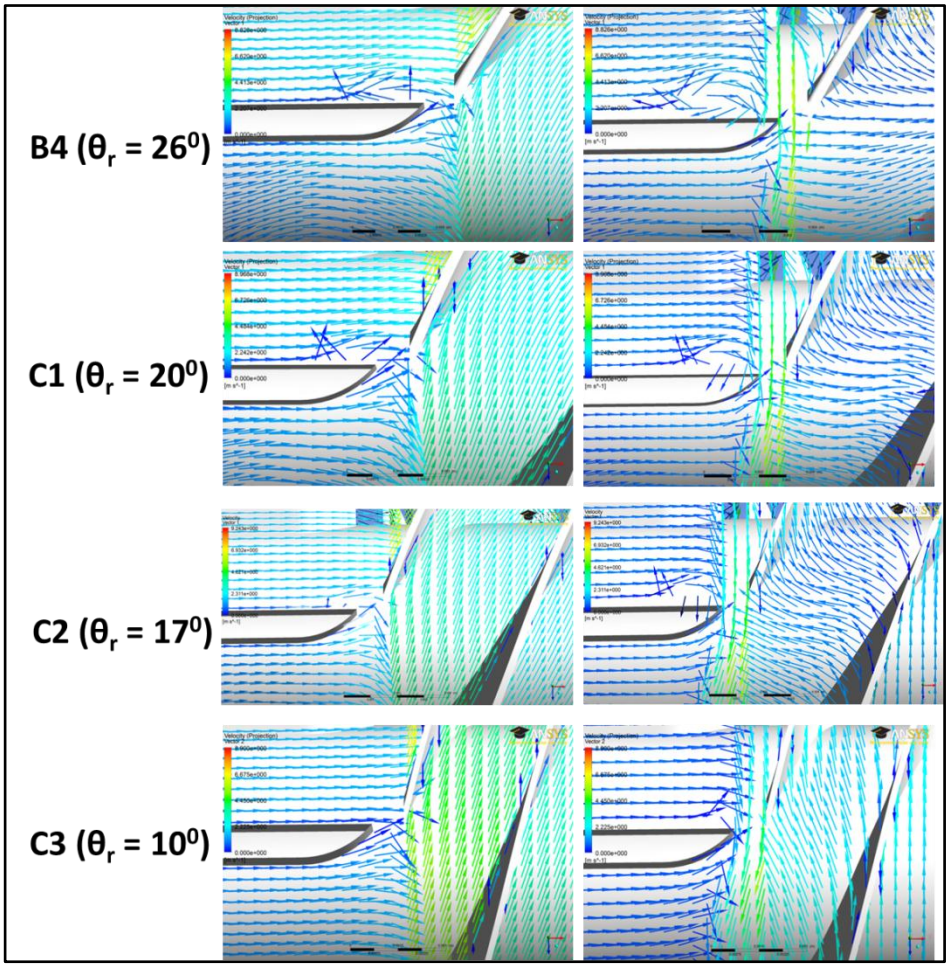

Fig 3.5: Velocity Vectors at Inducer-Rotor Interface, in Median and Tip Plane at Left and Right

As seen from velocity vectors at tip plane (frames at right hand side in Fig 3.5), flow vectors are at backward direction for prototype B4 that has 26^0 incidence. Backflow has high tangential velocity due to rotating blades and comes back to inducer section with high attack angle (almost orthogonal to inducer blades). Then, it collides to inducer blades and causes high shear stress at this zone. After collision, some part of backflow joins into forward flow and gets into rotor blades again. However, rest of backflow reaches interior of inducer due to continuously incoming backflow from rotary zone and then turns into forward direction. These actions due to continuous backflow cause vortex (circulative flow) in inducer core region.

Decreasing incidence to 10^0 significantly converted backward vectors to forward direction and eliminated vortex zone in inducer. Moreover in Table 3.6, reducing incidence to 10^0 from 26^0 reduced percentage backflow from ~%17 to ~%7. In

summary, reducing incidence provided better contact with fluid and reduced backflow at this section.

Prototype Code	%BF1 @ 5L	%BF2 @ 5L	%η @ 5L	ΔP @ 5L (mmHg)	%η max	%η mean	Q @ηmax (L/min)
B4	17,42%	32,92%	18,38%	102,4	22,81%	20,05%	8,2
C1	14,90%	33,52%	20,17%	108,7	24,04%	21,75%	7,9
C2	13,40%	32,58%	20,74%	108,4	24,33%	22,25%	7,6
C3	6,88%	32,16%	20,01%	96,4	20,33%	19,68%	6,0

Table 3.6: Performance of B4 and C1-3 on Optimization Objectives (ω = 1060 rad/sec)

Furthermore, reducing incidence angle shifted maximum efficiency point of pump to lower flow rates as well as increasing rotor trailing angle. Also, decreasing incidence up to optimum value increased nominal (at 5L/min), maximum and mean efficiency and head pressure at desired flow rate. After decreasing from optimum value reduced these optimization objectives.

In Plot 3.3, nominal (at 5L/min), maximum and mean efficiency and head pressure were scaled within 1 and 0; and plotted against incidence angle. So, optimum incidence for each optimization objectives is different; however all of them reach their maximum values at incidence within 20^0-17^0. So, C1 and C2 are between acceptable incidence ranges but C1 was selected for next optimization step.

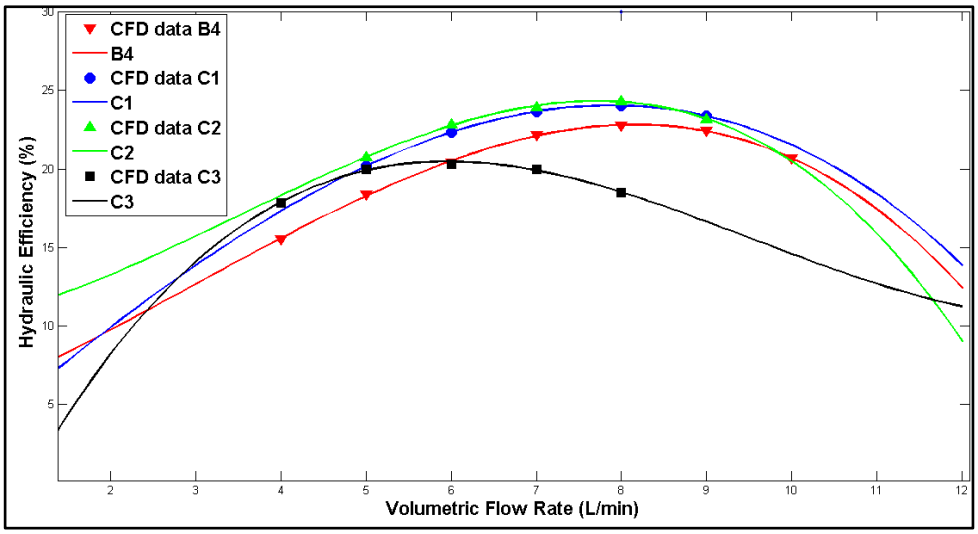

Plot 3.2: Hydraulic Efficiency vs. Volumetric Flow Rate of Prototype B4 and C1-3

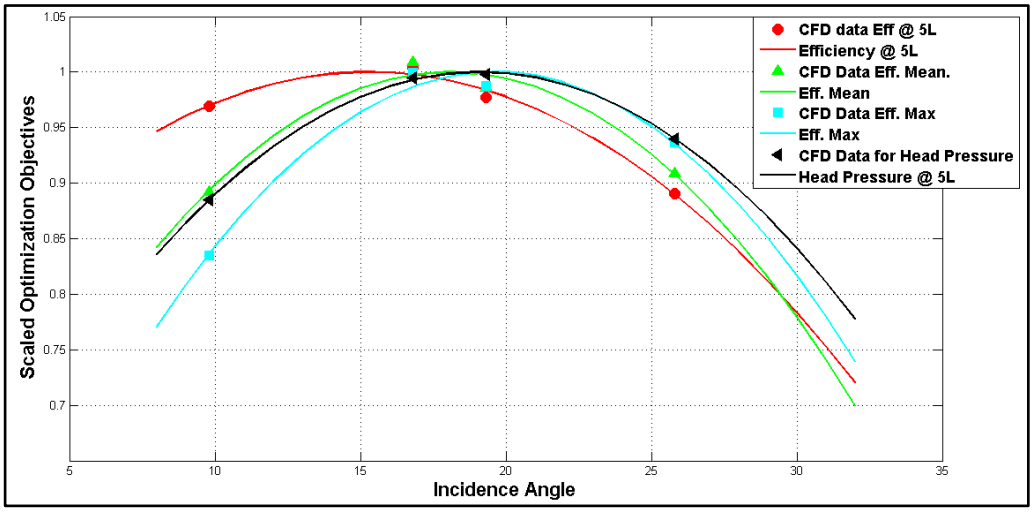

Plot 3.3: Optimization Objectives vs. Incidence Angle (%η @ 5L , %η max, %η mean and ΔH @ 5L; scaled by their maximum values).

Step 4: (Diffuser Attack Angle, β_{b3})

Firstly design C1 was modified by reducing gap between diffuser and rotor blades to 0.5mm from 1mm. After this modification, no difference on flow field at diffuser inlet was observed.

Then, diffuser attack angle was increased to minimize backflow at this section; in the other words incidence was reduced to provide better contact between fluid and diffuser blade attack edge. As known from Table 3.1, initially diffuser attack angle (β_{b3}) was selected as 66^0. However due to smooth curvature shape modification at pressure surface of diffuser attack edge, diffuser blade of C1 doesn't have sharp edge and hereby actual value of attack angle becomes less than 66^0. "p" sign was used before attack angle to define blades that has smooth curvature modification at pressure surface of attack edge. All other blade attack edges (if it doesn't have "p" sign before degree value) were designed by remaining pressure surface sharp, so β_{b3} for these type of blades represents actual value.

Then, 5 more prototypes (D1-5) were designed additionally to C1 by increasing attack angle from 56^0 to 75^0. By using Eq 2.9, fluid attack angle at diffuser inlet (β_{f3}) was calculated as 83^0. So, incidence angle varied from 27^0 to 8^0 as shown in Table 3.7.

Prototype Code	β_{b3}	θ_d
C1	$p66^0$	-
D1	56^0	27^0
D2	61^0	22^0
D3	66^0	17^0
D4	71^0	12^0
D5	75^0	8^0

Table 3.7: Technical Specifications of C1 and D1-5, $\beta_{f3} = 83^0$

Change on backflow field at rotor-diffuser interface in terms of incidence angle at diffuser inlet, were illustrated by Fig 3.6 by showing velocity vectors at mean plane. As seen from figure, velocity vectors through blade suction surface (dark blue vectors) tends to change flow direction from forward to backward and then passes to rotor section (backflow). Then flow turns to forward direction thanks to reaction with rotary blade and passes to diffuser region again. These actions with continuously incoming backflow create vortex zone in diffuser inlet region. From Fig 3.6, it seems that vortex zone becomes smaller by decreasing incidence angle from D1 to D5 and velocity vectors tend to flow more aligned with blades. Furthermore, backflow lines were directly visualized by illustrating in Fig 3.7. As seen, backflow streamlines are becoming less with decreased incidence angle. Both figures are evidence of decreased volumetric backflow at diffuser inlet section as a result of providing smoother contact between fluid and blade attack edge by decreasing incidence(θ_d). As listed in Table 3.8, decreasing incidence from 27^0 to 8^0 in designs D1-5 reduced percentage backflow from ~%27 to ~%13.

Furthermore, designs C1 and D3 have same type blade twisting ($\beta_{b3} = 66^0$), however only difference between them, C1 was formed with curvature while D3 was formed with sharp edge shape on pressure surface. Actually, sharp edge reduces incidence by depending on blade attack shape. So, sharp edge reduced percentage backflow from ~%34 to ~%23.

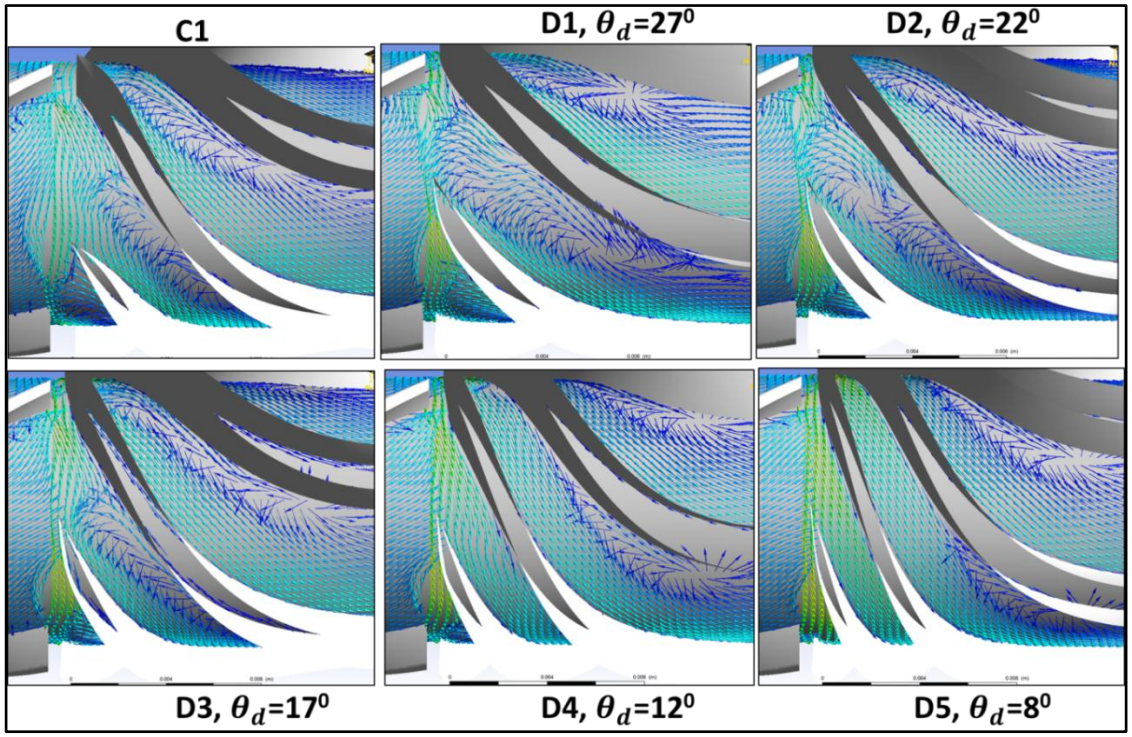

Fig 3.6:Velocity Vectors at Rotor-Diffuser Interface at Mean Plane

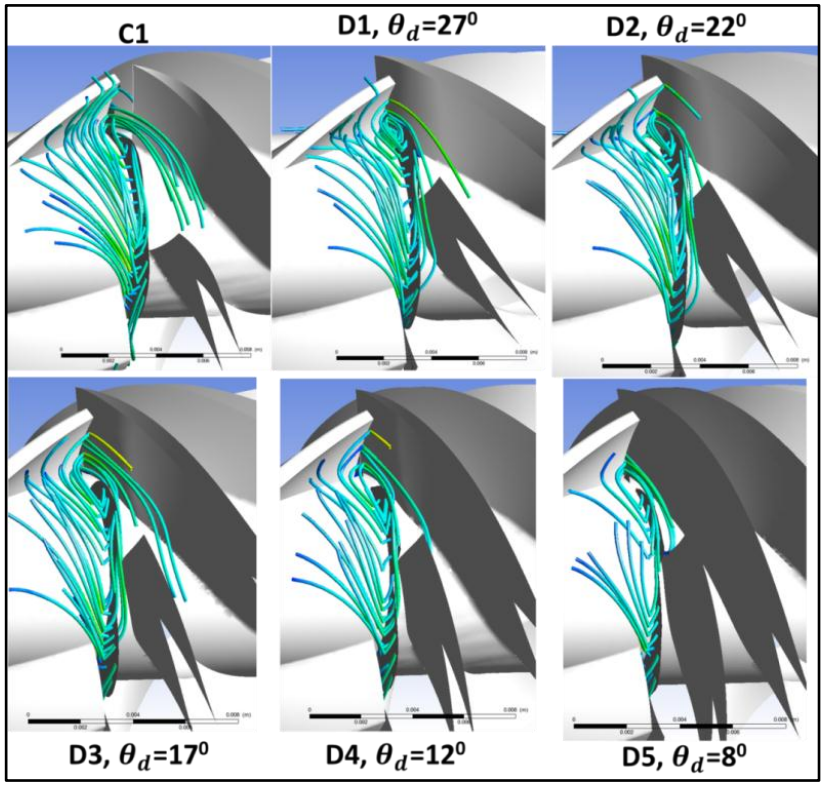

Fig 3.7:Backflow Streamlines (After 3ms Releasing from Rotor-Diffuser Interface)

Protot. Code	%BF1 @ 5L	%BF2 @ 5L	η @ 5L	ΔP @ 5L (mmHg)	η max	η mean	Q @ η max (L/min)	σ mean @ 5L (Pa)
C1	14,90%	33,52%	20,17%	108,7	24,04%	21,75%	7,9	519
D1	14,85%	27,18%	18,44%	92,3	21,95%	19,92%	7,6	508
D2	14,81%	25,22%	20,41%	99,7	22,91%	21,58%	6,8	507
D3	14,81%	23,35%	21,39%	100,0	22,80%	21,78%	6,3	505
D4	14,81%	19,33%	21,81%	96,5	22,30%	20,82%	5,5	505
D5	14,83%	12,95%	21,58%	88,5	21,50%	17,27%	4,7	508

Table 3.8:Performance of C1 and D1-5 on Optimization Objectives (ω = 1060 rad/sec , mean shear stress, σ was calculated by area averaging where shear > 400 Pa at shroud)

However, smooth curvature attack edge provided better hemodynamic performance with higher pressure rise and efficiency peak, ~109mmHg and ~%24 at 5 L/min flow and 1060 rad/sec rotational velocity. According to plot, curvature shape attack edge (C1, red plot in Plot 3.4) provides better hydraulic performance at higher flow rate than sharp edge prototypes. However, sharp edge which provides smaller incidence, was selected to minimize backflow at diffuser-rotor interface as a cost of head pressure drop, ~9mmHg at same volumetric flow rate and rotational velocity.

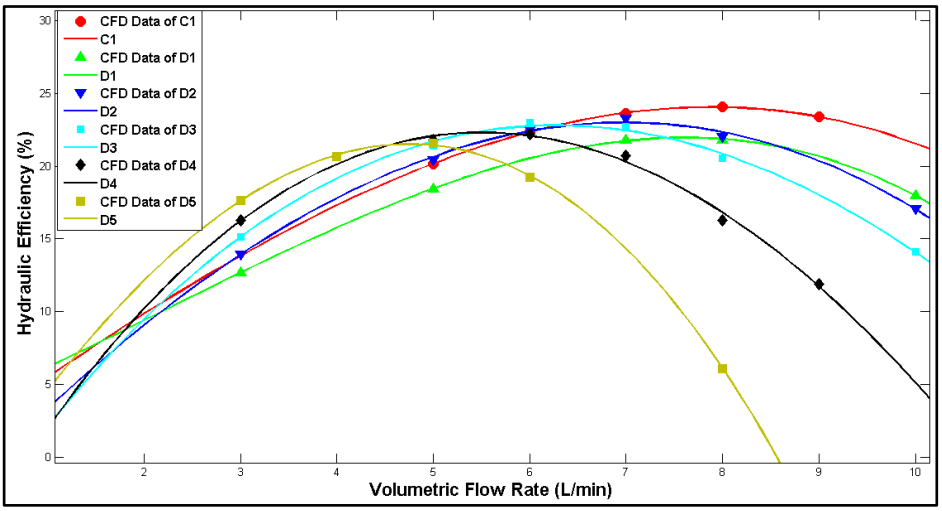

Plot 3.4:Efficiency vs. Volumetric Flow Rate of Prototype C1 and D1-5

Moreover incidence angle was decreased from 27^0 to 8^0 with designs D1-5 and it shifted peak of efficiency (Q@η max) to lower flow rates. Furthermore, it also shifted +x asymptote of curve to lower flow rates, so efficiency at higher flow rates dropped from ~%21.5 to ~%5 at 8L/min. Furthermore decreasing incidence to 17^0 increased

hemodynamic performance (D3), but then below the optimum incidence caused drop on head pressure. Moreover same quadratic characteristic was observed on nominal efficiency (at 5L/min), maximum and average efficiency by having different optimum incidence for each as occurred in rotor inlet incidence angle.

Decreasing incidence to 8^0 caused significant drop on head pressure which can only be recovered by increasing rotational velocity. So, prototype D5 was tested at higher rotational velocity to observe its performance at desired operation point (100mmHg at 5L/min). Head pressure was increased from ~88 to ~102 mmHg and matched with desired operation point by increasing rotational velocity from 1060 to 1105 rad/sec. However this time, higher blade linear velocity increased fluid attack angle and incidence angle. Hereby backflow at both interface increased. Furthermore, area averaged shear stress at shroud increased from 508 to 520 Pa (in Table 3.9 and Fig 3.8) and it is undesired result for hemocompatibility.

ω rad/s	**%BF1 @ 5L**	**%BF2 @ 5L**	**η @ 5L**	**ΔP @ 5L (mmHg)**	**η max**	**η mean**	**Q @η max (L/min)**	**mean σ (Pa)**
1060	14,8%	12,9%	21,58%	88,5	21,5%	17,3%	4,7	508
1105	16,2%	15,4%	21,66%	101,6	21,7%	18,4%	5,0	520

Table 3.9: Performance of D5 at Different Rotational Velocities.

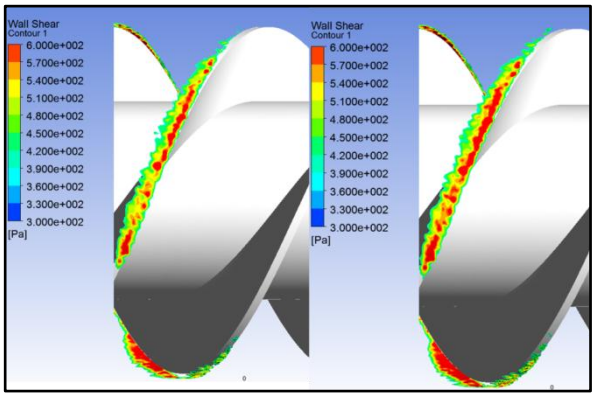

Fig 3.8: Shear Stress Contour of D5 at Shroud (ω = 1060 and 1105 rad/s at right and left respectively)

As seen from Table 3.8, D3 seems having best incidence angle, 17^0 as being optimum value for head pressure, nominal efficiency (at 5L/min) and mean efficiency. However, it couldn't succeed backflow criteria as being most important condition on hemocompatibility by effecting residence time of RBCs. Although reducing incidence to 8^0 decreased backflow more, hemodynamic performance significantly dropped and it was recovered by increasing rotational velocity which resulted higher stress on RBCs. As a result, any incidence value exists between them ($17^0$and 8^0) -that is not optimum for each, but best for all at the same time- and can be found by compromising from all optimization objectives as minimum as possible. Under this circumstance, 12^0 degree incidence (D4) was accepted as best for all optimization objectives at the same moment to not cause high drop on pressure rise and increment on backflow and shear stress. However, 12^0 incidence still didn't provide backflow within acceptable range. So, other pump geometric parameters should be modified together with diffuser attack angle to satisfy optimization objectives.

Step 5: (Cross Sectional Flow Area & Blade Hub-Tip Ratio)

As explained above, decreasing incidence below 12^0 via blade attack angle modifications isn't possible anymore to reduce backflow due to excessive drop on hemodynamic performance and efficiency at higher flow rates. By recalling Eq 2.14 and substituting fluid attack angle into, incidence was re-formulated. According to relation at below, narrowing cross sectional flow area is a way to reduce incidence angle by increasing axial velocity of fluid at same Q when it's not possible to modify blade attack angle, β_{b3}.

$$\theta_d = tan^{-1}\left(\frac{r_m\,\omega\,A_c}{Q} - tan(\beta_{f2})\right) - \beta_{b3}$$

Furthermore, pressure gradient at tip and hub plane are different due to linear velocity difference (u) at both plane and it causes dissimilarity on flow characteristic. So narrowing cross sectional flow area reduces blade height and minimizes difference between both planes (defined as hub-tip ratio, r_h/r_t); hereby it enhances flow field quality and reduces backflow.

As listed in Table 3.1, D4 has same dimensions with A1 as 7 and 4 mm radius at blade tip and hub ($A_c = 33\pi$ mm^2). Prototype H1 was designed by reducing A_c to 28.75 π by increasing hub radius to 4.5 mm without changing tip radius. Also, one more prototype (E1) was designed only by rearranging tip and hub radius 8 and 5.56 mm to increase hub to tip $\left({}^{r_h}/_{r_t}\right)$ ratio by keeping A_c same with D4.

Prototype Code	r_t (mm)	r_h (mm)	${}^{r_h}/_{r_t}$	A_c (mm^2)
D4	7	4,0	0,57	33π
H1	7	4,5	0,64	29π
E1	8	5,56	0,69	33π

Table 3.10: Technical Specification of Prototype D4, H1 and E1

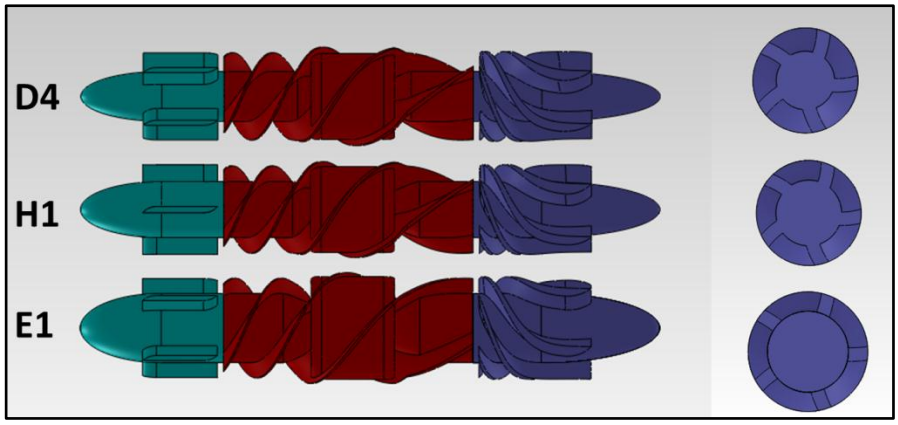

Fig 3.9: Side and Cross Sectional View of Prototype D4, H1 and E1, Respectively at Left and Right

	%BF1 @ 5L	%BF2 @ 5L	η @ 5L	ΔP @5L (mmHg)	η max	η mean	Q @ηmax (L/min)	mean σ @ 5L (Pa)	Ω rad/s
D4	14,8%	19,3%	21,8%	96,5	22,3%	20,8%	5,5	505	1060
H1	9,0%	13,5%	25,2%	103,0	25,1%	22,3%	5,1	530	1100
E1	11,5%	16,4%	26,1%	101,0	28,0%	26,5%	6,9	532	902

Table 3.11: Performance of Prototype D4, H1 and E1

As seen from Table 3.11, hemodynamic performance of H1 decreased because of reduced blade effective area as a result of smaller blade height and it was recovered by increasing rotational velocity up to 1100 rad/sec. Narrowed flow channel and increment on rotational velocity required as a result of modification, have opposite effects on incidence as seen in equation above. Nonlinear effect of cross sectional flow area on

incidence by changing operating conditions and 3D flow domain restricts to know actual value of incidence and its effects on backflow. However it obviously seen that H1 reduced percentage backflow to ~%9 from ~%14.8 and ~%13.5 from ~%19.3, respectively at inducer-rotor and rotor-diffuser interface by increasing hub-tip ratio$\left({}^{r_h}/_{r_t}\right)$. New design offered higher hydraulic efficiency as %25 and shifted optimum flow rate of pump to 5.1 from 5.5 L/min. Furthermore, increment on rotational velocity increased blade tip linear velocity and increased area averaged shear stress on shroud to 530 Pa from 505 Pa. All advantages of new design except shear stress increment were satisfactory, however nothing can be exactly known on hemocompatibility without doing in-vivo or in-vitro experiments to evaluate blood damage factor by using real blood.

Furthermore, in prototype E1 only hub-tip ratio was increased without changing cross sectional flow area. However, it was achieved by increasing tip radius and it changed all performance dynamics of pump. Increasing rotor blade tip radius to 8mm, increased pressure rise and offered possibility to reduce rotational velocity for same hydraulic output. So, prototype E1 operated at 902 rad/sec while D4 operated at 1060 rad/sec to satisfy 5L/min at ~100mmHg. Increasing hub-tip ratio significantly enhanced flow field and reduced backflow to ~%11.5 from ~%14.8 and ~%16 from ~%19.3, respectively at inducer-rotor and rotor-diffuser interface. However it should be noted that incidence at both blade attack edges differed due to change in rotational velocity and tip radius. Moreover, enhanced flow field resulted as increment on hydraulic efficiency of pump to ~%26 from ~%21.8. Furthermore, blade tip clearance-height ratio $\left({}^{g_t}/_{r_t - r_h}\right)$ increased in E1 and resulted as higher leakage flow which occurs at blade tip clearance due to pressure gradient difference between pressure and suction side of blade. Although increasing tip radius gave advantage to reduce rotational velocity, shear stress was increased due to higher leakage flow and centrifugal forces.

Furthermore higher leakage flow should cause increase on total backflow at inducer-rotor interface; however enhanced flow field via reduced tip-hub plane difference, possible decrement on incidence or both effects together had dominant role than leakage

flow and recovered backflow increment due to it. Hereby total backflow at this interface wasn't negatively affected by leakage flow.

Even though both optimization methods gave good results in terms of optimization aim, backflow at diffuser inlet still wasn't satisfactory. So, prototype E1 and H1 were used for further optimization steps respectively in way 1 and way 2.

Way 1 (Continue to develop E1):

Step 6.1: (Diffuser attack angle, β_{b3})

Diffuser attack angle couldn't be reduced below 12^0 in *step 4*, because of excessive drop on hemodynamic performance and efficiency at higher flow rates. Then, increment on tip radius and less hub-tip ratio enhanced flow field, increased hemodynamic performance and provided more flat efficiency curve that offers less hydraulic losses at higher flow rates. So, hub-tip ratio modification recovered drop on optimization objectives scarified as a cost of minimizing backflow via attack angle modification. And gave chance to modify β_{b3} more. So, prototypes E2-3 were designed additionally to E1, respectively by having 73^0 and 75^0 diffuser attack angle and 10^0 and 8^0 incidence angle when flow attacks with 83^0.[I]

Prototype Code	β_{b3}	θ_d	σ_d
E1	71^0	12^0	4,00
E2	73^0	10^0	4,08
E3	75^0	8^0	4,32

Table 3.12: Technical Specifications of Prototype E1 to E3

Decreasing incidence gave similar results on optimization objectives as occurred in *step 4*. As seen from Fig 3.10, backflow volume at rotor-diffuser interface significantly becomes less with decreased incidence. Furthermore, as seen from Table 3.13, decreasing incidence from 12^0 to 8^0 reduced percentage backflow from %18 to %14.5 without drop on hemodynamic performance. Also it shifted max efficiency point to the

[I] Incidence angle was calculated from 2D cascade analysis and it doens't give actual value in 3D flow domain.

lower flow rates, especially closer to the desired flow rate point, 5L/min (in Plot 3.5). However only disadvantage of E3 was reducing flatness of efficiency curve and causing more hydraulic losses when pump operates at higher flow rates. In short, it limited volumetric flow rate range for efficient usage of device.

It studied earlier that backflow can be eliminated by decreasing cross sectional flow area and increasing hub-tip ratio. Also effect of rotor-diffuser blade (g_2) gap wasn't studied yet. Before studying other geometric parameters effects that possibly offer alternative methods, modifying incidence for acceptable backflow as a cost of drop on other optimization objectives, is unnecessary. So 10^0 incidence (E2) was accepted for next optimization step.

	%BF1 @ 5L	%BF2 @ 5L	η @ 5L	ΔP @ 5L (mmHg)	η max	η mean	Q @ηmax (L/min)	ω rad/s
E1	12,5%	18,0%	25,8%	108,7	28,7%	27,0%	7,1	927
	11,5%	16,4%	26,1%	101,0	-	-	-	902
E2	12,1%	16,7%	26,3%	107,9	28,3%	26,9%	6,6	927
	11,6%	15,6%	26,8%	100,8	-	-	-	902
E3	12,2%	14,5%	27,0%	107,8	27,5%	26,1%	5,6	927

Table 3.13:Performance Results of Prototype E1 to E3

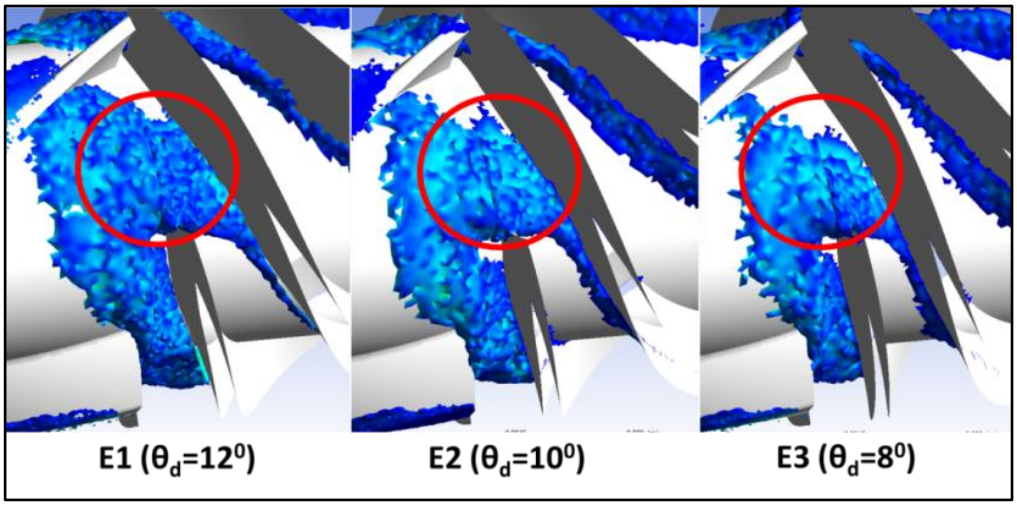

Fig 3.10: Flow Volume that Has Negative Axial Velocity (Backflow) at Rotor-Diffuser Interface of Prototype E1-3 (Q = 5L/min flow and ω = 927 rad/s)

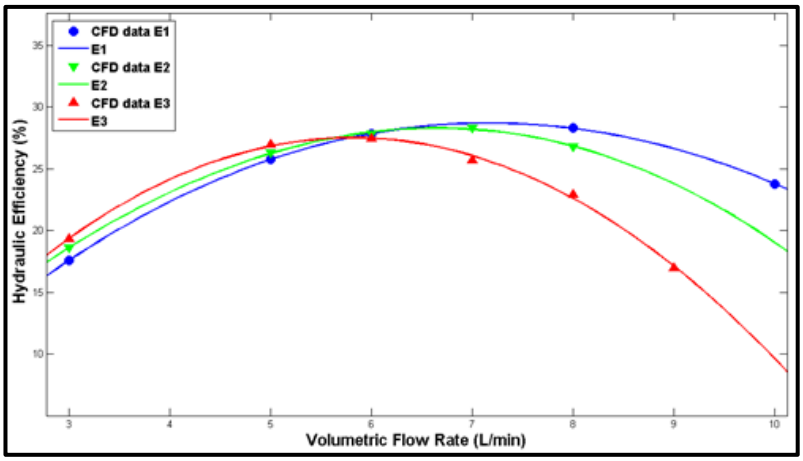

Plot 3.5: Hydraulic Efficiency vs. Volumetric Flow Rate of E1-3 (ω = 927 rad/s)

Step 7.1: (Cross Sectional Flow Area, A_c)

Prototype F1 was designed by decreasing cross sectional flow area to 30π mm^2 by increasing hub radius to 5.8 mm and keeping tip radius constant. So, hub-tip ratio was also increased ~%5 from 0.69 to 0.72 as a result of new configuration.

Prototype Code	r_t (mm)	r_h (mm)	r_h/r_t	A_c (mm^2)
E2	8	5,56	0,69	33π
F1	8	5,80	0,72	30π

Table 3.14: Technical Specifications of Prototypes E2 and F1

	%BF1 @ 5L	%BF2 @ 5L	η @ 5L	ΔP @ 5L (mmHg)	η max	η mean	Q @ ηmax (L/min)
E2	12,1%	16,7%	26,3%	107,9	28,3%	26,9%	6,6
F1	13,2%	12,8%	27,7%	104,3	-	-	-

Table 3.15: Performance of Prototypes E2 and F1 (ω = 927 rad/s)

New modification reduced pressure gradient difference between tip and hub plane and incidence at both blade attack edge thanks to narrowing flow channel. As seen from Table 3.15, F1 decreased percentage backflow at rotor-diffuser inlet to %12.8 from %16.7 by only dropping head pressure ~4 mmHg. As against, backflow at inducer-rotor interface increased which is opposite result according to previous studies (*step* 5).

Backflow at inducer-rotor interface is separately caused by non-smooth contact at attack edge (incidence), tip-hub plane linear velocity difference and leakage flow at blade tip clearance which occurs due to pressure gradient differences between pressure and suction side of blade tip. Although new modification reduced backflow by adjusting incidence and blade tip-hub ratio, increased tip clearance-blade height ratio $\left({}^{g_t}/_{r_t - r_h}\right)$ caused higher volumetric leakage flow at blade tip. Therefore total backflow at this location by combination of three reasons, increased to %13.2 from %12.1.

As a result, F1 provided satisfactory solution on backflow at rotor-diffuser interface even it caused drop on hemodynamic performance. However it didn't enhance flow field at inducer-rotor interface and it is possible to reduce leakage flow at this location by decreasing tip clearance later. So, presence of possible enhancement methods makes prototype F1 was acceptable as a result of this step.

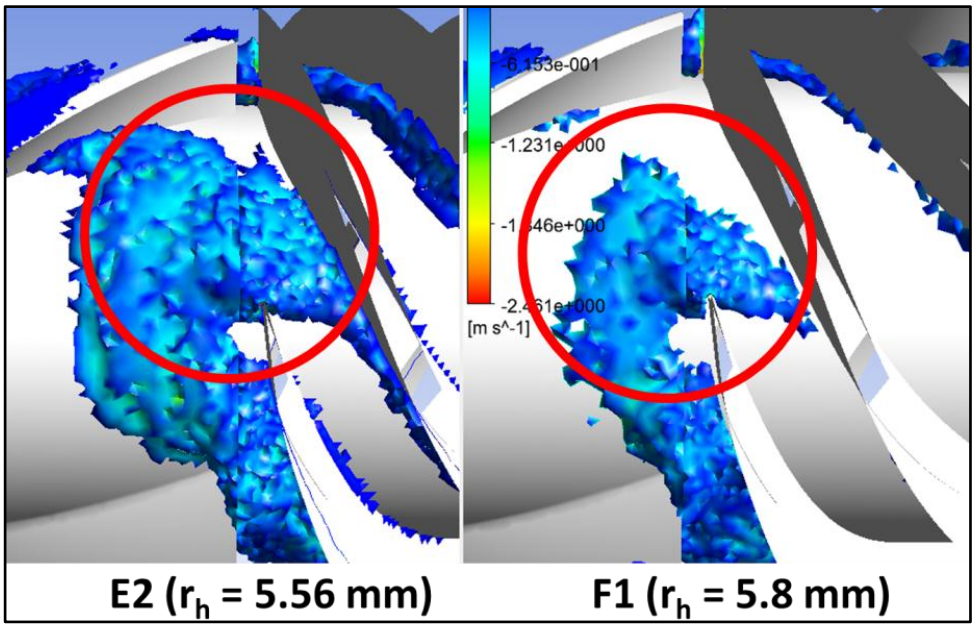

Fig 3.11: Flow Volume that has Negative Axial Velocity (Backflow) at Rotor-Diffuser Interface of Prototype E2 and F1 (Q = 5L/min and ω = 927 rad/s)

Step 8.1: (Rotor Blade Number, n_r)

As listed above, prototype F1 was selected with 8-5.8mm at tip and hub radius, 65^0 and 32^0 at rotor attack and trailing and 73^0 and 0^0 degree diffuser attack and trailing angles, respectively. Then another prototype (F2) was developed by increasing rotor blade numbers to 4 at both locations, continuous blades through all rotor and small height blades at exterior surface of magnetic cylinder. So, new design increased surface area of blade as an effective factor to sufficiently transfer energy to fluid, however also it may cause negative effects on flow dynamics due to decreased space between blades.

	n_r	σ_r
F1	3	6,021
F2	4	8,189

Table 3.16:Technical Specifications of Prototype F1-2

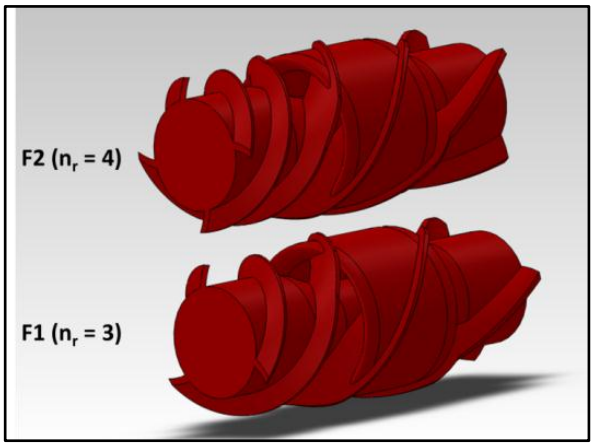

Fig 3.12:Isometric View of Prototype F1-2

As seen from Table 3.17, extra blade increased pressure rise ~4mmHg and nominal hydraulic efficiency up to ~%28.4. Better performance on energy transfer reduced leakage flow at blade tip clearance and it reduced total percentage backflow at inducer-rotor interface ~%50, to %7 from %13.2.

It's known that excessive shear stress on shroud at rotor inlet location, is caused by blade linear velocity and leakage flow at blade tip. Therefore, less leakage flow decreased shear stress to 510 Pa from 550 Pa which is significant positive result on hemocompatibility. Furthermore, increased hemodynamic performance also gave chance to reduce rotational velocity for same performance, hereby shear stress can be

reduced more. Although it enhanced flow field at inducer-rotor interface, extra blade didn't effect flow quality at rotor-diffuser interface.

	%BF1 @ 5L	%BF2 @ 5L	η @ 5L	ΔP @ 5L (mmHg)	η max	η mean	Q @ ηmax (L/min)	mean σ @ 5L
F1	13,2%	12,8%	27,7%	104,3	-	-	-	557
F2	7,0%	12,8%	28,4%	108,2	28,9%	27,5%	5,6	510

Table 3.17: Performance of Prototype F1-2 (ω = 927 rad/sec)

Step 9.1: (Rotor Attack Angle,β_{b1})

As explained in *step 3*, optimum incidence angle was evaluated within 20^0 and 17^0, and then, C1 was selected for further optimization steps with 64^0 β_{b1} and 20^0 incidence. However rotor attack angle modification is still optional by staying within its range to minimize backflow thanks to increased hemodynamic performance and efficiency at higher flow rates via hub-tip ratio and flow area modifications.

	β_{b1}	%BF1 @ 5L	%BF2 @ 5L	η @ 5L	ΔP @ 5L (mmHg)	η max	η mean	Q @ ηmax (L/min)
F2	$\mathbf{64^0}$	7,0%	12,8%	28,4%	108,2	28,9%	27,5%	5,6
F3	$\mathbf{67^0}$	5,7%	13,1%	29,4%	109,8	-	-	-

Table 3.18: Technical Specifications and Performance of Prototype F2-3 (ω = 927 rad/sec)

As known from Table 3.18, percentage backflow at inducer-rotor interface was around %7, so prototype F3 was designed by increasing rotor attack angle to 67^0 as being in acceptable incidence range to minimize backflow more. So, fewer incidence reduced backflow to %5.7 at inducer-rotor interface without causing drop on other optimization objectives.

Step 10.1: (Inducer-to-Rotor Gap, g_1)

Velocity vectors were illustrated with Fig 3.5. Flow firstly gains kinetic energy thanks to rotary blade, however it turns to backward direction (due to incidence, hub-tip ratio and blade clearance-height ratio) and gets into the inducer zone again with high radial velocity. Then backflow with high radial velocity, collides to inducer blades and causes high shear stress where collision occurs. After collision, flow separates into two ways.

In first, backflow turns to forward direction after interacting with incoming forward flow and immediately enters to rotor zone again, therefore this backflow stays in inducer with shorter duration. In second, backflow reaches core of inducer domain and then turns into the forward direction; however continuously incoming backflow from rotary zone forces transition of backflow into forward direction and converts forward flow into backward direction again. These continuous interactions causes vortex zone at core of inducer and increases residence time of flow particles into inducer region. In briefly, residence time in inducer section can be reduced by eliminating vortex which can be minimized by totally eliminating backflow or preventing collision.

In this step, inducer blades were moved further from rotor blades to see its effects on backflow and vortex. Another prototype (F4) was designed by increasing inducer-rotor distance to 2 mm from 1 mm by keeping all other parameters constant.

	g_1 mm	%BF1 @ 5L	%BF2 @ 5L	η @ 5L	ΔP @ 5L (mmHg)	Mean σ @ 5L (Pa)
F3	**1**	5,7%	13,1%	29,4%	109,8	512
F4	**2**	1,5%	13,3%	29,9%	108,8	503

Table 3.19: Technical Specifications and Performance of Prototype F3-4 (Q=5L/min, ω=927 rad/s)

As clearly seen from Table 3.19, increased inducer-rotor gap significantly reduced backflow at this location from %5.7 to %1.5. Possible reason on backflow minimization is quicken transition from backward to forward direction thanks to nonexistence of collision. Furthermore, eliminating collision decreased area averaged shear stress from 512 Pa to 503 Pa. In short, shorter residence time and less stress in F4 were good results for enhancing device hemocompatibility.

Step 11.1: (Rotor-to-Diffuser Gap, g_2)

Blade distance between two stages was tested in *step 10* and it resulted that larger gap between blades reduces contact between backflow and pre-stage blades; hereby flow field is eliminated from vortexes. Therefore, same method was applied to the rotor-diffuser interface with prototypes F5 and F6 designed with 1.5 and 2 mm gap, respectively.

As seen from Table 3.20 and Fig 3.13, increasing rotor-diffuser gap significantly reduced backflow; however it dropped head pressure too. Increasing gap from 0.5 to 1.5 mm reduced backflow and head pressure respectively %3 and 4.4 mmHg when increasing it from 1.5 to 2mm reduced backflow and head pressure around %1.7 and 5.1 mmHg. Widening gap more than 1.5mm reduced its effectiveness (weight) on optimization objectives and caused less reduction in backflow and higher drop on hemodynamic performance and efficiency at nominal point. Furthermore, F5 achieved %10 backflow as design criteria. In briefly, 1.5 mm rotor-diffuser gap was selected as best over the other prototypes, F4 and F6.

	g_2 mm	%BF1 @ 5L	%BF2 @ 5L	η @ 5L	ΔP @ 5L (mmHg)	Mean σ @ 5L (Pa)
F4	**0,5**	1,5%	13,3%	29,9%	108,8	503
F5	**1,5**	0,5%	10,3%	29,7%	104,4	502
F6	**2,0**	1,6%	8,5%	28,9%	99,3	505

Table 3.20: Technical Specifications and Performance of Prototype F4-6 (Q=5L/min, ω=927 rad/s)

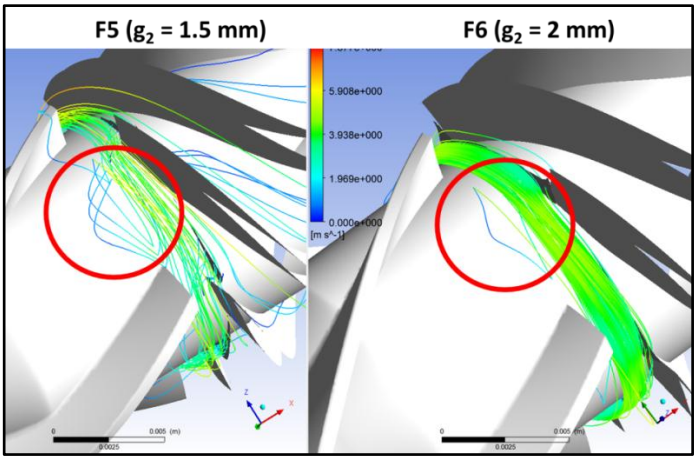

Fig 3.13: Streamlines of Backflow at Rotor-Diffuser Interface for prototype F5-6

Step 12.1: (Blade Tip-to-Shroud Clearance, g_t)

As explained earlier, pressure gradient difference between blade pressure and suction sides at blade tip, causes leakage flow at this location. Reducing rotor tip clearance doesn't change pressure difference, but effects volume of leakage flow via effecting tip clearance-blade height ratio $\left({}^{g_t}/_{r_t - r_h}\right)$. So, prototype F7 was designed by decreasing tip-shroud gap to 0.1 mm from 0.2 mm. Then both prototypes were tested via CFD method. As seen from Table 3.21, decreasing clearance at tip didn't give positive solution on backflow at rotor inlet, even though overall efficiency and hemodynamic performance increased. Furthermore, decreased gap caused excessive increment on shear stress level from 502 to 636 Pa (area averaged shear stress on shroud where shear stress is greater than 400 Pa) (Fig 3.14).

	g_t mm	%BF1 @ 5L	%BF2 @ 5L	η @ 5L	ΔP @ 5L (mmHg)	η max	η mean	Q@ηmax (L/min)	Mean σ @ 5L
F5	**0.2**	0,5%	10,3%	29,7%	104,4	29,6%	27,5%	5,37	502
F7	**0.1**	3,3%	7,5%	30,2%	105,6	30,3%	28,5%	5,15	636

Table 3.21 : Technical Properties and Performance of prototype F5-6 (Q =5L/min, ω=927 rad/s)

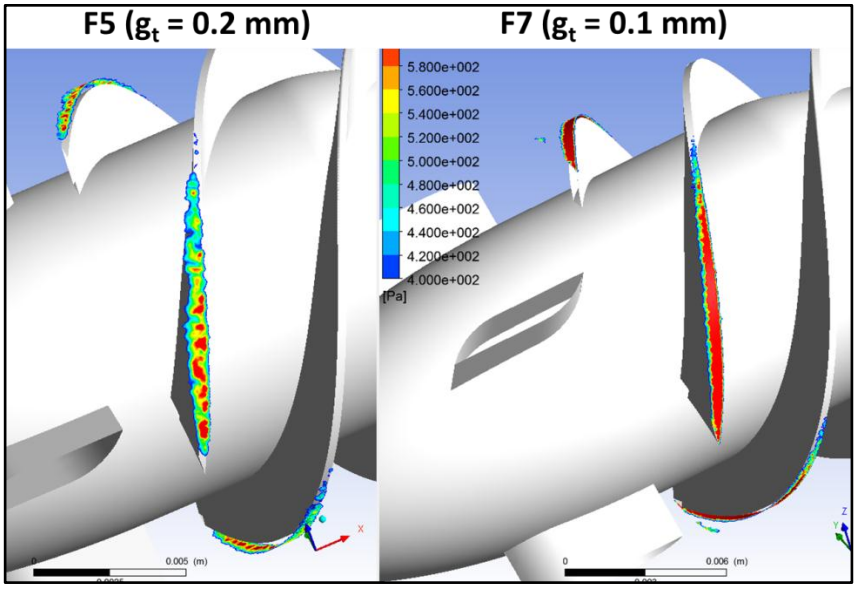

Fig 3.14: Shear Stress Contour of Shroud Surface that has greater than 400 Pa Wall Shear Stress

Way 2 (Continue to Prototype H1):

Step 6.2: (Gap at Interfaces)

As tested in *step 10* and *11*, reducing gap between inducer-rotor and rotor-diffuser blades significantly reduced backflow at both section. So, same method was applied to prototype H1 and H2 was developed. Respectively gap between inducer-rotor and rotor-diffuser were increased to 2 and 1.5 mm as in F4 and F5. As a result, backflow at both interface respectively reduced to %7.2 and % 12.4. However it also dropped head pressure ~7 mmHg.

	g_1	g_2
H1	1 mm	0,5 mm
H2	2 mm	1,5 mm

Table 3.22:Technical Specifications of Prototype H1-2

	%BF1 @ 5L	%BF2 @ 5L	η @ 5L	ΔP @ 5L (mmHg)	η max	η mean	Q @ ηmax (L/min)	mean σ @ 5L
H1	9,0%	13,5%	25,2%	103	-	-	-	530
H2	7,2%	12,4%	24,8%	96	25%	22,7%	5,3	522

Table 3.23: Performance of Prototype H1-2 (Q=5L/min, ω=1100 rad/s)

As a result of optimization process, prototype F5 and H2 [I] satisfied all optimization objectives in virtual domain. So, prototype development via CFD was completed with one-by-one parametric modification by showing their effects on flow dynamics and pump performance. However CFD results and pump performance, especially effects on hemolysis (backflow, shear stress and residence time) should be validated with in-vitro and in-vivo tests (PIV, Mock Circuit and clinical trials) to decide geometric parameters for commercial product. After all, if possible deviation between CFD and physical test results are observed, performance of device can be enhanced more in terms of modifications on geometric parameters that were listed between page 76-103.

[I] It just needs small modifications such in step 3, 4 or 8 (β_{b1}, β_{b3} or n_r)

3.2. FINAL PROTOTYPES (FPS) PERFORMANCES

3.2.1. Technical Details

As explained in "3.1.1-Step-by-Step Parametric Optimization Process:" section, two different prototypes F5 and H2 that satisfy all optimization objectives, were developed and respectively were named as "Final Prototype 1 (FP1)" and "Final Prototype 2 (FP2)". Basic pump geometric parameters for FP1 and FP2 were listed in Table 3.24.

		r_t (mm)	r_h(mm)	r_h/r_t	A_c (mm^2)	Blade Height up Magnet Cylinder	Attack angle	Trailing Angle	Blade Length (mm)	Blade numbers	Blade Thickness (mm)	Solidity	Gap (mm)
FP1 (F5)	**Rotor**	8	5,8	0,725	30,4π	0,8	β_{b1} 67^0	β_{b2} 32^0	l_r 40	n_r 4	t_r 0,7	σ_r 7,96	g_t 0,2
	Inducer						- -	α_1 0^0	l_i 5	n_i 4	- -	- -	g_1 2,0
	Diffuser						β_{b3} 73^0	β_{b4} 0^0	l_d 18	n_d 5	t_d 2,0	σ_d 4,30	g_2 1,5
FP2 (H2)	**Rotor**	7	4,5	0,643	28,7π	0,8	β_{b1} 65^0	β_{b2} 32^0	l_r 40	n_r 3	t_r 0,7	σ_r 6,29	g_t 0,2
	Inducer						- -	α_1 0^0	l_i 5	n_i 4	- -	- -	g_1 2,0
	Diffuser						β_{b3} 70^0	β_{b4} 0^0	l_d 18	n_d 5	t_d 2,0	σ_d 5,16	g_2 1,5

Table 3.24: Technical Specifications of Final Prototype 1&2 (F5 & H2)

Furthermore, blade twisting through length of blade was defined in terms of blade angle with axis. Rotor blade angle at each length of blade (1 to 40th mm) was plotted for FP1 and FP2 (blue and red line respectively in Plot 3.6 at top). In plot, rotor blade angle at 1st and 40th mm are respectively,$\beta_{b1}$and β_{b2}. Then blade angle was converted to pitch [I] parameter to easily use calculated parameters in CAD tools to form blade in 3D (Plot 3.6 at bottom). Then twisting shape of diffuser blades of FP1 and FP2 were also showed with same method in Plot 3.7. As seen, diffuser trailing angles were determined as 0^0, so blade pitch goes to infinity at diffuser outlet.

[I] Pitch is length, which twisting shape completes 360^0 rotation. It mostly used in screws to define space between two teeth.

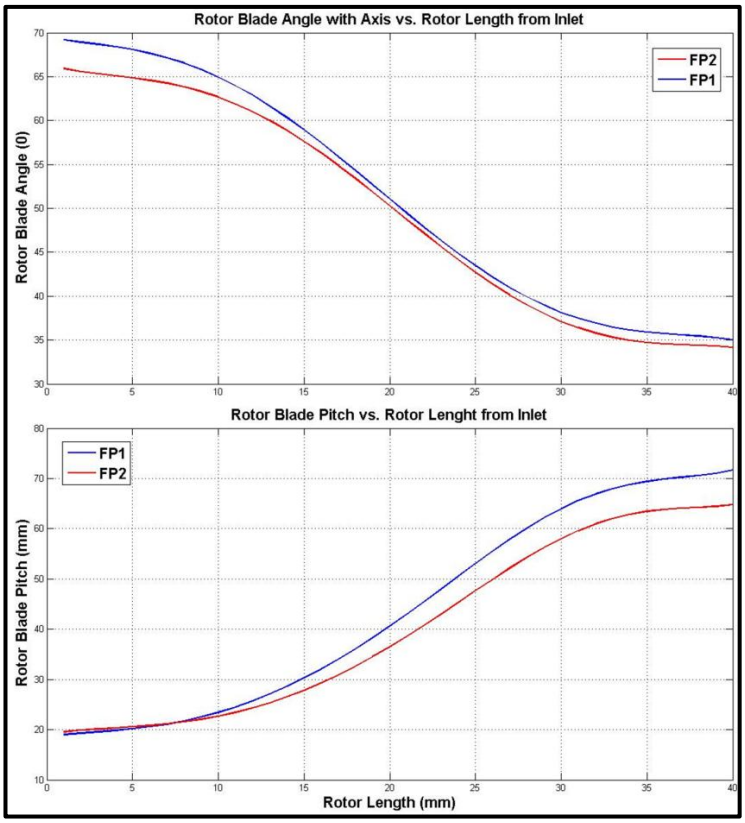

Plot 3.6:Rotor Blade Angle with Axis and Pitch vs. Blade Length at Top and Bottom Respectively

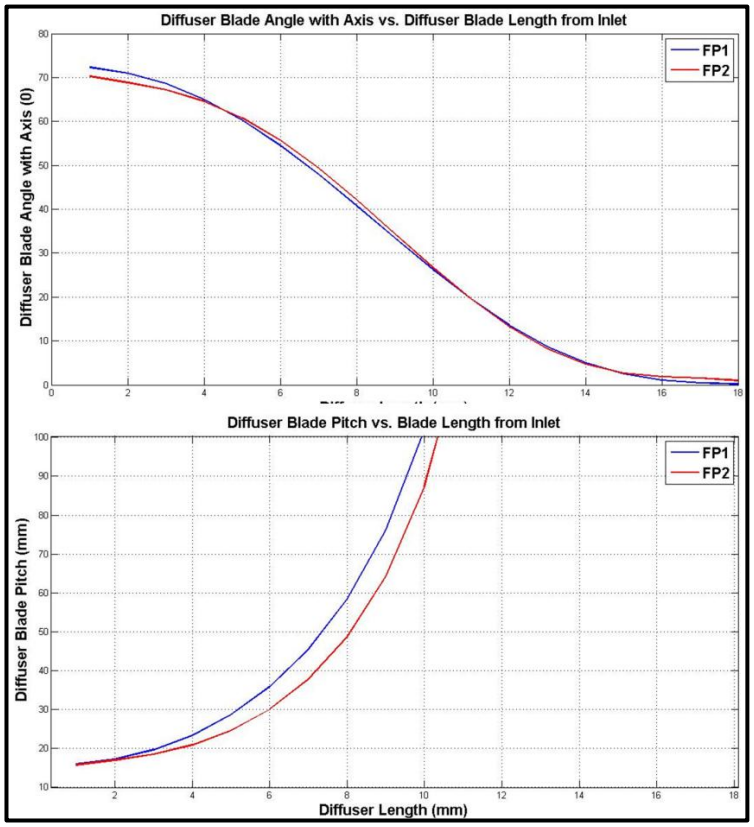

Plot 3.7: Diffuser Blade Angle with Axis and Pitch vs. Blade Length at Top and Bottom Respectively

Furthermore, geometric details of magnetic cylinder where permanent magnets of DC motor located, were descripted in Table 3.25 and listed parameters are just initial dimensions for magnetic cylinder; because magnet sizes and motor performance hadn't been tested via any simulation software or physical testing tools yet. So, permanent magnets dimensions and other motor parameters should be optimized via magnetic analysis to achieve mechanical performance to satisfy hydraulic performance. However, new magnet configuration doesn't restrict flow capacity of device by canalizing most of the flow via central channel. Therefore, optimization process of motor parameters via magnetic analysis, won't effect hemodynamic performance of pump thanks to flexibility on magnetic cylinder geometry.

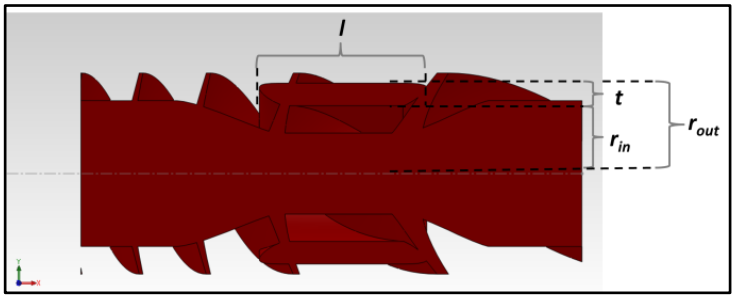

Fig 3.15: Magnetic Cylinder Technical Drawings of FP1

	l	r_{out}	r_{in}	t
FP1	13 mm	7.2 mm	5.4 mm	1.8 mm

Table 3.25: Initial Magnetic Cylinder Technical Specifications of FP1

	V (m^3)	**J ($Kg*m^2$)**	**m (gr)**
FP1	$4{,}149 * 10^{-6}$	$90{,}05 * 10^{-9}$	18,7
FP2	$3{,}035 * 10^{-6}$	$56{,}02 * 10^{-9}$	13,7

Table 3.26: Other Technical Parameters of FPs Rotor Components.

Furthermore, some other useful parameters final prototypes were listed in Table 3.26. Respectively "V", "J" and "m" represent volume, moment of inertia at rotation axis and mass of rotor component. Volume and moment of inertia was calculated from CAD tool by using 3D designs of prototypes. Then, mass of rotor component was calculated by forming it from titanium material that has 4506 kg/m^3 density by neglecting magnet and bearing mass.

3.2.2. Overall Hemodynamic Performance - Static

Hemodynamic performance at different rotational velocities and CFD results in terms of optimization parameters were showed in Table 3.27, for FP1 and FP2.

	BF1 L/min	%BF1 @ 5L	BF2 L/min	%BF2 @ 5L	η @ 5L	ΔP @5L mmHg	η max	η mean	Q @η max L/min	Area Av. σ shroud @5L Pa	ω rad/s
FP1	0,024	0,5%	0,546	10,3%	29,7%	104,4	29,6%	27,5%	5,37	502	927
	0,014	0,3%	0,489	9,3%	29,6%	98,7	29,2%	27,0%	5,23	496	910
	0,003	0,1%	0,345	6,7%	29,1%	80,6	29,2%	25,6%	4,70	484	850
FP2	0,402	7,2%	0,683	12,4%	24,8%	96,0	25,0%	22,7%	5,30	522	1100

Table 3.27: Performance of FP1 and FP2 (prototype F5 and H2)

As shown in Table 3.27, FP1 has 0.014 and 0.489 L/min volumetric backflow respectively at inducer-rotor and rotor-diffuser interface by being %0.3 and %9.3 of forward flow, at 910 rad/s rotational velocity which provides nominal hydraulic output (ΔP =100mmHg & Q =5L/min). Furthermore, FP2 provided 0.4 and 0.68 L/min backflow as being %7.2 and %12.4 of forward flow at inducer-rotor and rotor-diffuser interface. So, percentage backflow at both interfaces was reduced below %10 as being design criteria, in FP1. However, FP2 has greater than %10 backflow at rotor-diffuser interface; if it's necessary, backflow at this region can be reduced by increasing diffuser blade attack angle, narrowing cross sectional flow area or reducing difference between tip-hub plane.[I]

Furthermore, wall shear stress was calculated as 496 and 522 Pa respectively for FP1 and FP2 at 910 and 1100 rad/s (ΔP =100mmHg & Q =5L/min), by applying area averaging method for shroud surfaces where shear stress is greater than 400 Pa.

In Plot 3.8, hemodynamic performance of FP1 was showed by plotting efficiency and head pressure against volumetric flow rate at different rotational velocities.

[I] For details look, step 3, 4 or 5 (β_{b1}, β_{b3} or A_c)

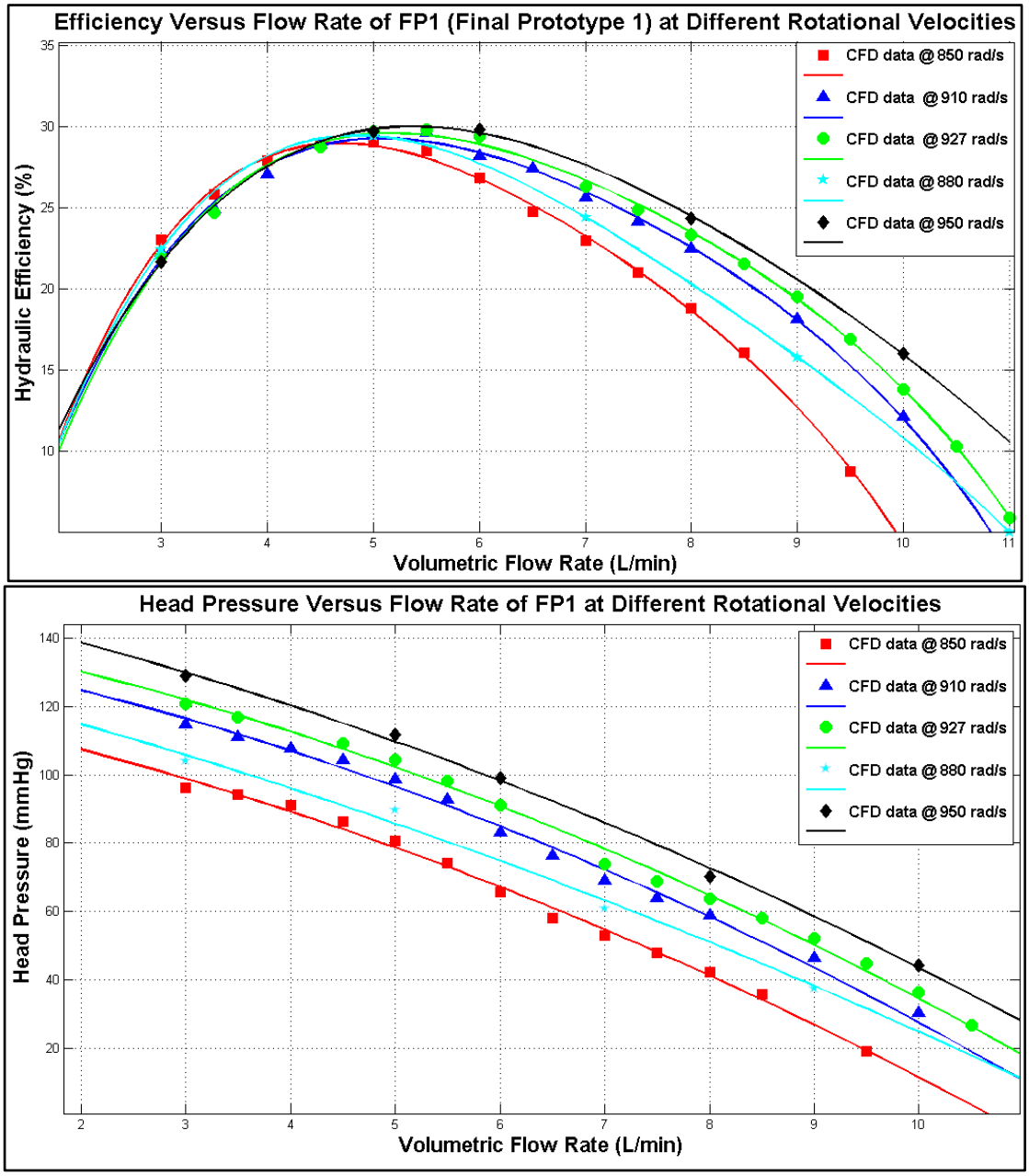

Plot 3.8: Hydraulic Efficiency and Head Pressure vs. Volumetric Flow Rate (for FP1)

Then, pump mathematical model of FP1 was derived by fitting CFD data to formulate pressure rise and efficiency as a function of flow rate (Q) and rotational velocity (ω). Pump head pressure was empirically formulated as;

$$\Delta P = aQ^2 + bQ + cQ\omega + d\omega + \mathrm{e} \qquad \textbf{Eq 3.1}$$

Where,

$$a = -0.4717$$
$$b = -5.634$$
$$c = -6.266 * 10^{-4}$$
$$d = 0.2944$$
$$e = -128.5$$

Also, hydraulic efficiency was modeled as;

$$\eta_h = a\,Q^3 + b\,Q^2 + c\,Q^2\omega + d\,Q\omega + e\,Q + f\omega + g \quad \textbf{Eq 3.2}$$

Where

$$a = 5.145 * 10^{-4}$$
$$b = -2.598 * 10^{-2}$$
$$c = 8.432 * 10^{-6}$$
$$d = 4.76 * 10^{-5}$$
$$e = 0.1064$$
$$f = -2.742 * 10^{-4}$$
$$g = 0.1839$$

In Eq 3.1 and Eq 3.2, Q is volumetric flow rate of pump in L/min , ΔP is head pressure in mmHg, ω is rotational velocity in rad/sec and η_h is hydraulic efficiency of pump as dimensionless ($0<\eta_h<1$).

Both equation models head pressure and efficiency of FP1 with coefficients in %95 confidence bounds. Degrees of system can be increased more to decrease mathematical model error e.g. adding ω^2 term. Furthermore, both equations were derived from CFD results within 750 and 950 rad/s, therefore they only model pump performance accurately where CFD tests were done. Out of range can be modeled with high error due to missing CFD data. Hereby, mathematical model should be developed to cover all operational range of device to use it for developing controller algorithm. In Plot 3.9 hemodynamic performance of pump was showed as 2D surface plot by using mathematical model of FP1.

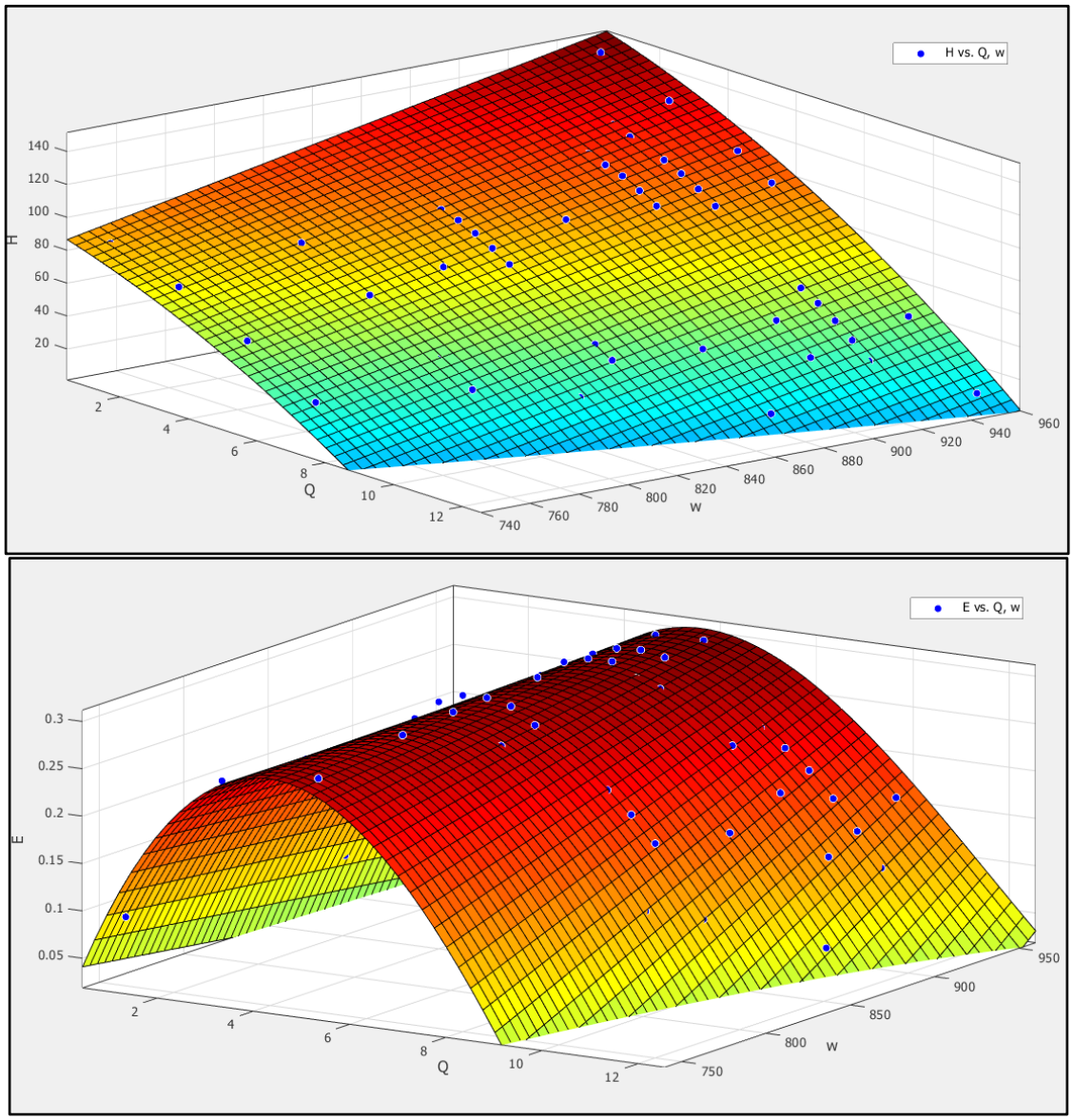

Plot 3.9: 2D Surface of Hemodynamic Performance. Head pressure and Efficiency vs. Flow Rate and Rotational Velocity at Top and Below (for FP1) (Q: L/min, H : mmHg, w: rad/s)

Furthermore, hemodynamic performance of FP2 was showed by plotting head pressure and hydraulic efficiency against flow rate in Plot 3.10. However, CFD tests were done only at 1100 rad/s rotational velocity. Hereby, FP2 pump mathematical model couldn't be derived due to non-enough CFD data. However, it should be derived with more CFD analysis which covers all operational range of FP2 for future tests and developing control algorithm.

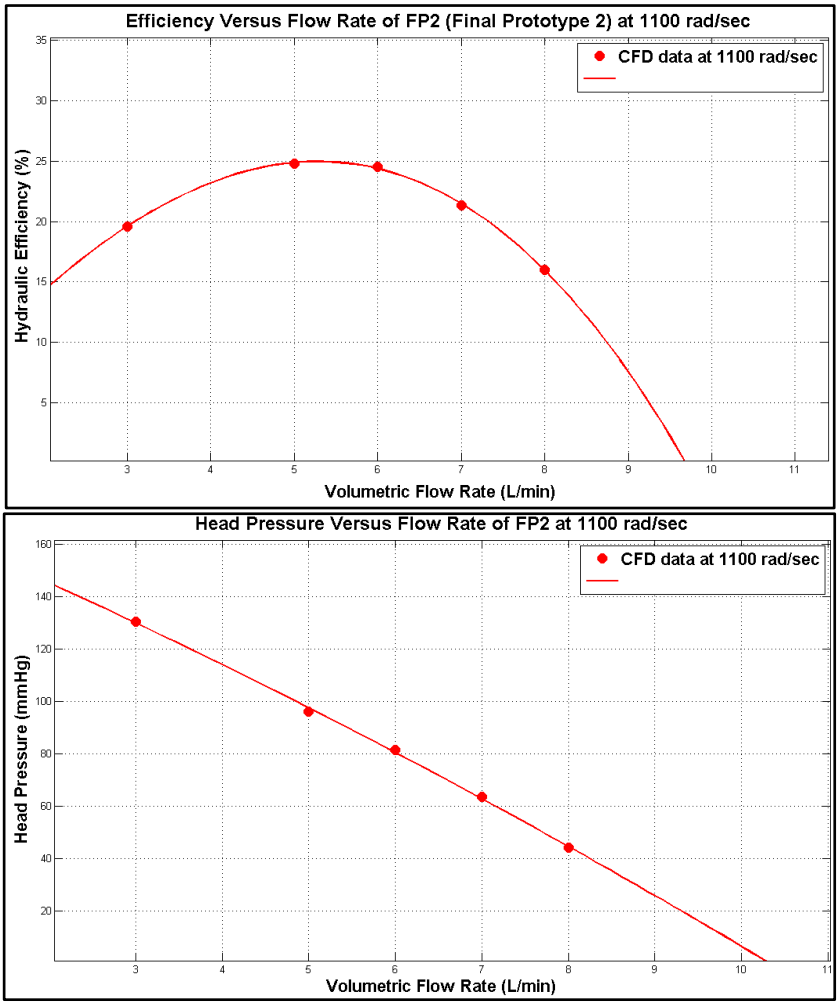

Plot 3.10: Hydraulic Efficiency and Head Pressure vs. Flow Rate (for FP2)

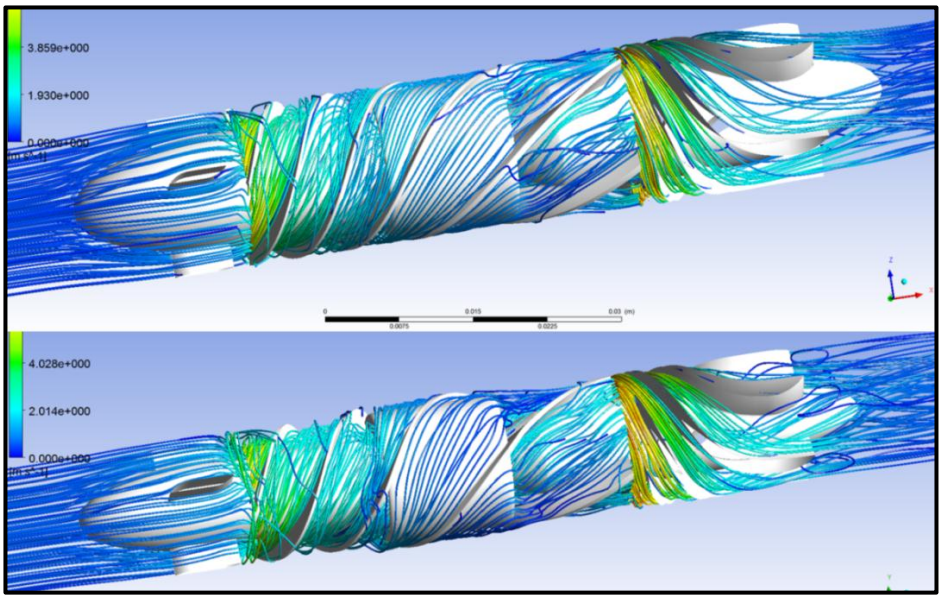

Fig 3.16: Streamlines of FP1 at Top and FP2 at Bottom (ω = 910 and 1100 rad/s, Q = 5L/min, ΔP = 100 mmHg)

3.2.3. Momentum, Axial Thrust and Power Characteristic - Static

When impeller pressurizes and accelerates fluid by exerting mechanical energy, fluid applies reactive force to the blade. Tangential component of this force (F_y) is torque (T_L, torque load of hydraulic system) required to be produced by impeller to overcome blood inertia and pressure difference to produce blood flow. Axial component of this force (F_x) exerts on blade at reverse of flow direction and pushes rotor to inducer direction. This axial thrust is important force factor for designing bearing mechanism to damp it.

According to CFD results on hemodynamic performance, force and power analysis were done and required mechanic output were listed in Table 3.28.

	Q (L/min)	**ΔP (mmHg)**	**ω (Rad/s)**	**T_L (mN.m)**	**F_x (N)**	**W_{in} (Watt)**	**W_{out} (Watt)**
FP1	5	104,4	927	4,2	0.4674	3,91	1,16
		98,7	910	4,1	0.4431	3,70	1,10
		80,6	850	3,6	0.3656	3,08	0,90
FP2		96,0	1100	3,9	0.4136	4,30	1,07

Table 3.28:Power Characteristic of FP1-2 (W_{in} is required input for hydraulic system or mechanical output)

It is also possible to model input power and torque requirement to simulate current draining from power source in electrical modeling or acceleration of device in mechanical modeling. W_{in}, W_{out} and T can be formulated by combining Eq 3.1 and Eq 3.2. However they weren't directly modeled in this project. Furthermore same modeling can be applied for FP2 if more CFD data are collected. So, all necessary results were listed in "APPENDIX A, A.5-PERFORMANCE RESULTS (ALL PROTOTYPES)" for future calculations and simulations. Moreover, some additional plots and 2D surfaces that show torque and power characteristic of FP1, were showed at below.

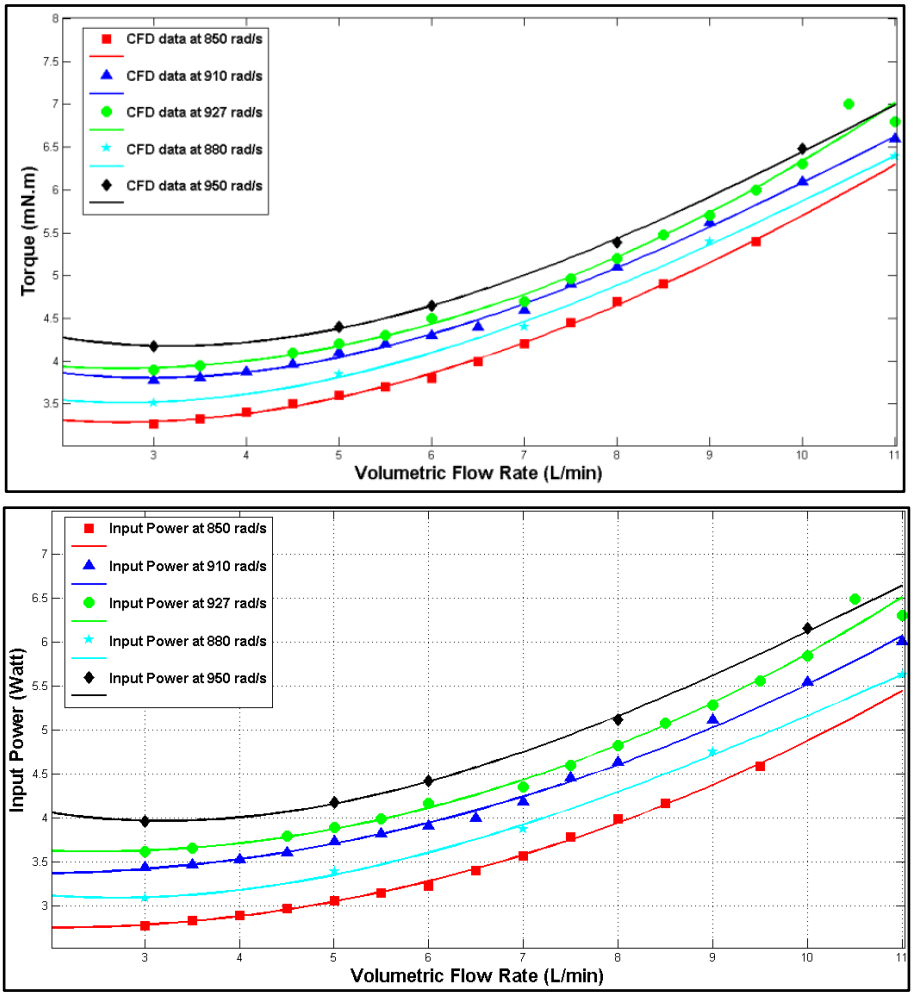

Plot 3.11: Torque and Input Power versus Volumetric Flow rate (FP1), at top and bottom

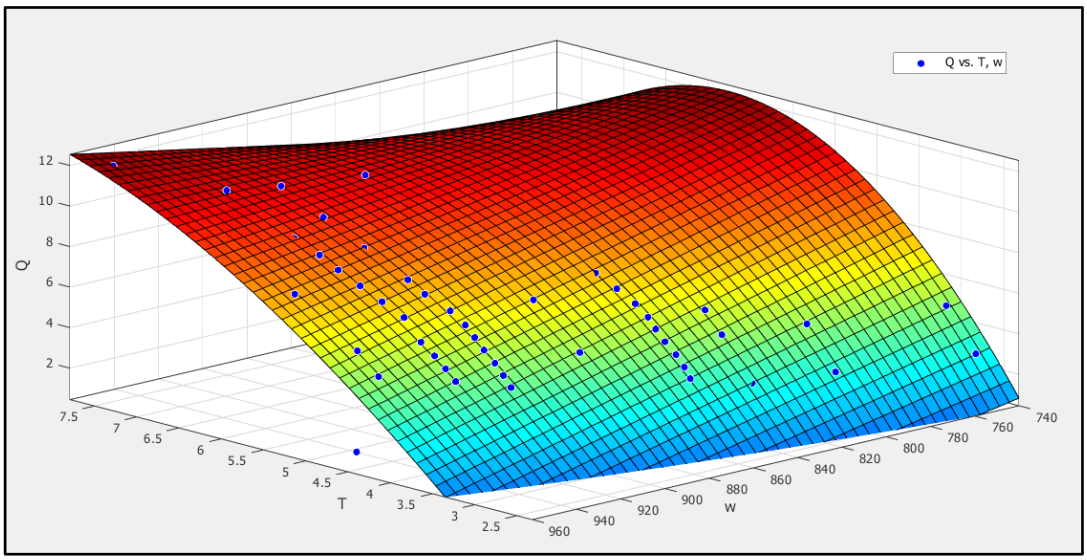

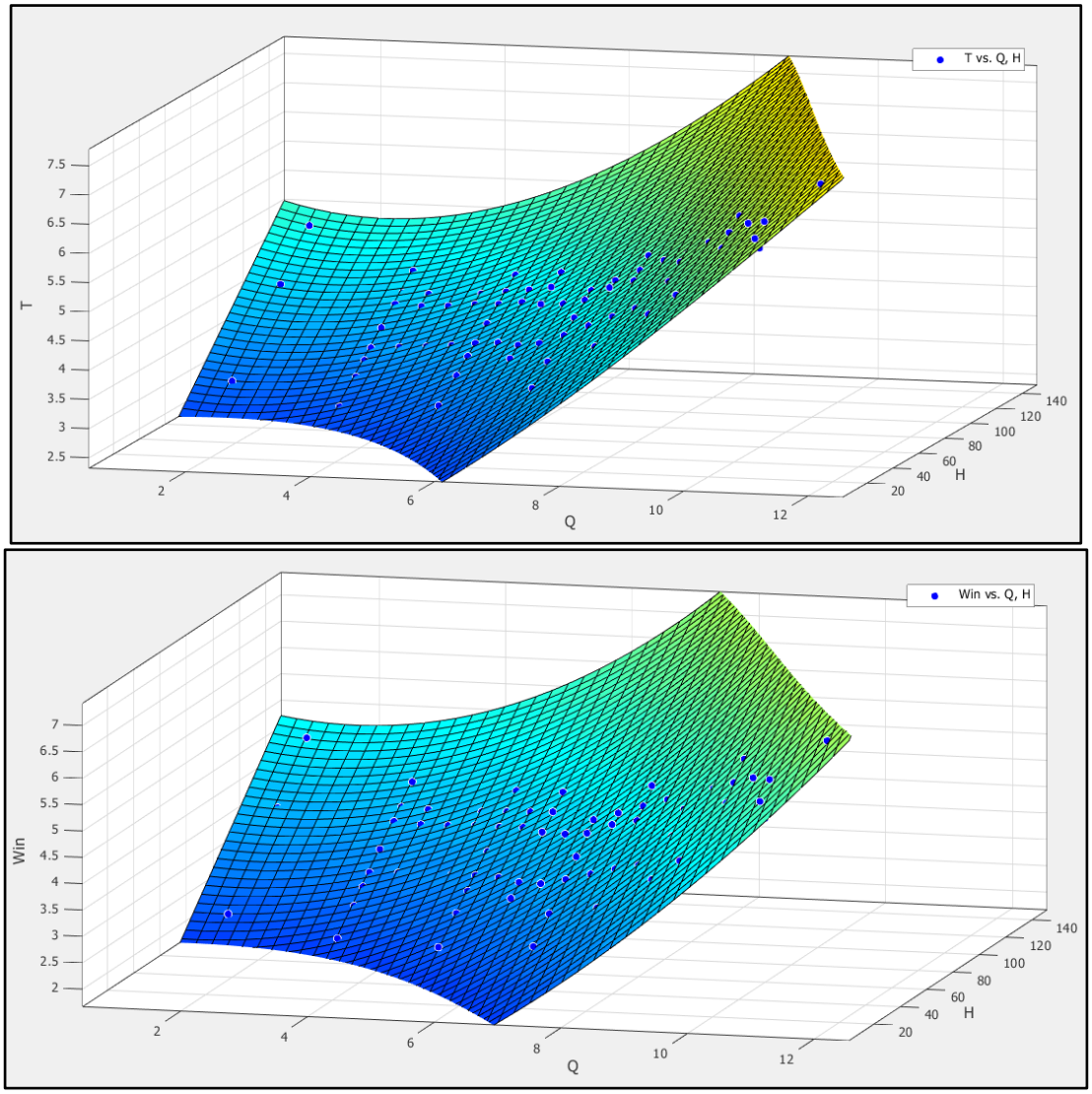

Plot 3.12: Surface Functions of FP1. Q: Flow Rate (L/min), w: Rotational Velocity (rad/s), T: Torque Load (mN.m), W_{in}: Input power (Watt), H: Head Pressure (mmHg)

3.2.4. Drag Coefficients

CFD tests gave hydraulic efficiency, head pressure and optimum flow rate ($Q(\eta_{max})$) at specific rotational velocity. So, drag coefficient ratios were calculated by using $Q(\eta_{max})$ in Eq 2.40. Then two unknown drag coefficients was reduced only one by using drag ratio, κ. After all, Eq 2.41 was used with hydraulic efficiency and ideal head pressure evaluated via CFD, to calculate C_D for rotor and diffuser blades.[I]

	$Q(\eta_{max})$ **L/min**	**ω rad/s**	$\kappa\ (C_{Dr}/C_{Dd})$
FP1	5,37	927	0,6026
	5,23	910	0,6011
	4,70	850	0,5941
FP2	5,30	1100	0,9163

Table 3.29: Drag Ratios of FP1-2

As seen from Plot 3.8, efficiency goes to zero at higher flow rates than $Q(\eta_{max})$, therefore drag coefficients goes to infinity. Plot 3.13 illustrates drag coefficient of rotor and diffuser blades for FP1 and FP2 at rotational velocity (respectively 910 and 1100 rad/s) which satisfies nominal design operation point.

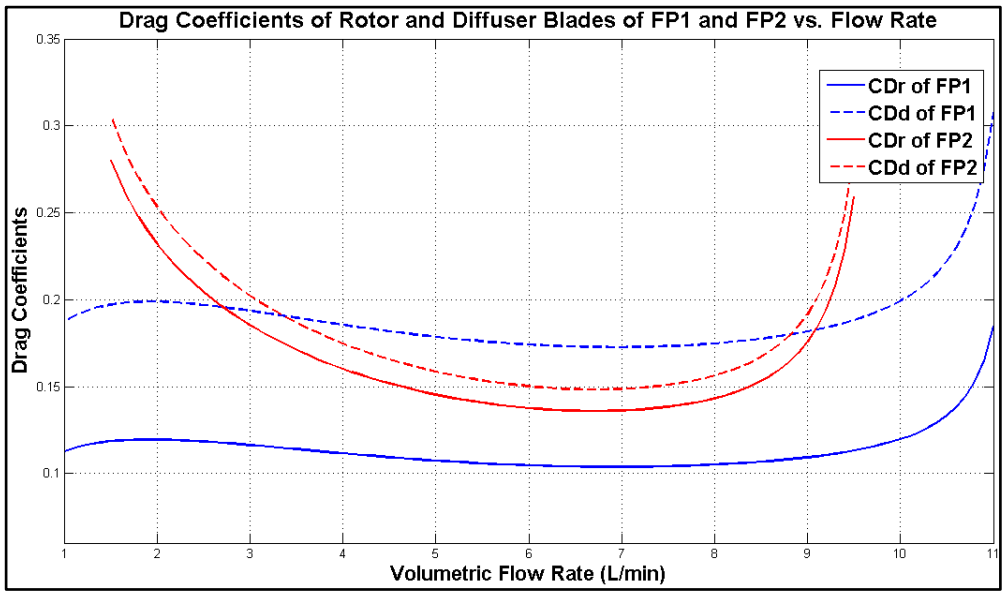

Plot 3.13: Drag Coefficient Graphs of FP1-2 (blue-red lines). Continuous and dashed lines respectively for rotor and diffuser.

[I] For details look Eq 2.41in P:43

3.2.5. Peripheral and Central Flow

	LF (L/min)	FF_p (L/min)	FF_c (L/min)	%LF	$\%FF_p$	$\%FF_c$	ω rad/s
FP1	0,0047	1,34	3,44	%0,13	%28,1	%72,0	910
FP2	0,0208	0,71	4,02	%0,52	% 15,0	%85,0	1100

Table 3.30: Volumetric Flow Analysis at Peripheral and Central Flow Channel (Q = 5L/min and ΔP = 100mmHg)

In Table 3.30, "LF" represents leakage flow from central to peripheral channel. "FF_p" and "FF_c" respectively defines forward flow rate through peripheral and central flow channel (exterior and interior flow channel). "%LF" and "%FF" signify percentage leakage flow from central to peripheral channel, $\left({}^{LF}/_{FF_c}\right)$ and forward flow at concerned flow channel according to total forward flow, $\left(\frac{FF_p}{FF_p+FF_c}\right)$. Flow rates were calculated at location where both channel combines (at end of magnetic cylinder).

As design possible disadvantage, pressure gradient in both flow channel can be different due to different linear velocities and blade surface areas. This difference may cause leakage flow from one channel to other channel. As seen from Table 3.30, 4.7ml/min blood flows at backward direction through peripheral channel. This value isn't exact volumetric leakage flow due to pressure gradient difference at both channel, however it is maximum value of possible leakage flow from central to the peripheral flow channel in FP1. In briefly, maximum %0.13 of forward flow through central channel turns into backward direction at the end of magnetic cylinder and gets in peripheral channel. This maximum leakage flow increases to 20.8 ml/min in FP2 by being %0.5 of forward flow through central channel.

Furthermore %28.1 and %72 of total forward flow passes through peripheral and central flow channel respectively, in FP1. This flow rates changes as %15 and %85 in FP2 due to changes on cross sectional flow area rates.

Moreover, Fig 3.17 illustrates streamlines that only pass through peripheral flow channel. As seen, flow lines have smooth pathway and don't cause any vortex or stagnant flow. As understood from results in table and visual objects, magnetic cylinder formation doesn't have any negative effects on flow dynamics and pump performance.

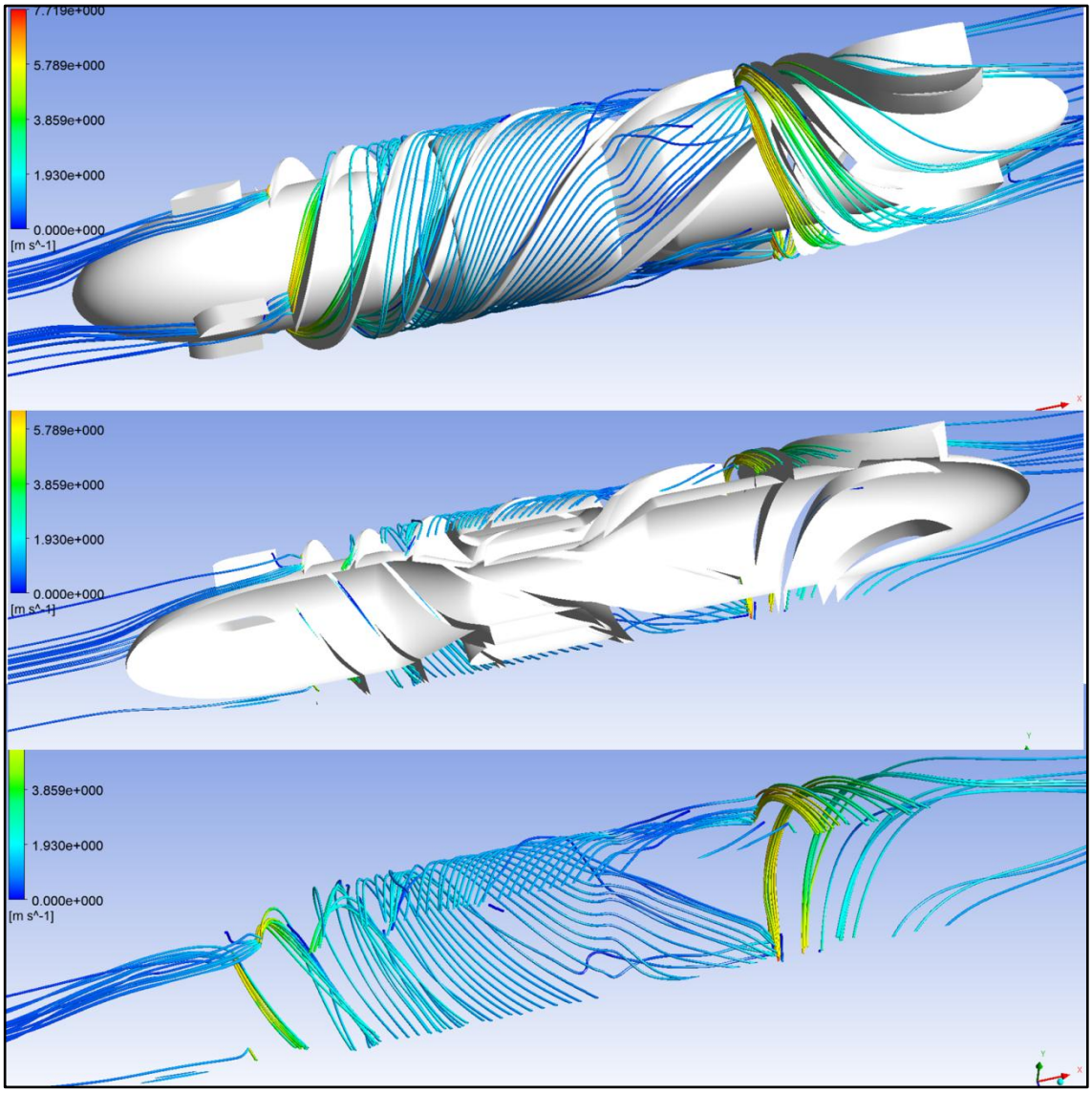

Fig 3.17:Streamlines Only Passes Through Peripheral Flow Channel (cross sectional view at middle and cross sectional view without blades at below)

3.2.6. Regurgitant Flow

In possible malfunction of pump, it doesn't work anymore and rotational velocity becomes zero. In this case when systolic cycle starts, aorta pressure gets larger than LV and blood flows at inverse direction (from outlet to inlet) through pump and it is called as regurgitant flow (Q_r). So, FP1 was tested by defining rotational velocity as zero. Then regurgitant flow was evaluated from CFD results. Furthermore, pump hydraulic resistance at inverse direction was calculated, $R_h = {}^{\Delta P}/_{Q_r}$ and listed.

	ΔP (mmHg)	Q_r (L/min)	R_h (10^8 kg/m^4.s)
FP1	50	-3,1686	1.2623
	80	-4,1476	1.5429
	100	-4,7621	1.6798

Table 3.31: Regurgitant Flow and Hydraulic Resistance of FP1 (ω= 0, $\Delta P = P_{Aort} - P_{LV}$)

3.2.7. Transition Time

Transition time of fluid can't be known exactly, because all fluid particles don't follow same pathway at same time. However it can be estimated by releasing streamlines from inlet and observing time when they reaches to outlet via CFD post processing tool. So 100 streamline were released from inlet and when most of them reached outlet (more than %50 streams), passing time were accepted as average transition time of fluid particles through pump. In Fig 3.19, most of the fluid particles (balls at exit of diffuser) reached outlet of pump in ~0.09 second after releasing from inlet for FP1. Same method applied to the FP2 and average transition time was observed as ~0.075 s.

	$t_{e_{ave}}$
FP1	85-90 ms
FP2	70-75 ms

Table 3.32: Average Transition Time of Fluid Particles Through Pump

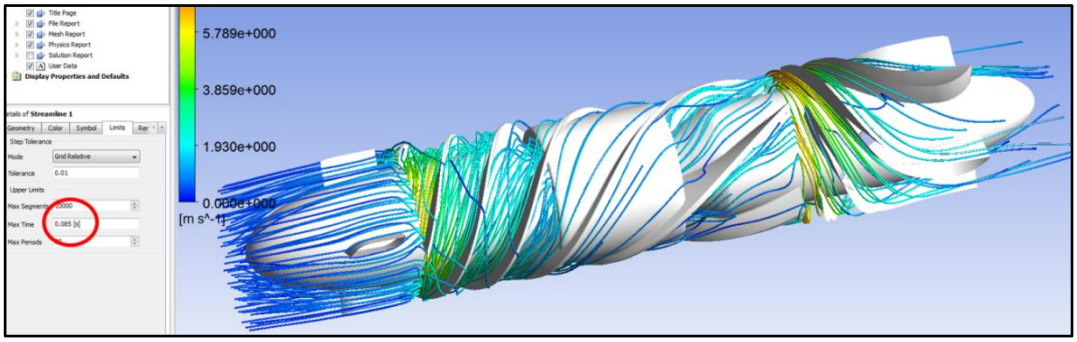

Fig 3.18: Streamlines of FP1, 85ms after releasing from inlet

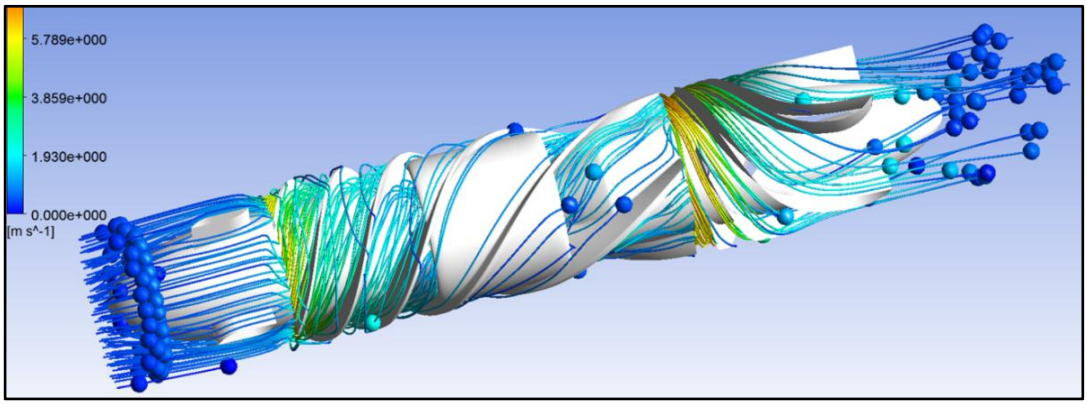

Fig 3.19: Balls at Outlet Shows the Location of Particles After 90ms Releasing From Inlet (in FP1)

3.2.8. Turbulence Quality

As explained in "2.3.1-Flow Modeling, P:59" section, dimensionless distance factor y^+ of boundary cells should be less than 5 in order to accurately use "enhanced wall treatment" for turbulence modeling at near wall zones. So, Eq 2.56 was used to calculate actual size of boundary cells to adjust y^+ below 5 by using preliminary wall shear stress value. However preliminary estimations on wall shear caused deviation from actual y^+ value, therefore CFD analysis was performed to see boundary cell locations and turbulence modeling quality at near wall zones.

In Fig 3.20, red zone shows the cell faces that has y^+ greater than 5. As obviously seen, red zone mostly covers area at inlet of rotor and diffuser blades where blood instantly accelerates and decelerates. Higher y^+ at this location was caused by high shear stress due to contact with incoming flow and blade. The other red face zone is interior side of magnetic cylinder where streamline direction changes.

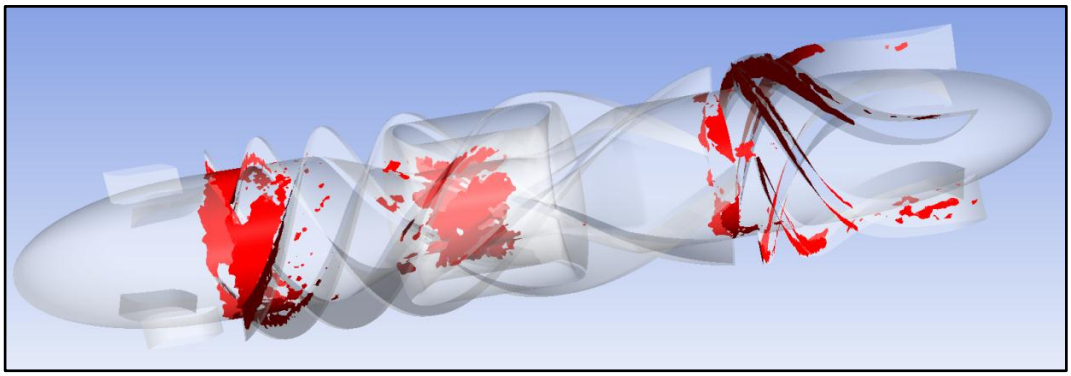

Fig 3.20: Boundary Layer y^+ Contour (Red zone, $y^+ > 5$), (FP1 at 5L/min, 100mmHg and 910 rad/s)

As showed in Fig 3.20, cell sizes of red zone should be smaller to move near wall nodes into the viscous sublayer. Fig 3.21 shows these surfaces as color schema from blue to red, y^+ from 5 to 8. By starting from red colored cells which are maximum in all pump, cell dimensions should be reduced more to enhance turbulence modeling to provide more accurate flow dynamic results. However, it possible to neglect if computation time is important criteria for R&D process and error due to turbulence is acceptable.

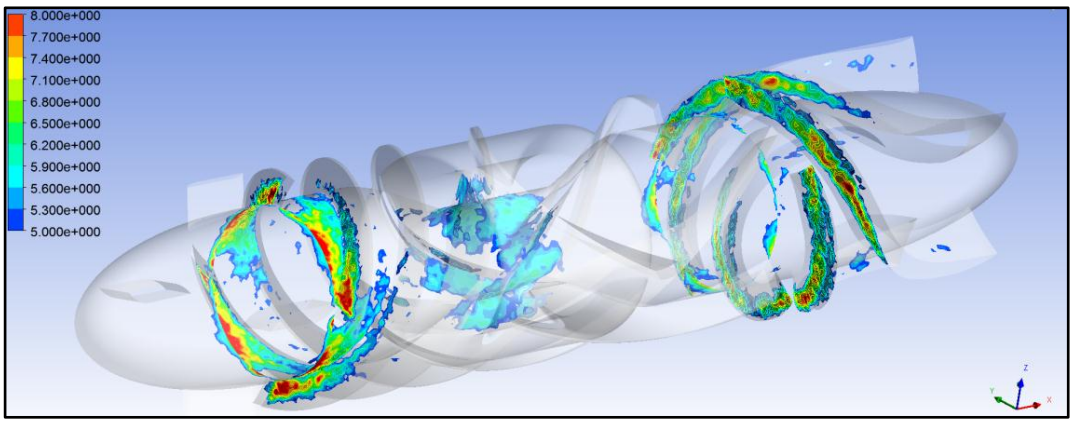

Fig 3.21: Boundary Layer y^+ Contour (Blue-to-Red colour schema shows y^+=5 to 8)

3.2.9. Time-Dependent Analysis

All calculations on FP1 and FP2 were done according to static analysis by being independent from time. However, static performance of prototypes should be tested and validated by transient analysis to see inertial effects and response time of hydraulic system according to time varying operation conditions. Furthermore, cavitation is also harmful for blood that depends on pressure change by depending on time (derivative of pressure). So, transient analysis is requirement of R&D process of LVAD via CFD.

Rotational velocity of FP1 was defined as a sinusoidal function and UDF (User Defined Function) was written to introduce this time dependent function to CFD solver (ANSYS Fluent). Output of UDF was a time varying sinusoidal function with 900 rad/s offset, 50 rad/s magnitude, 0.1592 Hz frequency and 6.28 sec. period. Rotational velocity was formulated as;

$$\omega(t) = 900 + 50 * \sin(t)$$

Then volumetric flow rate was defined as 5 L/min constant. Head pressure and torque were evaluated via CFD and plotted versus time (Plot 3.14).

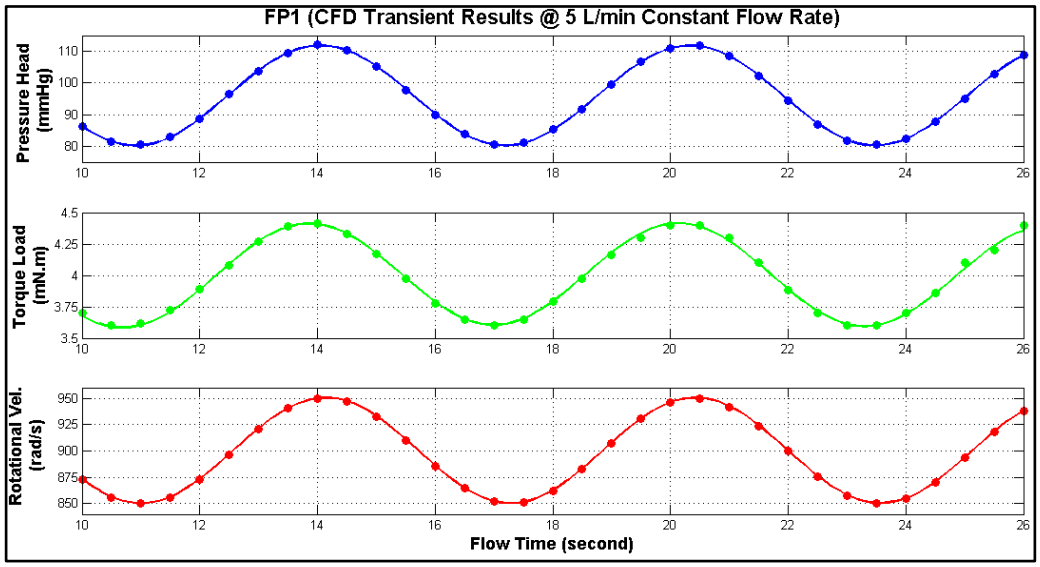

Plot 3.14: Hemodynamic Performance and Torque of FP1 with Time Varying Rotational Velocity at 5L/min Constant Flow

As seen from plot, transient results at 12.8 s. flow time matches with static analysis where rotational velocity becomes ~910 rad/s, head pressure reaches ~100 mmHg and torque becomes ~4.1 m.Nm (Table 3.33).

	ω (rad/s)	ΔP (mmHg)	T (mN.m)
Transient Result at 12.8 s	911,8	101,0	4,09
Static Result	910,0	98,7	4,10

Table 3.33: Comparing Transient and Static CFD Results at 5L/min (FP1)

Furthermore, it obviously seems that there is shift between peak of torque and rotational velocity and rotational velocity reaches its peak value with a delay ~0.3 s. Main reason for this delay is inertial effect of rotor component and its acceleration. Furthermore, inertial effects of blood doesn't seems distinct; because head pressure reaches to maximum almost at the same time with rotational velocity (Table 3.34).

FP1	
$t@T_{max}$	13,85 s
$t@\omega_{max}$	14,15 s
$t@\Delta P_{max}$	14,15 s

Table 3.34: Time at Peak Values for 5L/min (FP1)

3.3. INITIAL MOTOR CALCULATIONS (MATLAB®)

Torque load and rotational velocity which listed in Table 3.28 after CFD analysis, were used to make initial calculations on motor parameters. NdFeBr type magnet was selected with maximum energy product (BH_{max}) 28 to 49 MGOe and residual flux density (B_r) 1.0-1.3 Tesla.[I] So, if magnetic flux losses were neglected, magnetic field intensity at gap(B_g) becomes maximum 1.3 T. Furthermore, mechanical efficiency was accepted as %100 due to lack of data about friction losses at bearing location and inertial losses of rotary component. Moreover, wire diameter was initially selected as 0.6mm and copper material was used by having electrical resistivity 1.68*10^{-8} ohm.m. Magnet outer radius was specified as 7 and 6 mm, respectively for FP1 and FP2 by considering 0.8mm blade height at exterior surface of magnetic cylinder. Also, input voltage was selected as 12 Volt due to battery size limitations that explained in "*1.1.7-Design Criteria, P:24"* section.

$B_{g_{max}}$ (NdFeBr)	r_{wire}	r_{mag}	η_m	ρ_w (copper)
1.3 T	0.3 mm	7-6 mm	1	1.68*10^{-8}

Table 3.35: Design Variables for Motor Calculations

	T m.Nm	ω Rad/s	V_{in} Volt	i A.	R_e mΩ	W_{in} Watt	$W_{el-loss}$ mWatt	$l_m * N$ turn.m	K_b N.m/A
FP1	4,07	910	12	0,31	27,4	3,71	2,6	0,1152	0,0132
FP2	3,91	1100	12	0,36	26,4	4,31	3,4	0,1112	0,0109

Table 3.36: Calculated Motor Parameters. L_m*N is for all active coils (two coils). R_e is for all active phases. i is armature current

l_m	N
10,0 mm	12 turn
7,5 mm	16 turn
5,0 mm	24 turn

Table 3.37: Total Coil Turn Number (for all active phases together) vs. Magnet Length. $l_m * N = 0.1152\ Turn.meter$

[I] 1 Tesla = 10^4 Gauss ; 1 Oesterd = 1000/4π Amper/meter

4. CONCLUSION

At end of the “CFD analysis to optimize axial flow LVAD” project, two prototypes (FP1 and FP2) were successfully developed that recovers physiological need of heart failure patients by not causing excessive damage on RBCs in computational results. Furthermore new magnet configuration was applied to prototypes and no negative effects on hemocompatibility, were observed.

The success of prototype performances were corresponded to design criteria that are hemodynamic performance and hemocompatibility, respectively defines physiological need of circulatory system and non-negative effects on physiology during device support. These design criteria were related to optimization objectives to numerically define and compare device performances with concrete and visual data.

As a result of CFD analysis process, head pressure-flow rate characteristic and hydraulic efficiency were observed to characterize hemodynamic performance; backflow at interfaces and area averaged shear stress at shroud were studied to qualify hemocompatibility of prototypes. Then these performance results wanted to be enhanced to move them within acceptable range to satisfy hemocompatibility and hemodynamic requirements.

By following CFD analysis, prototypes were modified step-by-step parametric approach to enhance results on optimization objectives. In step-by-step parametric approach, only one geometric parameter was modified to see its individual effect on flow dynamics and performance by keeping rest of them constant. Then best option for this parameter was determined in terms of optimization objectives and then it kept constant for next steps. These steps were repeated for other geometric parameters and modifications were continued until reaching optimization objectives in acceptable range.

During CFD analysis and optimization process, more than 28 prototypes were developed by following step-by-step parametric modification and at the end of process,

two prototypes (FP1 and FP2) performed successful results in computational environment by satisfying all optimization objectives.

Then, time-dependent analysis was performed on FP1 to approve steady hemodynamic results. Rotational velocity of system was defined as periodic function of time and volumetric flow rate was taken as steady. Transient analysis showed that rotational velocity of rotor gives response to torque increment within 0.3 s delay because of rotor inertia. However no spectacular inertial effect of blood was observed, because pressure rise immediately responded to rotational velocity increment.

After matching static and transient results, performance of optimized prototype were modeled with numerous CFD analysis by collecting data at wide operation range, to use mathematical pump model of final prototype for future simulations and developing control algorithm to provide consistency between pump operation and patient physiological demands.

At the end, final prototypes were manufactured from plastic material with rapid prototyping method to use it in physical experiments.

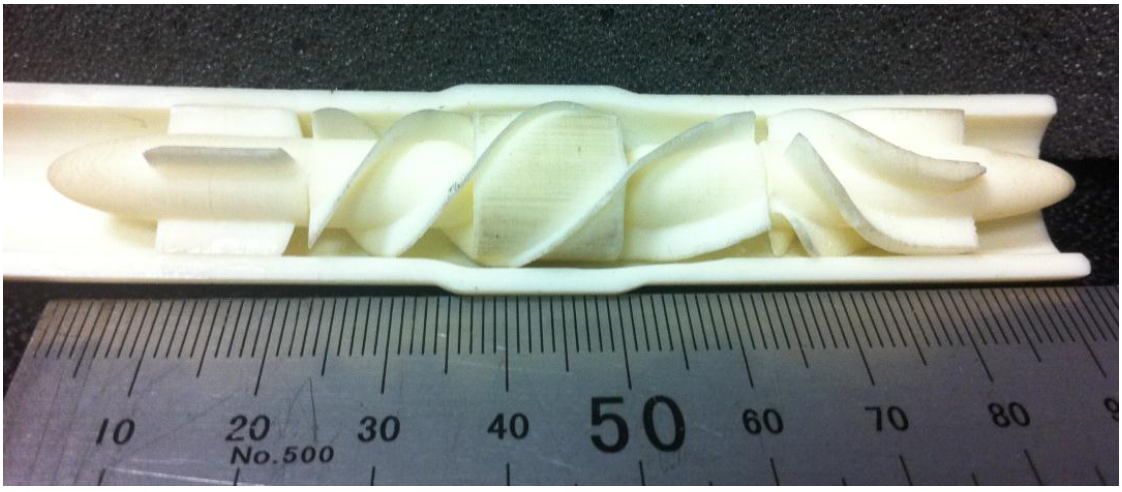

Fig 4.1: Plastic Prototype

Furthermore, power analysis (torque-velocity characteristic) were done to make initial calculations for motor design such as determining input armature current, coil turns, magnet length and thickness and etc.

4.1. STUDY ON OPTIMIZATION OBJECTIVES

- **Flow Field Quality (Backflow & Vortex Zones):**

According to preliminary CFD studies, most of the backflow occurs where blood flow enters to another blade stage. So, inducer-rotor and rotor-diffuser interfaces are important zones in pump to examine backflow.

Firstly flow exits from inducer blade and gets into rotary zone. Then it gains kinetic energy thanks to rotary blade, however it turns to backward direction due to non-smooth contact between attacking fluid and rotor blade attack edges. The reason of hard contact is difference between flow and blade attack angle (incidence angle). Furthermore, pressure gradient difference between tip and hub plane of rotor blade (hub-tip ratio) causes dissimilarity on energy transfer and causes reverse flow in rotor zone. Moreover, pressure gradient difference between pressure and suction side of blade tip causes leakage flow at this location from pressure to suction side direction (inverse of blade rotation direction). Volume of leakage flow directly is affected by tip clearance and blade clearance-height ratio. Then this flow turns into backward direction due to insufficient energy transfer at tip clearance.

Backflow which occurs as a result of these parameters, gets into inducer zone again with high radial velocity which gained by rotor blade. Then backflow collides to inducer blades almost orthogonally due to high radial velocity and causes high shear stress where collision occurs. After collision, flow separates into two ways. In first, backflow turns to forward direction after interacting with incoming forward flow and enters to rotor zone again, therefore this backflow stays in inducer with shorter duration. In second, backflow reaches core of inducer domain and then turns into the forward direction by interacting with incoming forward flow; however continuously incoming backflow from rotary zone forces transition of backflow into forward direction and converts forward flow into backward direction again. These continuous interactions cause vortex zone and increases residence time of flow particles into inducer region. In briefly, residence time and shears stress in inducer stage can be reduced by respectively

eliminating vortex and preventing collision which can be minimized by totally eliminating backflow. Furthermore, leakage flow causes increase on shear stress at rotor blade tip and shroud.

Therefore, rotor blade attack angle (β_{b1}) was increased to reduce incidence and provide smoother contact at rotor inlet. Then, cross sectional flow area (A_c) and blade height were reduced to decrease difference between hub and tip plane. Both modification methods enhanced flow lines and reduced backflow, however smaller blade height increased blade tip clearance-height ratio and resulted as increment on leakage flow which reduces second methods effectiveness weight on backflow minimization. Then, inducer-rotor blade gap(g_1) was increased and it prevented fluid collision to inducer blades. Because, incoming forward flow from inducer turned backflow into forward direction at gap before it reaches and collides to inducer blades. Hereby, no vortex occurred due to non-existence of collision and shear stress and residence time significantly decreased. Also, increasing rotor blade numbers (n_r) significantly decreased backflow at rotor inlet by reducing tendency of leakage flow to turning into backward direction thanks to more sufficiently transferring energy to fluid.

At rotor-diffuser interface, backflow occurs due to same reasons (incidence and hub-tip ratio) as in inducer-rotor interface except leakage flow. In addition, boundary layer flow separation also causes reverse flow in diffuser region. However, backflow dynamics (vortex and collision) and effects on shear stress and residence time seem same as in inducer-rotor interface.

Therefore, diffuser blade attack angle (β_{b3}) was increased to reduce incidence and provide smoother contact at diffuser inlet. In addition increasing rotor trailing angle (β_{b2}) decreased tangential velocity of fluid and its attack angle(β_{f3}) at diffuser inlet. As a result, flow lines enhanced thanks to smaller incidence. Then, cross sectional flow area was reduced to minimize deviation between tip and hub plane. Also rotor-diffuser gap (g_2) was increased and it resulted as quicker change in flow direction from backward to forward before backflow gets into rotor again. As a result, residence time

of backflow at interface reduced. Furthermore, diffuser blade amounts were modified to reduce boundary layer flow separation.

Furthermore parallelizing diffuser blade trailing edge($\beta_{b4} = 0^0$) with axis, eliminated fluid rotation at outlet cannula by reducing radial velocity. Also, it increased conversion of kinetic to potential energy more.

- **Hemodynamic Performance**

Increasing head pressure at same flow rate and hydraulic efficiency gives chance to reduce rotational velocity of device for same output and reduce power consumption to use lighter batteries for portability. As known shear stress at blade tip and shroud directly depends on blade linear velocity and decrement on it results as more hemocompatible device.

As studied in parametric modifications, reducing incidence at both interface via increasing blade angles (β_{b1}, β_{b2}& β_{b3}) increased head pressure and hydraulic efficiency ($\eta_{max}$and η_{mean}). However, both results were observed until reaching optimum incidence value and exceeding it caused drop on both; also optimum incidence for each optimization objects was different. Moreover they shifted optimum flow rate ($Q@\eta_{max}$) to closer to the desired nominal operation point (Q = 5L/min) and increased nominal efficiency (η @ $5L/min$).

Furthermore, reducing A_c modification affected head pressure in positive or negative way by depending on blade tip and hub radius modification. In first, hub radius was increased by keeping tip radius constant to reduce blade height. It caused drop on head pressure due to reducing blade effective area for energy transfer and drop was recovered by increasing rotational velocity. In second, both radii were increased to reduce A_c and increase hub-tip ratio. Head pressure increased thanks to higher linear velocity at blade tip and it gave chance to reduce required rotational velocity for same hydraulic output. Hydraulic efficiency increased for both thanks to enhanced flow field.

Moreover, enlarging gaps between adjacent blade stages (g_1&g_2)dropped head pressure and hydraulic efficiency, although reduced backflow and enhanced flow lines. Also,

reducing tip-shroud gap (g_t) increased hemodynamic performance as a result of reducing leakage flow at gap.

- **Summary of Optimization**

Design criteria of device were related to optimization objectives which are flow dynamic results. Then CFD results on optimization objectives was aimed to move in acceptable range for satisfying design criteria and it was performed with one-by-one parametric modification. In Table 4.1, all optimization objectives and modification methods on parameters to achieve these objectives, were listed. For example, 1st row and 1st column in Table 4.1 represents that rotor blade attack angle should be increased to minimize backflow at rotor inlet.

Optimization Objective	β_{b1}	β_{b2}	β_{b3}	g_1	g_2	g_t	n_r	r_t	r_h
Minimizing Backflow Rotor Inlet	↑	–	–	↑	–	↓	↑	↓	↑
Minimizing Backflow Diffuser Inlet	–	↑	↑	–	↑	↓	–	↓	↑
Maximizing Efficiency	↑	↑	↑	↑	↓	↓	↑	↑	↑
Maximixing Head Pressure	↑	↓	↑	↓	↓	↓	↑	↑	↓
Shifting Q@η max to lower Q	↑	↑	↑	?	?	?	?	↓	↑

Table 4.1: Modifications on Geometric Parameters to Achieve Optimization Objectives. Each Geometric Modification was made Individually by Holding Rest of Them Constant.

Symbol	Description
↑	Increasing geometric parameter to achieve optimization objective
↓	Decreasing geometric parameter to achieve optimization objective
–	Geometric parameter dont have effects on objective
↑	Increasing upto optimum value
?	Effect of parameter on object can't known exactly due to non-enough CFD experiments

Table 4.2: Descriptions of Symbols in Table 4.1

4.2. FINAL PROTOTYPE RESULTS

Since initial design to final prototype, percentage backflow at inducer-rotor and rotor-diffuser interface respectively decreased from %17.4 and %35.2 to %0.3 and %9.3 in FP1 and %7.2 and %12.4 in FP2 by being so close to %10 which was defined as design criteria.

Furthermore, maximum, mean (average within a range 4-8L/min)and optimal (at 5L/min) hydraulic efficiencies were increased from %19.5, %16.5 and %14.9 to %29.2,%27.0 and %29.6 in FP1 and %25.0, %22.7 and %24.8 in FP2. Deviation between maximum, mean and optimal efficiencies was reduced by shifting optimum flow rate of pump ($Q@\eta_{max}$), from 9.35 L/min to 5.23 L/min in FP1 and 5.3 L/min in FP2. Hereby, optimum operation point of pump ($Q\ @\ \eta_{max}$) was almost matched with desired operation point of pump ($\Delta P = 100\ mmHg\ and\ Q = 5\ L/min$).

Desired hemodynamic performance (ΔP=100mmHg and Q=5L/min) were succeeded at 910 and 1100 rad/s rotational velocity with 4.1 and 3.9 mN.m torque load by consuming 3.7 and 4.3 Watt, respectively in FP1 and FP2. Tip-hub blade dimensions for FP1 and FP2 were respectively 8-5.8 and 7-4.5 mm. By considering blade dimensions with rotational velocity, blade linear velocities became 7.3 m/s in FP1 and 7.7 m/s in FP2 and it respectively caused 496 and 522 Pa, area averaged wall shear stress at shroud. Furthermore, blood exited from pump averagely in 90 and 75 ms for FP1 and FP2. However, these results about shear stress and transition time don't give accurate estimation about hemocompatibility which requires in-vivo or in-vitro testing to evaluate blood damage in international medical standards.

Furthermore, evaluating optimum flow rate of prototypes and pressure losses through both stage gave chance to apply backward engineering method for hydraulic efficiency formula in theory. Then drag coefficients of rotor and diffuser blades were calculated as 0.115 and 0.185 for FP1 and 0.145 and 0.155 for FP2.

- **Magnetic Cylinder**

Furthermore, magnetic cylinder formation which includes flow channel inside, was developed as new configuration for permanent magnet installation method. Canalizing blood flow through interior (central channel) instead of exterior channel (peripheral channel), removed necessity for wide exterior channel and gave chance to narrow it. Therefore, magnetic gap between permanent magnets and stator coils was reduced. Furthermore, cylinder formation provided flexibility on magnet volume which is limited when magnets installed in rotor blades. Both advantages increased magnetic performance and gave chance to use less coil turn or armature current for same mechanic output. Although these advantages, this configuration could cause negative effects on flow dynamics such as leakage flow from one channel to other due to pressure gradient differences. Furthermore, narrowing exterior channel could cause stagnant flow which results as coagulation. So, both possible results could increase blood damage of device.

As a result of CFD on FP1, maximum 4.7ml/min blood flows from central to peripheral channel at where magnetic cylinder ends and both channel combines. So, leakage flow from central-to-peripheral channel was evaluated as %0.13 of central channel forward flow. Furthermore, blades with 0.8 mm height located at exterior of magnet to transfer energy to blood and increase flow through exterior channel to keep away from possible stagnation. So, %28 and %72 of total forward flow passed through peripheral and central channel respectively and no-stagnation was observed at peripheral channel. So, magnetic cylinder formation with extra blades located at peripheral channel, didn't cause excessive leakage flow from central-to-peripheral channel and stagnation.

- **Initial Motor Calculations**

According to hydraulic system requirements of FP1, motor torque constant and armature current were initially calculated as 0,0132 N.m/A and 0,31 A by neglecting mechanical and magnetic losses. Then, product of motor active length and total coil turn number for all active phases (l_m*N) was calculated as 0,1152 Turn.meter.

5. DISCUSSION

Although successful prototypes were developed at the end of project, there are some missing works that should be filled. Mathematical model of pumps (Eq 3.1 and Eq 3.2) simulate pump performance within range where CFD analyses were done, however out of range can be simulated with error. Therefore more accurate model should be derived by widening its range with more CFD analyses to use formulas for developing controller algorithm in order to run pump in consistency with physiology.

Furthermore, more time-dependent analyses should be performed to observe pump characteristic with inertial effects of device and blood when it produces pulsatile flow. Especially, derivative of flow rate is important to be known under time varying rotational velocity and head pressure to study on possible physiologic effects of pulsatile flow.

Moreover, only observing shear stress and transition time isn't enough to define device hemocompatibility. CFD package offers chance to use Lagrangian method to track fluid particles, therefore empirical formula to estimate pfHb level (Eq 2.57) can be calculated for released particles (RBCs in virtual domain) with small time steps in transient CFD analysis. However this method still doesn't provide accurate estimations of blood damage. Best way is evaluating pfHb level and calculating NIH after in-vivo and in-vitro tests.

In the further projects on R&D of LVAD program, magnetic analyses should be performed to optimize pump motor parameters which initially calculated in this project. Furthermore, mechanical structural analysis should be performed on rotor blades to see their strength against high rotational velocity.

It is known that most important locations in pump that effect hemocompatibility are interfaces between blades and this location includes mechanical bearings which support rotation. Therefore, bearing design is important by effecting hemocompatibility of pump. In further projects, it should be designed and tested via CFD to see possible

effects on flow dynamics. Furthermore, its strength and effect on vibration should be tested via mechanical structural and vibration analyses.

In addition to computational testing process, as shown in Fig 1.3 physical tests are required to validate virtual performance of pump in physical domain. So, particle image velocimetry should be applied by using transparent glass or plastic prototype to map pathways of fluid particles for observing backflow and vortex zones. Furthermore, NIH factor of pump can be evaluated by using real blood in this step. Then, metal wear physical prototype should be operated in mock circuit to validate consistency of controller algorithm with physiology. Later, clinical trials can be started with metal wear prototype which includes cannula, battery and all other accessories.

APPENDIX A

A.1. APPLYING BERNOULLI EQUATION TO BOTH STAGES

$\tau_a = \ tan(\alpha_1)$
$\tau_b = tan(\beta_{f2})$
$\tau_c = tan(\beta_{f4})$
$\gamma = \frac{u}{v_x}$
$X = \ \tau_a + \tau_b$
$Y = \tau_c - \tau_b$
$Z = \tau_a - \tau_b$

Table A.1: Some Shortening to Simplify Equations

A.1.1. Rotor Stage

As known from methods section, ideal pressure rise through rotor (ΔH_r) was expressed as

$$\Delta H_r = \ \rho \ u \ \Delta v_{ur} \qquad \textbf{Eq 2.25}$$

By substituting Δv_{ur}, ideal pressure rise through rotor became,

$$\Delta H_r = \ \rho(u^2 + u \ v_x \tau_a - u \ v_x \tau_b) \qquad \textbf{Eq A.1}$$

Static pressure rise through rotor was formulated as (k=+1 for rotary stage),

$$\Delta P_r = \ \rho \ v_x \Delta v_{ur} \tan(\beta_{mr}) - \frac{\rho \ C_D \ \sigma \ {v_x}^2}{2 \cos(\beta_m)^3} \qquad \textbf{Eq A.2}$$

By recalling $tan(\beta_{mr})$and substituting it into the ΔP_rformula

$$\tan(\beta_{mr}) = \frac{1}{2}\left(\frac{u}{v_x} + \ \tau_a + \tau_b\right) \qquad \textbf{Eq 2.16}$$

ΔP_r became,

$$\Delta P_r = \left(\frac{\rho\, v_x\left(u + v_x(\tau_a - \tau_b)\right)\left(\frac{u}{v_x} + \tau_a + \tau_b\right)}{2} \right) - \frac{\rho\, C_{Dr}\, \sigma\, {v_x}^2}{2\cos(\beta_{mr})^3} \qquad \textbf{Eq A.3}$$

$$\Delta P_r = \frac{\rho}{2}\left(u^2 + 2uv_x\tau_a + {v_x}^2{\tau_a}^2 - {v_x}^2{\tau_b}^2\right) - \frac{\rho\, C_{Dr}\sigma_r\, {v_x}^2}{2\cos(\beta_{mr})^3}$$

Moreover, dynamic pressure rise through rotor was formulated as below, if we assume axial velocity of fluid is uniform through stage.

$$\Delta KE_r = \rho\, \frac{({v_{u2}}^2 - {v_{u1}}^2)}{2} \qquad \textbf{Eq A.4}$$

By substituting $v_{u2} = u - v_x\tau_b$ and $v_{u1} = -v_x\tau_a$ into the dynamic pressure rise formula, it became

$$\Delta KE_r = \frac{\rho}{2}\left((u - v_x\tau_b)^2 - (-v_x\tau_a)^2\right)$$
$$\Delta KE_r = \frac{\rho}{2}\left(u^2 - 2uv_x\tau_b + {v_x}^2{\tau_b}^2 - {v_x}^2{\tau_a}^2\right) \qquad \textbf{Eq A.5}$$

Bernoulli equation defines energy transfer of system. By substituting ideal pressure, static pressure and dynamic pressure rise formula to Bernoulli equation; pressure loss through rotor became,

$$\Delta H_r = \Delta P_r + \Delta KE_r + h_{loss_r} \qquad \textbf{Eq A.6}$$

$$h_{loss_r} = \frac{\rho\, C_{Dr}\, \sigma\, {v_x}^2}{2\cos(\beta_{mr})^3} \qquad \textbf{Eq A.7}$$

As seen, pressure loss through rotor depends on drag coefficient of rotor blades (C_{Dr}).

A.1.2. Diffuser Stage

For diffuser stage static pressure rise can be expressed as below (k=-1 for diffuser stage).

$$\Delta P_d = -\rho\, v_x \Delta v_{ud} \tan(\beta_{md}) - \frac{\rho\, C_{Dd}\, \sigma\, {v_x}^2}{2\cos(\beta_{md})^3} \quad \textbf{Eq A.8}$$

By recalling $tan(\beta_{md})$ and substituting it into the ΔP_d formula

$$tan\,(\beta_{md}) = \frac{1}{2}\left(\frac{u}{v_x} + \tau_c - \tau_b\right) \quad \textbf{Eq 2.16}$$

Static pressure rise through diffuser became,

$$\Delta P_d = -\frac{\rho\, v_x(v_x\,(\tau_c + \tau_b) - u)\left(\frac{u}{v_x} + \tau_c - \tau_b\right)}{2} - \frac{\rho\, C_{Dd}\, \sigma_d\, {v_x}^2}{2\cos(\beta_{md})^3}$$
$$\Delta P_d = \frac{\rho}{2}\,(u^2 - 2uv_x\tau_b + {v_x}^2{\tau_b}^2 - {v_x}^2{\tau_c}^2) - \frac{\rho\, C_{Dd}\sigma_d\, {v_x}^2}{2\cos(\beta_{md})^3} \quad \textbf{Eq A.9}$$

Moreover dynamic pressure decrease through diffuser can expressed as,

$$\Delta KE_d = \rho\,\frac{({v_{u4}}^2 - {v_{u3}}^2)}{2} \quad \textbf{Eq A.10}$$

By substituting $v_{u4} = v_x\,\tau_c$ and $v_{u3} = u - v_x\tau_b$ to dynamic pressure equation, it became

$$\Delta KE_d = \frac{\rho}{2}((v_x\,\tau_c)^2 - (u - v_x\tau_b)^2)$$
$$\Delta KE_d = \frac{\rho}{2}(-u^2 + 2uv_x\tau_b - {v_x}^2\,{\tau_b}^2 + {v_x}^2\,{\tau_c}^2) \quad \textbf{Eq A.11}$$

It's known that u equals to zero in stationary stage, so there is no external energy transfer occurs through diffuser blades ($\Delta H_d = 0$). So, Bernoulli equation became as below

$$0 = \Delta P_d + \Delta KE_d + h_{loss_d} \quad \textbf{Eq A.12}$$

Then, by substituting dynamic and static pressure change to Bernoulli equation, pressure loss through diffuser became a function of drag coefficient of these blades (C_{Dd}).

$$h_{loss_d} = \frac{\rho\, C_{Dd}\, \sigma_d\, {v_x}^2}{2\cos(\beta_{md})^3} \quad \textbf{Eq A.13}$$

A.2. HYDRAULIC EFFICIENCY

Hydraulic efficiency is rate of input and output energy. Input energy of system was described as sum of ideal pressure rise through both stages.

$$\begin{aligned} \Delta H_{in} &= \Delta H_r + \Delta H_d \\ \Delta H_{in} &= \rho(u^2 + u\, v_x \tau_a - u\, v_x \tau_b) \end{aligned} \quad \textbf{Eq A.14}$$

Moreover, output energy of system is difference between ideal head pressure and total pressure losses through all pump (diffuser and rotor stage losses together).

$$\Delta H_{out} = \Delta H_i - h_{loss_{total}} \quad \textbf{Eq A.15}$$

Where $h_{loss_{total}}$ represents total pressure losses through all stages (rotor and diffuser together) and it was defined as;

$$\begin{aligned} h_{loss_{total}} &= h_{loss_r} + h_{loss_d} \\ h_{loss_{total}} &= \frac{\rho\, C_{Dr}\, \sigma_r\, {v_x}^2}{2\cos(\beta_{mr})^3} + \frac{\rho\, C_{Dd}\, \sigma_d\, {v_x}^2}{2\cos(\beta_{md})^3} \end{aligned} \quad \textbf{Eq A.16}$$

So, hydraulic efficiency can be expressed as

$$\eta_h = \frac{\Delta H_{out}}{\Delta H_{in}}$$

$$\eta_h = \frac{\Delta H_{in} - h_{loss_{total}}}{\Delta H_{in}}$$

$$\eta_h = 1 - \frac{h_{loss_{total}}}{\Delta H_{in}} \qquad \textbf{Eq A.17}$$

$$\eta_h = 1 - \frac{\left(\frac{{v_x}^2}{2}\right)\left(\frac{C_{Dr}\,\sigma_r}{\cos(\beta_{mr})^3} + \frac{C_{Dd}\,\sigma_d}{\cos(\beta_{md})^3}\right)}{u^2 + u\,v_x(\tau_a - \tau_b)}$$

A.3. DERIVATIVE OF EFFICIENCY

If we divide up and down of division part of $\eta_h$formula with ${v_x}^2$,

$$\eta_h = 1 - \frac{1}{2}\frac{\left(\frac{C_{Dr}\,\sigma_r}{\cos(\beta_{mr})^3} + \frac{C_{Dd}\,\sigma_d}{\cos(\beta_{md})^3}\right)}{\gamma^2 + \gamma(\tau_a - \tau_b)} \qquad \textbf{Eq A.18}$$

Where $\gamma = \frac{u}{v_x}$ and it must be remembered that $\gamma = \frac{u\,A_c}{Q}$. It is known that from trigonometric relations, cosine of any angle can described as

$$\cos(\theta) = \sqrt{\left(tan\,(\theta)\right)^2 + 1}$$

After trigonometric equivalences, equation at above became,

$$\eta_h = 1 - \frac{1}{2}\frac{C_{Dr}\,\sigma_r\left(\left(tan\,(\beta_{mr})\right)^2 + 1\right)^{3/2} + C_{Dd}\,\sigma_d\left(\left(tan\,(\beta_{md})\right)^2 + 1\right)^{3/2}}{\gamma^2 + \gamma(\tau_a - \tau_b)} \qquad \textbf{Eq A.19}$$

By recalling Eq 2.16 and using γ instead of $\frac{u}{v_x}$,

$$tan\,(\beta_{mr}) = \frac{1}{2}(\gamma + X)$$
$$tan\,(\beta_{md}) = \frac{1}{2}(\gamma + Y)$$

Eq A.20

Where

$$X = \tau_a + \tau_b \qquad \& \qquad Y = \tau_c - \tau_b$$

Then we can write,

$$\left(\left(tan\,(\beta_{mr})\right)^2 + 1\right)^{3/2} = \frac{\{(\gamma + X)^2 + 4\}^{3/2}}{8}$$
$$\left(\left(tan\,(\beta_{md})\right)^2 + 1\right)^{3/2} = \frac{\{(\gamma + Y)^2 + 4\}^{3/2}}{8}$$

Eq A.21

So, by substituting these equivalences to $\eta_h$equation,

$$\eta_h = 1 - \frac{1}{16}\frac{C_{Dr}\,\sigma_r\,\{(\gamma + X)^2 + 4\}^{3/2} + C_{Dd}\,\sigma_d\,\{(\gamma + Y)^2 + 4\}^{3/2}}{\gamma^2 + \gamma Z}$$

Eq A.22

Where

$$Z = \tau_a - \tau_b$$

$\eta_h$was simplified by separating it to three different functions of γ, simplified efficiency formula is,

$$\eta_h = 1 - \frac{f_1(\gamma) + f_2(\gamma)}{g(\gamma)}$$

Eq A.23

Where

$$f_1(\gamma) = C_{Dr}\,\sigma_r\{(\gamma + X)^2 + 4\}^{3/2}$$
$$f_2(\gamma) = C_{Dd}\,\sigma_d\{(\gamma + Y)^2 + 4\}^{3/2}$$
$$g(\gamma) = 16(\gamma^2 + \gamma\,Z)$$

Formulas were written by depending on γ, so partial derivative according to γ had to be derived firstly ,then it should be multiplied with derivative of γ according to flow rate (Q).

$$\frac{d(\eta_h)}{dQ} = \frac{\partial \eta_h}{\partial \gamma} \frac{\partial \gamma}{\partial Q} \quad \textbf{Eq A.24}$$

Second component of derivative can expressed as,

$$\frac{\partial \gamma}{\partial Q} = -\frac{A_c u}{Q^2} \quad \textbf{Eq A.25}$$

Its known that this component cannot be equal to zero. So, in order to make derivative of hydraulic efficiency zero $\left(\frac{d(\eta_h)}{dQ} = 0\right)$, first component of Eq A.24 must be zero $\left(\frac{\partial \eta_h}{\partial \gamma} = 0\right)$. Flow rates which provide this condition is optimum flow rate $(Q@\eta_{max})$ of current design. First component of derivative can be expressed as,

$$\frac{\partial \eta_h}{\partial \gamma} = -\frac{1}{g^2}\left(g\frac{\partial(f_1)}{\partial \gamma} - f_1\frac{\partial(g)}{\partial \gamma} + g\frac{\partial(f_2)}{\partial \gamma} - f_2\frac{\partial(g)}{\partial \gamma}\right) \quad \textbf{Eq A.26}$$

Then derivative of f_1, f_2 and g were derived as below,

$$\frac{\partial(f_1)}{\partial \gamma} = 3\, C_{Dr}\, \sigma_r(\gamma + X)\sqrt{(\gamma + X)^2 + 4}$$
$$\frac{\partial(f_1)}{\partial \gamma} = 3\, C_{Dd}\, \sigma_d(\gamma + Y)\sqrt{(\gamma + Y)^2 + 4} \quad \textbf{Eq A.27}$$
$$\frac{\partial(g)}{\partial \gamma} = 16\,(2\gamma + Z)$$

According to condition $\frac{\partial \eta_h}{\partial \gamma} = 0$; f_1, f_2 , g and their partial derivatives according to γ were substituted in equation above, following simplified conditional equation was observed

$$0 = 16\ (C_{Dr}\ \sigma_r\ K_r + \ C_{Dd}\ \sigma_d\ K_d\ ) \qquad \textbf{Eq A.28}$$

Where $K_r(\gamma)$ and $K_d(\gamma)$are function of γ,

$$K_r = \left((2\gamma + Z)\ ((\gamma + X)^2 + 4) - 3(\gamma^2 + \gamma\ Z)(\gamma + X)\right)\sqrt{(\gamma + X)^2 + 4}$$

$$K_d = \left((2\gamma + Z)\ ((\gamma + Y)^2 + 4) - 3(\gamma^2 + \gamma\ Z)(\gamma + Y)\right)\sqrt{(\gamma + Y)^2 + 4} \qquad \textbf{Eq A 29}$$

Then equation above was rewritten in form such that,

$$\frac{C_{Dr}\ \sigma_r}{C_{Dd}\ \sigma_d} = -\frac{K_d}{K_r} \qquad \textbf{Eq A.30}$$

Then taking square of both side to remove square root terms in $K_r(\gamma)$ and $K_d(\gamma)$;

$$\left(\frac{C_{Dr}\ \sigma_r}{C_{Dd}\ \sigma_d}\right)^2 = \left(\frac{K_d}{K_r}\right)^2 \qquad \textbf{Eq A.30}$$

As said earlier, drag coefficient of helical type blades are unknown, so these constants cannot be used to determine design optimal flow rate. However for commonly used cascades, this formula can be used to evaluate optimum flow rate after finding its roots. So, right hand side terms of equivalence should be written in form of polynomial to find its roots. After opening parenthesis, K_r & K_d functions became as,

$$K_r = \left(-\gamma^3 + \gamma^2(X - 2Z) + \gamma^1\ (2X^2 - XZ + 8) + (X^2Z + 4Z)\right)\sqrt{(\gamma + X)^2 + 4}$$

$$K_d = \left(-\gamma^3 + \gamma^2(Y - 2Z) + \gamma^1\ (2Y^2 - YZ + 8) + (Y^2Z + 4Z)\right)\sqrt{(\gamma + Y)^2 + 4} \qquad \textbf{Eq A 29}$$

$K_r\ and\ K_d$terms are in same form, so they were simplified in form such that,

$$K(\gamma) = \left(-\gamma^3 + \gamma^2(N - 2Z) + \gamma^1\,(2N^2 - NZ + 8) + (N^2Z + 4Z)\right)\sqrt{(\gamma + N)^2 + 4} \quad \textbf{Eq A 29}$$

Where

$$N = X\ for\ K_r, \qquad N = \left(tan(\alpha_1) + tan(\beta_{f2})\right)$$

$$N = Y\ for\ K_d, \qquad N = \left(tan(\beta_{f4}) - tan(\beta_{f2})\right)$$

Then taking square of K,

$$K^2 = (\gamma^2 + 2\gamma N + N^2 + 4) *$$
$$\{$$
$$\boldsymbol{\gamma^6}$$
$$+\boldsymbol{\gamma^5}(4Z - 2N)$$
$$+\boldsymbol{\gamma^4}(-3N^2 - 2NZ + 4Z^2 - 16)$$
$$+\boldsymbol{\gamma^3}(4N^3 - 12N^2Z + 4NZ^2 + 16N - 40Z) \quad \textbf{Eq A 29}$$
$$+\boldsymbol{\gamma^2}(4N^4 - 2N^3Z - 3N^2Z^2 - 8NZ + 32N^2 - 16Z^2 + 64)$$
$$+\boldsymbol{\gamma^1}(4N^4Z - 2N^3Z^2 + 32N^2Z - 8NZ^2 + 64Z)$$
$$+\boldsymbol{\gamma^0}(N^4Z^2 + 8N^2Z^2 + 16Z^2)$$
$$\}$$

$$K^2 =$$
$$\boldsymbol{\gamma^8}$$
$$+\boldsymbol{\gamma^7}(4Z)$$
$$+\boldsymbol{\gamma^6}(4Z^2 - 6N^2 + 6NZ - 12)$$
$$+\boldsymbol{\gamma^5}(-4N^3 - 12N^2Z + 12NZ^2 - 24N - 24Z) \quad \textbf{Eq A 29}$$
$$+\boldsymbol{\gamma^4}(9N^4 - 28N^3Z + 9N^2Z^2 - 96NZ + 36N^2)$$
$$+\boldsymbol{\gamma^3}(12N^5 - 12N^4Z - 4N^3Z^2 - 72N^2Z - 24NZ^2 + 96N^3 + 192N - 96Z)$$

$$+\boldsymbol{\gamma^2}(4N^6 + 6N^5Z - 6N^4Z^2 + 48N^4 + 48N^3Z - 36N^2Z^2 + 96NZ + 192N^2 - 48Z^2 + 256)$$
$$+\boldsymbol{\gamma^1}(4N^6Z + 48N^4Z + 192N^2Z + 256Z)$$
$$+\boldsymbol{\gamma^0}(N^6Z^2 + 12N^4Z^2 + 48N^2Z^2 + 64Z^2)$$

Then we can write 1x9 P_r & P_d matrix which includes gains of 8th order polynomials of ${K_r}^2$ and ${K_d}^2$,

$$P = \begin{matrix} 1 \\ (4Z) \\ (4Z^2 - 6N^2 + 6NZ - 12) \\ (-4N^3 - 12N^2Z + 12NZ^2 - 24N - 24Z) \\ (9N^4 - 28N^3Z + 9N^2Z^2 - 96NZ + 36N^2) \\ (12N^5 - 12N^4Z - 4N^3Z^2 - 72N^2Z - 24NZ^2 + 96N^3 + 192N - 96Z) \\ (4N^6 + 6N^5Z - 6N^4Z^2 + 48N^4 + 48N^3Z - 36N^2Z^2 + 96NZ + 192N^2 - 48Z^2 + 256) \\ (4N^6Z + 48N^4Z + 192N^2Z + 256Z) \\ (N^6Z^2 + 12N^4Z^2 + 48N^2Z^2 + 64Z^2) \end{matrix} \quad \textbf{Eq A.31}$$

Where

$$Z = \left(tan(\alpha_1) - tan(\beta_{f2})\right)$$

1x9 P_r & P_d matrix were formed via P matrix,

$$P \xrightarrow{N=\left(tan(\alpha_1)+tan(\beta_{f2})\right)} P_r$$
$$P \xrightarrow{N=\left(tan(\beta_{f4})-tan(\beta_{f2})\right)} P_d$$

So we can form Eq A.30 in form,

$$\xi^2 = \frac{\gamma^8 P_{d1} + \gamma^7 P_{d2} + \gamma^6 P_{d3} + \gamma^5 P_{d4} + \gamma^4 P_{d5} + \gamma^3 P_{d6} + \gamma^2 P_{d7} + \gamma^1 P_{d8} + P_{d9}}{\gamma^8 P_{r1} + \gamma^7 P_{r2} + \gamma^6 P_{r3} + \gamma^5 P_{r4} + \gamma^4 P_{r5} + \gamma^3 P_{r6} + \gamma^2 P_{r7} + \gamma^1 P_{r8} + P_{r9}} \quad \textbf{Eq A.32}$$

Where $\xi = \left(\frac{C_{Dr}\,\sigma_r}{C_{Dd}\,\sigma_d}\right)$ .Then this equation became,

$$0 = \gamma^8(P_{d1} - P_{r1}\xi^2) + \gamma^7(P_{d2} - P_{r2}\xi^2) \ldots . + \gamma^0(P_{d9} - P_{r9}\xi^2) \quad \textbf{Eq A. 33}$$

Then by substituting actual value of γ,

$$0 = \left(\frac{u\,A_c}{Q}\right)^8 (P_{d1} - P_{r1}\xi^2) + \left(\frac{u\,A_c}{Q}\right)^7 (P_{d2} - P_{r2}\xi^2) \ldots \ldots . + \left(\frac{u\,A_c}{Q}\right)^0 (P_{d9} - P_{r9}\xi^2) \quad \textbf{Eq A.34}$$

By multiplying equation with Q^8,

$$0 = Q^8(u\,A_c)^0(P_{d9} - P_{r9}\xi^2) + Q^7(u\,A_c)^1(P_{d8} - P_{r8}\xi^2) \ldots . + Q^0(u\,A_c)^8(P_{d1} - P_{r1}\xi^2) \quad \textbf{Eq A.35}$$

Then formula above was simplified as,

$$0 = \sum_{k=0}^{8} \left(Q^{(8-k)}(u\,A_c)^k \left(P_{d_{(9-k)}} - \xi^2\, P_{r_{(9-k)}} \right) \right) \quad \textbf{Eq A.36}$$

By rewriting this equation, equivalence below was found.

$$0 = \sum_{k=0}^{8} \left(Q^{(8-k)}(u\,A_c)^k \left(P_{d_{(9-k)}} - P_{r_{(9-k)}} \left(\frac{C_{Dr}\,\sigma_r}{C_{Dd}\,\sigma_d}\right)^2 \right) \right) \quad \textbf{Eq A.36}$$

A.4. DRAG COEFFICIENTS

If optimum flow rate ($Q(\eta_{max})$) at specific rotational velocity is known from CFD tests or experiments in real environment, drag coefficient ratios can be calculated by using $Q(\eta_{max})$ in equation above. Let's say drag ratio is κ.

$$\kappa = \frac{C_{Dr}}{C_{Dd}} \qquad \textbf{Eq A.37}$$

By recalling Hydraulic efficiency formula, Eq A.17;

$$\eta_h = 1 - \frac{\left(\rho \frac{{v_x}^2}{2}\right)\left(\frac{C_{Dr}\,\sigma_r}{\cos(\beta_{mr})^3} + \frac{C_{Dd}\,\sigma_d}{\cos(\beta_{md})^3}\right)}{\Delta H_i}$$

After substituting κ, hydraulic efficiency formula became;

$$\eta_h = 1 - \frac{C_{Dd}\left(\rho \frac{{v_x}^2}{2}\right)\left(\frac{\kappa\,\sigma_r}{\cos(\beta_{mr})^3} + \frac{\sigma_d}{\cos(\beta_{md})^3}\right)}{\Delta H_i} \qquad \textbf{Eq A.38}$$

Then, any of drag coefficient can be written by depending on drag ratio, hydraulic efficiency and head pressure which can be evaluated by CFD analysis.

$$C_{Dd} = \frac{2\,(1 - \eta_h)\,\Delta H_i}{{v_x}^2\left(\frac{\kappa\,\sigma_r}{\cos(\beta_{mr})^3} + \frac{\sigma_d}{\cos(\beta_{md})^3}\right)} \qquad \textbf{Eq A.39}$$

A.5. PERFORMANCE RESULTS (ALL PROTOTYPES)

Prototype Code	%BF rotor inlet	%BF diffuser inlet	%η @ 5L	$\%\eta_{max}$	$\%\eta_{mean}$	Q @ η_{max}	ΔH @ 5L	T_L @ 5L	ω	Area Av. σ at shroud
	%	%	%	%	%	L/min	mmHg	m.Nm	rad/s	Pa
B1	17,20%	35,23%	14,93%	19,50%	16,50%	9,35	96,79	6,793	1060	-
A2	17,48%	36,91%	16,85%	21,31%	18,16%	9,20	107,20	6,829	1060	-
B2	17,40%	35,04%	17,00%	21,95%	18,71%	9,00	107,00	6,596	1060	-
B3	17,40%	34,44%	17,47%	22,38%	19,30%	8,60	106,40	6,383	1060	-
B4	17,42%	32,92%	18,38%	22,81%	20,05%	8,20	102,40	5,837	1060	-
B5	17,40%	32,69%	19,00%	22,62%	20,47%	7,60	101,80	5,593	1060	-
C1	14,90%	33,52%	20,17%	24,04%	21,75%	7,90	108,67	5,647	1060	519
C2	13,40%	32,58%	20,74%	24,33%	22,25%	7,60	108,40	5,481	1060	519
C3	6,88%	32,16%	20,01%	20,33%	19,68%	6,00	96,40	5,048	1060	503
D1	14,85%	27,18%	18,44%	21,95%	19,92%	7,60	92,30	5,244	1060	508
D2	14,81%	25,22%	20,41%	22,91%	21,58%	6,80	99,72	5,12	1060	507
D3	14,81%	23,35%	21,39%	22,80%	21,78%	6,30	100,00	4,900	1060	505
D4	14,81%	19,33%	21,81%	22,30%	20,82%	5,50	96,52	4,638	1060	505
D5	14,83%	12,95%	21,58%	21,50%	17,27%	4,70	88,48	4,297	1060	508
	16,20%	15,41%	21,66%	21,66%	18,40%	5,00	101,60	4,705	1105	520
E1	12,48%	18,04%	25,81%	28,71%	26,98%	7,10	108,70	5,045	927	542
	11,48%	16,38%	26,09%	-	-	-	101,00	4,765	902	532
E2	12,15%	16,72%	26,33%	28,30%	26,93%	6,60	107,90	4,909	927	537
	11,58%	15,57%	26,80%	-	-	-	100,81	4,634	902	532
E3	12,23%	14,46%	26,98%	27,46%	26,07%	5,65	107,78	4,786	927	539
F1	13,18%	12,85%	27,67%	-	-	-	104,28	4,515	927	557
F2	6,98%	12,81%	28,42%	28,87%	27,54%	5,60	108,25	4,554	927	510
F3	5,74%	13,15%	29,43%	-	-	-	109,77	4,467	927	512
F4	1,50%	13,33%	29,92%	-	-	-	108,79	4,356	927	503
F5 (FP1)	0,07%	6,74%	29,07%	29,20%	25,56%	4,70	80,64	3,626	850	484
	0,29%	**9,30%**	**29,62%**	**29,21%**	**27,05%**	**5,23**	**98,72**	**4,070**	**910**	**496**
	0,50%	10,27%	29,69%	29,63%	27,50%	5,37	104,37	4,211	927	502
F6	1,58%	8,52%	28,89%	-	-	-	99,27	4,116	927	505
F7	2,77%	5,65%	29,81%	29,72%	27,23%	4,90	90,26	3,822	880	614
	3,15%	6,80%	30,05%	30,13%	28,09%	5,05	99,81	4,055	910	630
	3,30%	7,55%	30,17%	30,31%	28,49%	5,15	105,58	4,192	927	636
H1	7,84%	12,00%	25,01%	25,10%	22,24%	4,90	90,76	3,803	1060	521
	8,99%	13,53%	25,19%	-	-	-	103,00	4,132	1100	530
H2 (FP2)	**7,18%**	**12,42%**	**24,80%**	**25,00%**	**22,70%**	**5,30**	**96,00**	**3,913**	**1100**	**522**

	ROTOR						DIFFUSER						INDUCER			GAPS			DIMENSIONS			
	β_{b1}	β_{b2}	n_r	l_r	t_r	σ_r	β_{b3}	β_{b4}	n_d	l_d	t_d	σ_d	α	n_i	l_i	g_1	g_2	g_t	r_t	r_h	r_h/r_t	A_c
	°	°	-	mm	mm	-	°	°	-	mm	mm	-	°	-	mm	mm	mm	mm	mm	mm	-	mm^2
A1	58°	14°	3	40	0,7	-	p66°	-11°	6	18	1	-	0°	5	12	1,0	1,0	0,2	7,0	4,0	0,57	33π
A2	"	"	"	"	"	"	"	0°	5	"	2	3,29	"	"	"	"	"	"	"	"	"	"
A3	"	"	"	"	"	"	"	"	4	"	"	-	"	"	"	"	"	"	"	"	"	"
B1	"	0°	"	"	"	-	"	"	5	"	"	3,29	"	"	"	"	"	"	"	"	"	"
B2	"	18°	"	"	"	-	"	"	"	"	"	"	"	"	"	"	"	"	"	"	"	"
B3	"	23°	"	"	"	-	"	"	"	"	"	"	"	"	"	"	"	"	"	"	"	"
B4	"	32°	"	"	"	5,78	"	"	"	"	"	"	"	"	"	"	"	"	"	"	"	"
B5	"	37°	"	"	"	-	"	"	"	"	"	"	"	"	"	"	"	"	"	"	"	"
C1	64°	32°	"	"	"	6,31	"	"	"	"	"	"	"	"	"	"	"	"	"	"	"	"
C2	67°	"	"	"	"	6,49	"	"	"	"	"	"	"	"	"	"	"	"	"	"	"	"
C3	74°	"	"	"	"	7,49	"	"	"	"	"	"	"	"	"	"	"	"	"	"	"	"
D1	64°	"	"	"	"	6,31	56°	"	"	"	"	-	"	"	"	"	0,5	"	"	"	"	"
D2	"	"	"	"	"	"	61°	"	"	"	"	-	"	"	"	"	"	"	"	"	"	"
D3	"	"	"	"	"	"	66°	"	"	"	"	-	"	"	"	"	"	"	"	"	"	"
D4	"	"	"	"	"	"	71°	"	"	"	"	-	"	"	"	"	"	"	"	"	"	"
D5	"	"	"	"	"	"	75°	"	"	"	"	-	"	"	"	"	"	"	"	"	"	"
E1	"	"	"	"	"	-	71°	"	"	"	"	4,00	"	"	"	"	"	"	8,0	5,56	0,69	33π
E2	"	"	"	"	"	"	73°	"	"	"	"	4,08	"	"	"	"	"	"	"	"	"	"
E3	"	"	"	"	"	"	75°	"	"	"	"	4,32	"	"	"	"	"	"	"	"	"	"
F1	"	"	"	"	"	6,02	73°	"	"	"	"	4,30	"	"	"	"	"	"	8,0	5,8	0,72	30π
F2	"	"	4	"	"	8,19	"	"	"	"	"	"	"	"	"	"	"	"	"	"	"	"
F3	67°	"	"	"	"	7,96	"	"	"	"	"	"	"	"	"	"	"	"	"	"	"	"
F4	"	"	"	"	"	"	"	"	"	"	"	"	"	4	5	2,0	"	"	"	"	"	"
F5 (FP1)	"	"	"	"	"	"	"	"	"	"	"	"	"	"	"	"	**1,5**	"	"	"	"	"
F6	"	"	"	"	"	"	"	"	"	"	"	"	"	"	"	"	2,0	"	"	"	"	"
F7	"	"	"	"	"	"	"	"	"	"	"	"	"	"	"	"	1,5	0,1	"	"	"	"
H1	64°	"	3	"	"	6,29	71°	"	"	"	"	5,17	"	5	12	1,0	0,5	0,2	7,0	4,5	0,64	29π
H2 (FP2)	"	"	"	"	"	"	"	"	"	"	"	"	"	"	"	**2,0**	**1,5**	"	"	"	"	"

Red : selected parameter for next iteration

A.7. CFD DATA OF FINAL PROTOTYPES

	Hemodynamic Perf.					Flow Field Study			
	ω	Q	ΔP	T	η	BF1		BF2	
	rad/s	L/min	mmHg	m.Nm	%	L/min	%	L/min	%
FP1	0	-3,1686	50,00	-	-	-	-	-	-
		-4,148	80,00	-	-	-	-	-	-
		-4,76	100,00	-	-	-	-	-	-
	750	1,0	85,04	2,76	9,14%	-	-	-	-
		3,0	71,89	2,57	24,89%	-	-	-	-
		5,0	52,35	2,92	26,52%	-	-	-	-
		7,0	28,30	3,61	16,24%	-	-	-	-
	800	3,0	84,58	2,92	24,23%	-	-	-	-
		5,0	66,1	3,26	28,12%	-	-	-	-
		7,0	40,37	3,91	20,07%	-	-	-	-
		8,0	28,64	4,36	14,58%	-	-	-	-
	830	3,0	91,25	3,12	23,47%	-	-	-	-
		5,0	74,83	3,48	28,76%	-	-	-	-
		6,0	59,27	3,68	25,88%	-	-	-	-
		9,0	21,94	5,04	10,49%	-	-	-	-
	850	3,0	96,23	3,27	23,07%	0,4846	12,95%	1,1710	29,46%
		3,5	94,13	3,33	25,84%	-	-	-	-
		4,0	91,00	3,40	27,94%	0,1289	3,03%	0,7338	16,19%
		4,5	86,39	3,50	28,98%	-	-	-	-
		5,0	80,64	3,63	29,07%	0,0032	0,07%	0,3451	6,74%
		5,5	74,13	3,74	28,51%	-	-	-	-
		6,0	65,60	3,83	26,87%	-	-	0,0835	1,43%
		6,5	58,00	3,98	24,76%	-	-	-	-
		7,0	52,93	4,20	22,98%	-	-	-	-
		7,5	47,83	4,45	21,05%	-	-	-	-
		8,0	42,23	4,70	18,81%	-	-	-	-
		8,5	35,80	4,94	16,10%	-	-	-	-
		9,5	19,20	5,43	8,79%	-	-	-	-
	880	1,0	122,51	3,94	7,86%	-	-	-	-
		3,0	104,17	3,51	22,46%	-	-	-	-
		5,0	89,64	3,85	29,43%	-	-	-	-
		7,0	60,88	4,40	24,43%	-	-	-	-
		9,0	37,52	5,40	15,78%	-	-	-	-
		11,0	11,51	6,39	5,01%	-	-	-	-
	910	3,0	114,89	3,78	22,27%	0,6157	15,75%	1,3978	33,35%
		3,5	111,21	3,81	24,93%	-	-	-	-
		4,0	107,78	3,88	27,12%	0,249	5,62%	0,9354	19,81%
		4,5	104,40	3,97	28,92%	-	-	-	-
		5,0	98,72	4,07	29,62%	0,0143	0,29%	0,4891	9,30%
		5,5	92,75	4,20	29,65%	-	-	-	-
		6,0	83,13	4,31	28,25%	0,0097	0,17%	0,1972	3,32%
		6,5	76,42	4,42	27,45%	-	-	-	-
		7,0	69,05	4,60	25,68%	-	-	-	-
		7,5	63,99	4,90	24,16%	-	-	-	-
		8,0	58,83	5,10	22,51%	-	-	-	-
		9,0	46,50	5,62	18,19%	-	-	-	-
		10,0	30,57	6,10	12,14%	-	-	-	-
		11,0	7,94	6,60	3,20%	-	-	-	-

	Hemodynamic Perf.					Flow Field Study			
	ω	Q	ΔP	T	η	BF1		BF2	
	rad/s	L/min	mmHg	m.Nm	%	L/min	%	L/min	%
FP1	927	3,0	120,68	3,90	22,04%	0,6549	16,54%	1,4147	33,72%
		3,5	116,75	3,95	24,74%	-	-	-	-
		4,5	109,30	4,09	28,75%	-	-	-	-
		5,0	104,37	4,21	29,69%	0,0244	0,49%	0,5459	10,27%
		5,5	98,27	4,34	29,86%	-	-	-	-
		6,0	91,20	4,50	29,41%	0,0076	0,13%	0,2303	3,86%
		7,0	74,00	4,70	26,35%	-	-	0,0118	0,18%
		7,5	68,73	4,96	24,89%	-	-	-	-
		8,0	63,61	5,22	23,35%	-	-	-	-
		8,5	58,12	5,48	21,58%	-	-	-	-
		9,0	52,17	5,70	19,56%	-	-	-	-
		9,5	44,82	6,00	16,94%	-	-	-	-
		10,0	36,30	6,30	13,83%	-	-	-	-
		10,5	26,84	6,60	10,31%	-	-	-	-
		11,0	15,26	6,80	5,90%	-	-	-	-
	950	1,0	144,80	4,66	7,27%	-	-	-	-
		3,0	128,82	4,17	21,69%	-	-	-	-
		5,0	111,71	4,4	29,72%	-	-	-	-
		6,0	98,96	4,65	29,84%	-	-	-	-
		8,0	70,19	5,39	24,38%	-	-	-	-
		10,0	44,36	6,48	16,01%	-	-	-	-
		12,0	10,88	7,54	4,05%	-	-	-	-
FP2	1100	3,0	130,19	4,00	19,60%	1,0044	22,58%	1,6204	36,65%
		5,0	96,00	3,90	24,80%	0,4019	7,18%	0,6827	12,42%
		6,0	81,31	4,00	24,56%	0,1452	2,36%	0,3197	5,24%
		7,0	63,44	4,20	21,35%	0,0894	1,30%	0,0973	1,42%
		8,0	43,90	4,40	15,98%	-	-	-	-

REFERENCES

Books

ANSYS Inc., April 2005, *ANSYS Fluent 12.0 Theory Guide*, Chapter 4.12-Turbulence:Near Wall treatments for Wall Bounded Turbulent Flows, Page: 4.72-74

Brennen E. Christopher, 1994, *Hydrodynamics of Pumps*, NREC, Chapter 3:Two-Dimensional Performance Analysis

Dixon S.I. and Hall C.A., 2010, *Fluid Mechanics and Thermodynamics of Turbomachinery 6.th Edition*, Elsevier, Chapter 3: Two-Dimensional Cascades, P:64-66

Hanselman Duane, 2003, *Brushless Permanent Magnet Motor Design Second Edition*, Magna Physics Publishing, Chapter 4: Brushless Motor Fundamentals, Page 76-79

Osman Gurdal, September 2001, *Design of Electric Machines* (Elektrik Makinalarının Tasarımı), Atlas Publishing, Chapter 3:General Subjects and Limitations of Rotating Machine Design (Döner Makina Tasarımının Genel Kavramları ve Sınırlamaları), Page:44-46

Tu J., Yeoh G.H. and Liu C., 2007, *Computational Fluid Dynamics A Practical Approach*, Butterworth-Heinemann

Turton R.K., 1994, *Rotodynamic Pump Design*, Cambridge University Press, Chapter 1:Fundamental Principles, Page:1-3

Turton R.K., 1995, *Principles of Turbomachinery Second Edition*, Chapmann & Hall, Chapter 1:Fundamental Principles, Page:8-9

Periodicals

Akdis M. and Reul HM., 2000, Blood Pumps for Circulatory Support, *Perfusion*, 15:295-311, Aachen-Germany

Anderson JB, Wood HG, Allaire PB and Olsen DB, 2000, Numerical Analysis of Blood Flow in the Clearance Regions of a Continuous Flow Artificial Heart Pump, *Artificial Organs*, 24:492-500

Anderson JB et al., 2000, Computational Flow Study of the Continuous Flow Ventricular Assist Device, Prototype Number 3 Blood Pump, *Artificial Organs*, 24(5):377-385

Antaki JF and Burgreen GW et al., 2000, Development Progress of the University Pittsburg Streamliner: a Mixed Flow Blood Pump with Magnetic Bearings, *ASAIO Journal*, 46:194

Behbahani M. et al., 2009, A Review of Computational Fluid Dynamics Analysis of Blood Pumps, *European Journal of Applied Mathematics*, 20:363-397

Bozkurt S., Şafak K., Sorgüven E., Küçükaksu S., Çıblak N., Okyar A.F., Akgün M.A., Ahn H.J., Eğrican A.N. and Lazoğlu İ., 2009, Control Strategies for Left Ventricle Assist Devices (Sol Ventrikül Destek Cihazları İçin Kontrol Stratejileri), *IEEE*

Burke DJ et al., 2001, The HeartMate II: Design and Development of a Fully Sealed Axial Flow Left Ventricular Assist System, *Artificial Organs*, 25:380-385

Butler KC. and Wampler RK. et al., 1990, The Hemopump New Cardiac Prosthesis Device, *IEEE Transactions on Biomedical Engineering*, Vol. 37, No 2

Chan WK. et al., 2005, Numerical Investigation of the Effects of the Clearance Gap between the Inducer and Impeller of an Axial Blood Pump, *Artificial Organs*, 29(3):250-258

Chua LP. et al,2007, Numerical Simulation of an Axial Blood Pump, *Artificial Organs*, 31(7):560-570

Curtas AR and Wood HG et al., 2002, Computational Fluid Dynamic Modeling of Impeller Designs for the HeartQuest LVAD, *ASAIO Journal*, 48:552-561

DeBakey ME., 2000, The Odyssey of the Artificial Heart, *Artificial Organs*, 24(6):405-411

Fan Hui-Min et al, 2009, Design of Implantable Axial-Flow Blood Pump and Numerical Studies on Its Performance, *Science Direct*, 21(4):445-452, Shanghai-China

Fan Hui-Min et al, 2010, Applications of CFD Technique in the Design and Flow Analysis of Implantable Axial-Flow Blood Pump, *Science Direct*, 22(4):518-525, Shanghai-China

Henaine R. et al., 2010, Right Ventricular Recovery After Cervical Extra Corporeal Membrane Oxygenation in a Four-Month-Old Male Leading to Left Berlin Heart Excor Assistance, *Interact CardioVascular Thorac Surg*, 11:840-842

Jingchun Wu et al., 2009, Computational Fluid Dynamics Analysis of Blade Tip Clearances on Hemodynamic Performance and Blood Damage in a Centrifugal Ventricular Assist Device, *Artificial Organs*, 34(5):402-411

Kaplon RJ. and Jarvik RK. et al, 1996, Miniature Axial Flow Pump of Ventricular Assistance in Children and Small Adults, *The Journal of Thoracic and Cardiovascular Surgery*, 111:13-18

Karamanoğlu Y., Mobedi M. and Ertöz AÖ., 2006, Using CFD for Developing Pump Designs (Pompa Tasarımının Geliştirilmesinde Hesaplamalı Akışkanlar Dinamiğinin Kullanılması), *Tesisat Mühendisliği Dergis*i, 91:46-55

Liebermann LN., 1949, The Second Viscosity of Liquids, *American Physical Society* ,Vol. 75,Issue 9

Miller LW. et al, 2007, Use of a Continuous-Flow Device in Patients Awaiting Heart Transplantation, *The New England Journal of Medicine*, 357:885-96

Mitamura Y. and Nakamura H. et al., 1999, Development of Valvo Pump: An Axial Flow Pump Implanted at the Heart Valve Position, *Artificial Organs*, 23:708-711

Miyazoe Y., Sawairi T. and Ito K. et al., 1999, Computational Fluid Dynamics to Establish the Design Process of a Centrifugal Blood Pump: Second Report, *Artificial Organs*, 23:762-768

Olsen DB. et al., 2000, The History of Continuous Flow Blood Pumps, *Artificial Organs*, 24(6):401-404

Robbins RC., Kown MH., Portner PM. and Oyer PE., 2001, The Totally Implantable Novacor Left Ventricular Assist System, *Ann Thorac Surg*., 71:162-165

Samuels et al., 2008, Hybrid Ventricular Assist Device: HeartMate XVE LVAD and Abiomed AB5000 RVAD, *ASAIO Journal*, 54(3):332-334

Siess T., Nix C. and Menzler F., 2001, From a Lab Type to a Product: A Retrospective View on Impella's Assist Technology, *Artificial Organs*, 25:414-421

Song X. & Olsen DB. et al, 2003, Axial Flow Blood Pumps, *ASAIO Journal*, 49:355-364

Song X., Wood HG., Dayn SW. and Olsen DB., 2003, Studies of Turbulence Models in a Computational Fluid Dynamics Model of a Blood Pump, *Artificial Organs*, 27(10):935-937

Song X. et al., 2004, Transient and Quasi Steady Computational Fluid Dynamics Study of a Left Ventricular Assist Device, *ASAIO Journal*, 50:410-417

Song X. et al., 2004, Design and Transient Computational Fluid Dynamics Study of a Continuous Axial Flow Ventricular Assist Device, *ASAIO Journal*, 50:215-224

Stücker M. et al., 1996, Capillary Blood Cell Velocity in Human Skin Capillaries Located Perpendicular to the Skin Surface: Measured by a New Laser Doppler Anemometer, *Microvascular Research*, 52:188-192

Throckmorton AL. et al., 2004, Computational Analysis of an Axial Flow Pediatric Ventricular Assist device, *Artificial Organs*, 28(10):881-891

Tamez D. and Conger JI et al., 2000, In Vivo Testing of the Totally Implantable Jarvik 2000 Heart System, *ASAIO Journal*, 46:168

Timms D., 2011, A Review of Clinical Ventricular Assist Devices, *Medical Engineering & Physics*, 33:1041-47

Tschirkov Alexander et al., 2007, The Berlin Heart EXCOR® in an 11-Year Old Boy, A Bridge to Recovery After Myocardial Infraction, *Texas Heart Institute Journal*, 34(4):445-448

Untaroiu A. et al., 2005, Computational Design and Experimental Testing of Novel Axial Flow LVAD, *ASAIO Journal*, 51:702-710

Untaroiu A. & Olsen DB. et al., 2005, Numerical and Experimental Analysis of an Axial Flow LVAD: The Influence of the Diffuser on Overall Pump Performance, *Artificial Organs*, 29(7): 581-591

Wernickle JT. and DeBakey ME. et al, 1995, A Fluid Dynamic Analysis Using Flow Visualization of the Baylor/NASA Implantable Axial Flow Blood Pump for Design Improvement, *Artificial Organs* 19(2):161-177

Wu H. et al., 2001, Design and Simulation of Axial Flow Maglev Blood Pump, *Information Engineering and Electronic Business*, 2:42-48

Wu J. et al., 2005, Design Optimization of Blood Shearing Instrument by Computational Fluid Dynamics, *Artificial Organs*, 29(6):482-489

Yamane T. et al, 1996, Fluid Dynamics of Turbo Pumps for Artificial Hearts, *Materials Science and Engineering*, C4:99-106

Yamazaki K., Umezu M. and Koyanagi H. et al., 1996, Development of a Miniature Intra-Ventricular Axial Flow Blood Pump, *ASAIO Journal*, 39:224-230

Zhang Y. et al., 2005, A Novel Integrated Rotor of Axial Flow Blood Pump Designed with Computationally Fluid Dynamics, *Artificial Organs*, 31(7):580-585

Zhang Y. and Zhan Z. et al., 2008, Design Optimization of an Axial Blood Pump with Computational Fluid Dynamics, *ASAIO Journal*, 54:150-155

Zhang T. et al., 2011, Study of Flow-Induced Hemolysis Using Novel Couette-Type Blood-Shearing Devices, *Artificial Organs*, Vol. 35, 12:1180-1185

Zhu X. et al., 2006, Numerical Investigation on Hydrodynamics and Biocompatibility of a Magnetically Suspended Axial Blood Pump, *ASAIO Journal*, 52:624-629

Zhu L. et al. 2010, Shape Optimization of the Diffuser Blade of an Axial Blood Pump by Computational Fluid Dynamics, *Artificial Organs*, 34(3):185-192

Other Sources

American Society for Testing and Materials, Standard Practice for Assesment of Hemolysis in Continuous Flow Blood Pumps, Designation: F1841-97

Arora D., Behr M. and Pasquali M., 2003, Blood Damage Measures for Ventricular Assist Device Modeling, Proceedings of 7th International Conference on Computational Modeling of Free and Moving Boundary Problems, Santa Fe-New Mexico

Cahners Business Information, 5 June 2000, Maglev Pumps Sustain the Wounded Heart, Design News, Page 98-102

Chua LP. and Su B., 2011, Numerical Study on the Impeller of an Axial Flow Blood Pump, 4th International Conference on Biomedical Engineering and Informatics

European Hearth Network, 2009, Annual Report

Fabbri S. et al., 20-22 Sep. 2012, Hybrid Bearing for a Hollow-Rotor-Axial Flow VAD (Hotor), International Society for Rotary Blood Pumps 20th Annual Congress Poster Section #27, Istanbul-Turkey

Fuster Valentin, R.Wayne Alexander and Robert A. O'Rourke, 2004, Hurst's the Heart Heart Failure, Vol. 1, Part 3

Gieras A.Izabella and Gieras F.Jacek, 2006, Recent Advancements in Permanent Magnet Motor Technology for Medical Applications, Proceedings of Electrotechnical Institute, Issue 229

Jeker M. et al., 20-22 Sep. 2012, Feasibility of a Hollow Rotor Axial Flow Pump (Hotor) as VAD, International Society for Rotary Blood Pumps 20th Annual Congress Poster Section #15, Istanbul-Turkey

Kirklin JK, Naftel DS, Stevenson LW, Kormos RL et al, 2008, INTERMACS Database for Durable Devices for Circulatory Support: First Annual Report, 27:1065-72

Kirklin JK. et al., 2011, Third INTERMACS Annual Report: The Evolution of Destination Therapy in the United States, J. Heart Lung Transplant, 30:115–23

Küçükaksu DS., Göksedef D. and Bülbül S. et al., 2006, The Prototype of The First Turkish Axial Pump for the Treatment of End-Stage Cardiac Failure: Heart Turcica-1, 14th Congress of the International Society for Rotary Blood Pumps (ISRBP), Leuven-Belgium

Küçükaksu DS., Göksedef D. and Bülbül S. et al., 2006, Turkish Product New Centrifugal Blood Pump for Long-Term Support: Heart Turcica II (Uzun Süreli Destek Tedavisinde Türk Yapımı Yeni Bir Sentrifugal Kan Pompası: Heart Turcica-2), Turkish Society of Heart and Artery Surgery, IX. National Congress (Türk Kalp ve Damar Cerrahisi Derneği IX.Ulusal Kongresi), Belek-Antalya

Lazoğlu Ismail, 2010, Heart Turcica Centrifugal-Development of the First Miniature& Implantable LVAD Heart Pump System in Turkey, Manufacturing & Automation Research Center, Koç University

Ministry of Health - Republic of Turkey, 2008, National Disease Burden and Cost-Effectiveness, Preventing and Controlling Cardiovascular Diseases Program in Turkey, No 743, Ankara

Ministry of Health of Republic of Turkey, 2008, National Organ and Tissue Transplant Coordination System

Mudge GH, 2008, Living With Heart Failure, Harvard Health Publications

Sinnott MD. and Cleary PW., 9-11 December 2009, Effect of Rotor Blade Angle and Clearance on Blood Flow Through a Non-pulsatile Axial Heart Pump, Seventh International Conference on CFD in the Minerals and Process Industries, CSIRO, Melbourne, Australia

Sorgüven E., Akgün MA., Ahj H., Çiblak N., Eğircan AN., Lazoğlu İ., Okyar AF., Şafak KK. and Küçükaksu S., 2007, Flow Simulation and Optimization of a Left Ventricular Assist Device, ASME Int ME Congress and Expo, 8, pp:1401-7

Stehlik J. et al, 10/2010, The Registry of the International Society for Health and Lung Transplantation: Twenty-Seventh Official Adult Heart Transplantation Report-2010, The Journal of Heart and Lung Transplantation, Vol. 20, Issue 10,1089-1103

Texas Heart Institute Journals, 21 Dec. 2009, Published by the Texas Heart Institute, Houston-Texas,

Tuna Yıldırım, 25 January 2007, First Artificial Heart Pump System of Turkey (Türkiye'nin ilk yapay kalp pompa sistemi), Medical Tribune, Year 1, No 1

Turkish Society of Organ Transplantation, 16 October 2010, 7th Annual Congress (Türk Organ Nakli Derneği 7. Yıllık Kongresi), Eskişehir, Turkey